

**EFFECT OF JOINT FREQUENCY AND ORIENTATION
ON COMPRESSIVE STRENGTH AND
DEFORMABILITY OF SMALL-SCALE ROCK
MASS MODELS**

Kiattisak Seephan



**A Thesis Submitted in Partial Fulfillment of the Requirements for the
Degree of Master of Engineering in Civil, Transportation
and Geo-resources Engineering
Suranaree University of Technology
Academic Year 2018**

อิทธิพลของความคิดและทิศทางของรอยแตกต่อกำล้างคดและการเปลี่ยนแปลง
รูปร่างของแบบจำลองมวลหินขนาดเล็ก



วิทยานิพนธ์นี้เป็นส่วนหนึ่งของการศึกษาตามหลักสูตรปริญญาวิศวกรรมศาสตรมหาบัณฑิต
สาขาวิชาวิศวกรรมโยธา ขนส่ง และทรัพยากรธรณี
มหาวิทยาลัยเทคโนโลยีสุรนารี
ปีการศึกษา 2561

**EFFECT OF JOINT FREQUENCY AND ORIENTATION ON
COMPRESSIVE STRENGTH AND DEFORMABILITY OF
SMALL-SCALE ROCK MASS MODELS**

Suranaree University of Technology has approved this thesis submitted in partial fulfillment of the requirements for a Master's Degree.

Thesis Examining Committee



(Asst. Prof. Dr. Akkhapun Wannakomol)

Chairperson



(Asst. Prof. Dr. Decho Phueakphum)

Member (Thesis Advisor)



(Assoc. Prof. Dr. Pornkasem Jongpradist)

Member



(Prof. Dr. Santi Maensiri)

Vice Rector for Academic Affairs
and Internationalization



(Assoc. Prof. Ft. Lt. Dr. Kontorn Chamniprasart)

Dean of Institute of Engineering

เกียรติศักดิ์ สี่พันธ์ : อิทธิพลของความถี่และทิศทางของรอยแตกต่อกำลังกดและการเปลี่ยนแปลงรูปร่างของแบบจำลองมวลหินขนาดเล็ก (EFFECT OF JOINT FREQUENCY AND ORIENTATION ON COMPRESSIVE STRENGTH AND DEFORMABILITY OF SMALL-SCALE ROCK MASS MODELS) อาจารย์ที่ปรึกษา : ผู้ช่วยศาสตราจารย์ ดร. เดโซ เพ็ชร์ภูมิ, 94 หน้า.

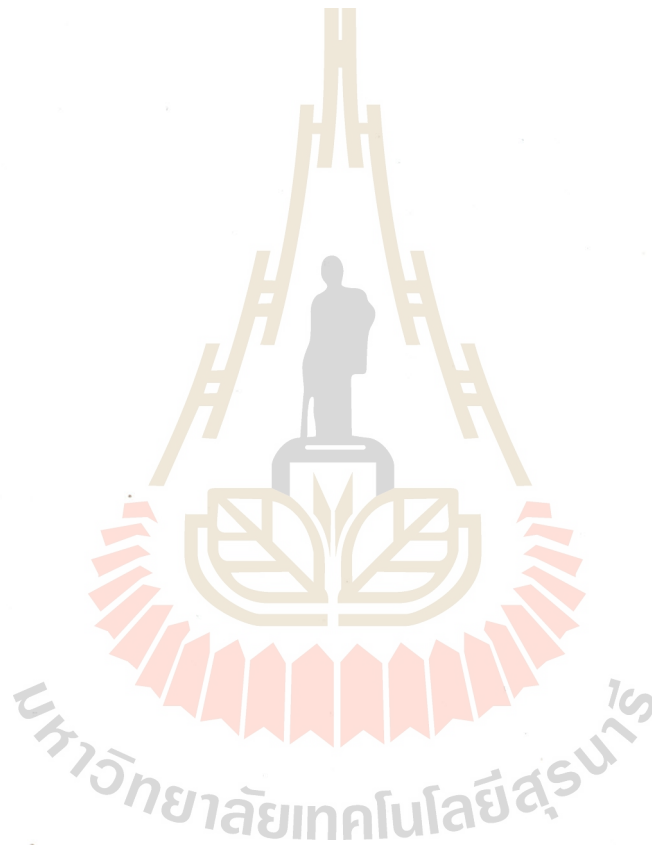
วัตถุประสงค์ของการศึกษานี้คือ เพื่อหาลำดับการเปลี่ยนแปลงรูปร่างของแบบจำลองมวลหินขนาดเล็กที่มีจำนวนและความถี่ของรอยแตกที่แตกต่างกันภายใต้ความดันล้อมรอบสูงถึง 12 เมกะปาสกาล ตัวอย่างหินทรายทรงลูกบาศก์ (55×55×55 ลูกบาศก์ มิลลิเมตร) ที่มีรอยแตกซึ่งจำลองด้วยรอยแตกแบบดิ่งได้ถูกทดสอบจนกระทั่งเกิดการวิบัติโดยใช้โครงให้แรงแบบหลายแกน ความถี่ของรอยแตกเทียบเท่ามีค่าอยู่ในช่วงจาก 36 และ 54 รอยแตกต่อเมตร ผลการทดสอบระบุว่าเมื่อจำนวนความถี่และจำนวนของรอยแตกเพิ่มขึ้นเป็นผลให้ค่ากำลังกดของตัวอย่างมีค่าลดลง ข้อสรุปนี้เป็นจริงสำหรับทุกความดันล้อมรอบ การเพิ่มขึ้นของกำลังกดของตัวอย่างตามความดันล้อมรอบมีแนวโน้มไม่เป็นเส้นตรงขึ้น โดยเฉพาะอย่างยิ่งสำหรับตัวอย่างที่มีสามรอยแตก สำหรับตัวอย่างที่มีรอยแตกเพียงชุดเดียวนั้น กำลังกดของตัวอย่างที่มีรอยแตกตั้งฉากกับแกนของความเค้นหลักสูงสุดจะมีค่าสูงกว่าตัวอย่างที่มีรอยแตกขนานกับแกนของความเค้นหลักสูงสุด ตัวอย่างที่รอยแตกทำมุม 45 องศา กับแกนของความเค้นหลักสูงสุดจะมีค่าต่ำที่สุด เกณฑ์กำลังที่เสนอโดย Hoek-Brown (1980), Sheorey และคณะ (1989), Yudhbir และคณะ (1983) และ Ramamurthy-Arora (1004) มีความสอดคล้องเป็นอย่างดีกับผลการทดสอบ โดยมีค่าสัมประสิทธิ์สหสัมพันธ์มากกว่า 0.9 สำหรับตัวอย่างหินที่มีรอยแตกหนึ่งชุดนั้น ค่าสัมประสิทธิ์การเปลี่ยนแปลงรูปร่างในทิศทางที่ขนานกับระนาบรอยแตกจะมีค่าสูงกว่าในทิศทางที่ตั้งฉาก สำหรับตัวอย่างหินที่มีสามรอยแตกจะมีสัมประสิทธิ์การเปลี่ยนแปลงรูปร่างเท่ากันทุกทิศทาง ค่าสัมประสิทธิ์การเปลี่ยนแปลงรูปร่างลดลงมีค่าลดลงตามการเพิ่มขึ้นของความถี่ของรอยแตกและมีแนวโน้มเพิ่มขึ้นตามการเพิ่มขึ้นของความดันล้อมรอบ

KIATTISAK SEEPHAN : EFFECT OF JOINT FREQUENCY AND
ORIENTATION ON COMPRESSIVE STRENGTH AND DEFORMABILITY
OF SMALL-SCALE ROCK MASS MODELS. THESIS ADVISOR : ASST.
PROF. DECHO PHUEAKPHUM, Ph.D., 94 PP.

TRIAXIAL COMPRESSION/ROCK MASS/DEFORMATION MODULUS/
STRENGTH

The objective of this study is to determine compressive strength and deformability of small-scale rock mass models with different joint sets and frequencies under confining stresses up to 12 MPa. The cubical sandstone specimens ($55 \times 55 \times 55$ mm³) with joint sets simulated by tension-induced fractures are compressed to failure using a polyaxial load frame. The equivalent joint frequencies range from 36 and 54 joints per meter. Results indicate that the larger numbers of joint frequencies and joint sets show the lower compressive strengths of the specimen. This is true for all confining pressures. The increase of the specimen strength with the confining pressure tends to be non-linear, particularly for the three joint sets specimens. For single joint set specimens, the compressive strength of the specimens with joints normal to major principal stress axis always shows greater strength than those with joints parallel to major principal stress axis. The lowest compressive strengths are obtained when the joint planes making angles of 45° with the major principal stress. The Hoek-Brown (1980), Sheorey et al. (1989), Yudhbir et al. (1983) and Ramamurthy-Arora (1994) strength criteria give equally good correlation with the test results, showing $R^2 > 0.9$. For one joint set specimens, the deformation moduli in direction with parallel to the

joint planes are higher than those in direction with normal to the joints planes. For three joint set specimens, the deformation moduli are similar for all principal directions. The deformation modulus decreases with increasing joint frequency, and tends to increase with the confining pressure.



ACKNOWLEDGMENTS

I wish to acknowledge the funding supported by Suranaree University of Technology (SUT).

I would like to express my sincere thanks to asst. Prof. Dr. Decho Phueakphum, for his valuable guidance and efficient supervision. I appreciate his strong support, encouragement, suggestions and comments during the research period. My heartiness thanks to Dr. Supattra Khamrat and Dr. Thanittha Thongprapha for their constructive advice, valuable suggestions and comments on my research works as thesis committee members. Grateful thanks are given to all staffs of Geomechanics Research Unit, Institute of Engineering who supported my work.

Finally, I would like to thank beloved parents for their love, support and encouragement.

Kiattsak Seephan

มหาวิทยาลัยเทคโนโลยีสุรนารี

TABLE OF CONTENTS

	Page
ABSTRACT (THAI)	I
ABSTRACT (ENGLISH)	II
ACKNOWLEDGEMENTS	IV
TABLE OF CONTENTS	V
LIST OF TABLES	VIII
LIST OF FIGURES	XI
SYMBOLS AND ABBREVIATIONS	XIV
CHAPTER	
I INTRODUCTION	1
1.1 Background and rationale	1
1.2 Research objectives	2
1.3 Scope and limitations	2
1.4 Research methodology	3
1.4.1 Literature review	3
1.4.2 Sample preparation	3
1.4.3 Triaxial testing	4
1.4.4 Strength criteria	5
1.4.5 Deformation modulus	5
1.4.6 Empirical criterion	5

TABLE OF CONTENTS (Continued)

	Page
1.4.7 Discussions and conclusions	6
1.5 Thesis contents	6
II LITERATURE REVIEW	7
2.1 Introduction	7
2.2 Effects of joint set on rock mass	7
2.3 Effects of joint orientation	8
2.4 Rock mass strength criterion	11
2.5 Strength comparison	20
2.6 Deformation modulus of rock mass	27
III SAMPLE PREPARATION	36
3.1 Introduction	36
3.2 Sample preparation	36
IV TEST METHOD	40
4.1 Introduction	40
4.2 Test apparatus	40
4.3 Test method	42
V TEST RESULTS	44
5.1 Introduction	44
5.2 Stress-strain curves	44
5.3 Post-test observations	44

TABLE OF CONTENTS (Continued)

	Page
5.4 Strength results	53
5.5 Deformation moduli.....	61
VI ANALYSIS	70
6.1 Introduction.....	70
6.2 Strength criteria	70
6.3 Deformability criteria	77
6.4 Modified Goodman's equation by Thaweeboon et al. (2017)	82
6.5 Relationship between deformation modulus and RMR system.....	86
VI DISCUSSIONS AND CONCLUSIONS	92
7.1 Discussions and conclusions.....	92
7.2 Recommendations for future studies	95
REFERENCES	96
APPENDIX.....	102
BIOGRAPHY	106

LIST OF TABLES

Table	Page
2.1 Results of statistical analyses involving non-linear least squares estimation method (Colak and Unlu, 2004).....	10
2.2 Expressions of the uniaxial compressive strength of the rock mass for the elected estimation methods (Edelbro et al., 2007).....	23
2.3 Methods with reasonable agreement with the measured strengths (Edelbro et al., 2007).....	23
2.4 Physical properties of welded-tuff (Ohya-stone) (Yoshinaka and Yamabe, 1986).....	28
2.5 Comparison of E_j values obtained from different approaches (Tiwari and Rao, 2006).....	33
3.1 Specimens prepared for triaxial compression test with confining pressures of 0, 1, 3, 5, 7 and 12 MPa.	38
5.1 Strength results for intact rock specimens	46
5.2 Strength results for case I.....	46
5.3 Strength results for case II	47
5.4 Strength results for case III	47
5.5 Strength results for case IV	48
5.6 Strength results for case V.....	48
5.7 Strength results for case VI.....	49

LIST OF TABLES (Continued)

Table	Page
5.8 Strength results for case VII.....	49
5.9 Some post-test specimens.....	52
5.9 Some post-test specimens (continuou).	53
5.10 Octahedral shear stresses at failure (case I)	59
5.11 Octahedral shear stresses at failure (case II).....	59
5.12 Octahedral shear stresses at failure (case III)	60
5.13 Octahedral shear stresses at failure (case IV)	60
5.14 Octahedral shear stresses at failure (case IV)	60
5.15 Octahedral shear stresses at failure (case VI)	61
5.16 Octahedral shear stresses at failure (case VII).....	61
5.17 Deformation moduli for intact rock specimens	64
5.18 Deformation moduli for case I.....	64
5.19 Deformation moduli for case II	65
5.20 Deformation moduli for case III.....	65
5.21 Deformation moduli for case IV.....	66
5.22 Deformation moduli for case V	66
5.23 Deformation moduli for case VI.....	67
5.24 Deformation moduli for case VII.....	67
6.1 Strength criteria and their constants calibrated from the test data	73
6.2 Parameter N defined for modified Goodman's equation	79
6.3 Joint factors calculated for this study.....	80

LIST OF TABLES (Continued)

Table	Page
6.4	Parameter N defined for modified Goodman equation by Thaweeboon et al. (2017)..... 83
6.5	Coefficients of correlation of each criterion. 84
6.6	Rock Mass Rating system for I (after Bieniawski 1989) 87
6.7	Rock Mass Rating system for II (after Bieniawski 1989)..... 87
6.8	Rock Mass Rating system for III (after Bieniawski 1989) 88
6.9	Deformation modulus ratio and rock mass rating for case I..... 88
6.10	Deformation modulus ratio and rock mass rating for case II 89
6.11	Deformation modulus ratio and rock mass rating for case III..... 89
6.12	Deformation modulus ratio and rock mass rating for case IV 90
6.13	Deformation modulus ratio and rock mass rating for case V 90
A.1	Intact rock specimens..... 103
A.2	Rock specimens for case I..... 103
A.3	Rock specimens for case II..... 103
A.4	Rock specimens for case III 104
A.5	Rock specimens for case IV 104
A.6	Rock specimens for case V 104
A.7	Rock specimens for case VI..... 105
A.8	Rock specimens for case VII 105

LIST OF FIGURES

Figure	Page
1.1	Research methodology 4
2.1	Anisotropic strength of rock masses with different dip angle: (a) type A; and (b) type B (Yang et al., 1998) 8
2.2	Variation of the normalized m_i parameter with the orientation angle for all sedimentary rock type considered (Colak and Unlu, 2004)..... 11
2.3	Relationship between compressive strength of jointed specimens and joint factor (Ramamurthy, 2001) 12
2.4	Plot of proposed criterion for types of rocks (Hashemnejad, 2013)..... 19
2.5	Comparison between predicted and measured strength of marble, quartzite, granite and tuff (Hashemnejad, 2013) 20
2.6	Experimental and predicted curves of uniaxial compressive strength of slates (Goshashi et al., 2006) 25
2.7	Variation of strengths versus orientation angles (Goshashi et al., 2006)..... 25
2.8	Comparison between predicted and experimental strength at $\sigma_3 = 3$ MPa (Goshashi et al., 2006) 26
2.9	Comparison between predicted and experimental strength at $\sigma_3 = 5$ MPa (Goshashi et al., 2006)..... 26
2.10	Comparison between predicted and experimental strength at $\sigma_3 = 10$ MPa (Goshashi et al., 2006)..... 27

LIST OF FIGURES (Continued)

Figure	Page
2.11 Model of a jointed rock mass subjected to three principal stresses (Yoshinaka and Yamabe, 1986)	29
2.12 Mechanical model for jointed rock mass with two sets of joints (Yoshinaka and Yamabe, 1986)	29
2.13 Relationship between E_{tj}/E_{ti} and joint factor for jointed specimens (Ramamurthy, 2001)	31
2.14 Prediction of modulus at different confining pressures using Janbu's coefficients approach (Tiwari and Rao, 2006)	32
3.1 Line load applied to obtain tension-induced fracture in specimen all tests are conducted under ambient temperature and dry condition	39
4.1 Polyaxial load frame developed for compressive and tensile strength testing under true triaxial stress (Fuenkajorn et al., 2012)	41
4.2 Cantilever beam weighed at outer end applies lateral stress to the rock specimen (Fuenkajorn et al., 2012)	42
4.3 Sample preparation before installed into the load frame. (Thaweeboon et.al., 2017)	43
5.1 Axial and lateral strains measured from various confining pressures for specimens with three mutually perpendicular joint sets, and inclined joint sets	45

LIST OF FIGURES (Continued)

Figure	Page
5.2	Major principal stresses at failure as a function of confining pressure for various joint orientation 54
5.3	Octahedral shear stresses at failure ($\tau_{oct,f}$) as a function of mean stress (σ_m) 58
5.4	Deformation moduli calculated along the intermediate and minor principal axes as a function of the major principal axis68
5.5	Deformation modulus as a function of confining pressure69
6.1	Major principal stresses at failure are comparing the model with tension-induced fractures (solid lines) with those of smooth fractures (dash line) of Thaweeboon et al. (2017) 74
6.2	Test data (points) and curve fits of four strength criteria..... 75
6.3	Hoek–Brown parameters m (a) and s (b) comparing the model with tension-induced fractures (solid lines) with those of smooth fractures (dash lines) of Thaweeboon et al. (2017) 76
6.4	Comparisons between the test data (points) and predictions (lines)..... 81
6.5	Comparisons between the test data (points) and modified Goodman equation by Thaweeboon et al. (2017) (lines) 85
6.6	Deformation moduli for tension-induced fractures (solid lines) and smooth fractures (dash lines) of Thaweeboon et al. (2017) 86
6.7	Deformation modulus ratio as a function of rock mass rating (RMR)..... 91

SYMBOL AND ABBREVIATIONS

ε_1	=	Major principal strains
ε_2	=	Intermediate principal strains
ε_3	=	Minor principal strains
α	=	Empirical constant for equation (6.4)
β	=	Empirical constant for equation (6.4)
θ_1	=	Empirical constant for equation (6.9)
θ_2	=	Empirical constant for equation (6.9)
ν	=	Poisson's ratio
σ_1	=	Compressive strength at failure
σ_2	=	Intermediate stress
σ_3	=	Minor principal stress
σ_c	=	Uniaxial compressive strength of intact rock
σ_{cm}	=	Uniaxial compressive strength of rock mass
σ_m	=	Mean stress
σ_{tm}	=	Uniaxial tensile strength of rock mass
$\tau_{oct,f}$	=	Octahedral shear stresses at failure
A	=	Empirical constant for equation (6.3)
B	=	Empirical constant for equation (6.3)
b_m	=	Empirical constant for equation (6.2)

SYMBOL AND ABBREVIATIONS (Continued)

E_1	=	Deformation modulus along the major directions
E_2	=	Deformation modulus along the intermediate directions.
E_3	=	Deformation modulus along the miner directions.
E_i	=	Empirical constant for equation (6.12)
E_m	=	Empirical constant for equation (6.12) and (6.13)
E_r	=	Empirical constant for equation (6.8)
E_{ij}	=	Empirical constant for equation (6.10)
J_F	=	Empirical constant for equation (6.11)
J_f	=	Empirical constant for equation (6.11)
k_n	=	Empirical constant for equation (6.8), (6.12) and (6.13)
k_{n1}	=	Empirical constant for equation (6.9)
k_{n2}	=	Empirical constant for equation (6.9)
k_{s1}	=	Empirical constant for equation (6.9)
k_{s2}	=	Empirical constant for equation (6.9)
L_1	=	Empirical constant for equation (6.9)
L_2	=	Empirical constant for equation (6.9)
m	=	Empirical constant for equation (6.1)
n	=	Empirical constant for equation (6.11)
N	=	Empirical constant for equation (6.12) and (6.13)
s	=	Empirical constant for equation (6.1), (6.8), (6.12) and (6.13)
r	=	Empirical constant for equation (6.11)

CHAPTER I

INTRODUCTION

1.1 Background and rationale

The reliable strength estimation of a jointed rock mass is necessary to develop safe and economical designs for tunnels, open pits, dam foundations and underground chambers. Rock mass is an inhomogeneous and anisotropic material with complex behavior, which contains random planes of discontinuities. The effects of joints on the compressive strength and elastic modulus of rock mass have long been recognized. One of the most common methods of estimating the rock mass strength is by using a failure criterion. Several researchers have proposed rock mass strength criteria based on laboratory testing (Ramamurthy and Arora, 1994; Colak and Unlu, 2004; Saroglou and Tsiambaos, 2008; Rafiai, 2011; Singh and Singh, 2012), case studies (Sheorey et al., 1989) and numerical analyses (Halakatevakis and Sofianos, 2010) to determine the effects of joint frequency, joint orientation and joint set number on rock mass strengths. It has been found that compressive strength of rock mass decreases with increasing joint frequency (Ramamurthy and Arora, 1994) and joint set number (Yang et al., 1998). The effect of joint on strength depends on the orientation. The lower strengths are obtained when the joint planes make angles between 30° - 40° with the major principal stress (Ramamurthy and Arora, 1994; Colak and Unlu, 2004; Goshtasbi et al., 2006). The existing strength criteria for rock mass have been verified by comparing with the actual in-situ conditions (Edelbro, 2004). Even though several rock mass strength criteria have

been proposed, the development of criteria to describe the deformation moduli as affected by joint orientation has been rare.

1.2 Research objectives

The objective of this study is to determine rock mass strength and deformability in the laboratory by simulating joints in sandstone specimens with one, two and three joint sets under various confining pressures and joint frequencies. The results are used to assess the predictive capability of the strength criteria developed by Hoek and Brown (1980), Ramamurthy and Arora (1994), Yudhbir et al. (1983) and Sheorey et al. (1989). Empirical criteria developed by Goodman (1970), Yoshinaka and Yamabe (1986) and Ramamurthy (2001) criteria are used to predict the deformation modulus of jointed rock specimens. Triaxial compressive strength tests have been performed on cubical sandstone specimens with nominal dimensions of $55 \times 55 \times 55 \text{ mm}^3$ using a true triaxial load frame. The confining pressures are varied from 0, 1, 3, 5, 7 to 12 MPa. The simulated joints are tension-induced fractures. The evaluation of the existing rock mass failure criteria and their parameters are useful to appropriately apply in the design and stability analysis of geologic structures.

1.3 Scope and limitations

The scope and limitations of the research include as follows:

- 1) Laboratory testing is conducted on cubical specimens prepared from the Phra Wihan sandstone.
- 2) Triaxial compression tests are performed with confining pressures of 0, 1, 3, 5, 7 and 12 MPa.

- 3) The specimens are prepared to have one, two and three joint sets with number of joint varies from 1, 2 joints for each set.
- 4) Up to 70 samples are tested, with the nominal dimensions of $55 \times 55 \times 55$ mm³ for one, two and for three joint sets.
- 5) For one joint set specimen, the joint are parallel, inclined at 45° and perpendicular to the applied major principal stress.
- 6) All tests are conducted under ambient temperature and dry condition.
- 7) The tested joint is artificially made in the laboratory by tension induced method.

1.4 Research methodology

The research methodology shown in Figure 1.1 comprises 8 steps; including literature review, sample preparation, triaxial testing, strength criteria, deformation modulus, empirical criterion, discussions and conclusions, and thesis writing.

1.4.1 Literature review

The research methodology shown in Figure 1.1 comprises 8 steps; including literature review, sample preparation, triaxial testing, strength criteria, deformation modulus, empirical criterion, discussions and conclusions, and thesis writing.

1.4.2 Sample preparation

The rock samples used in this study are Phra Wihan sandstone. This rock is classified as fine-grained quartz sandstones with highly uniform texture and density. They are prepared to obtain cubic specimens with nominal dimensions of $55 \times 55 \times 55$ mm³.

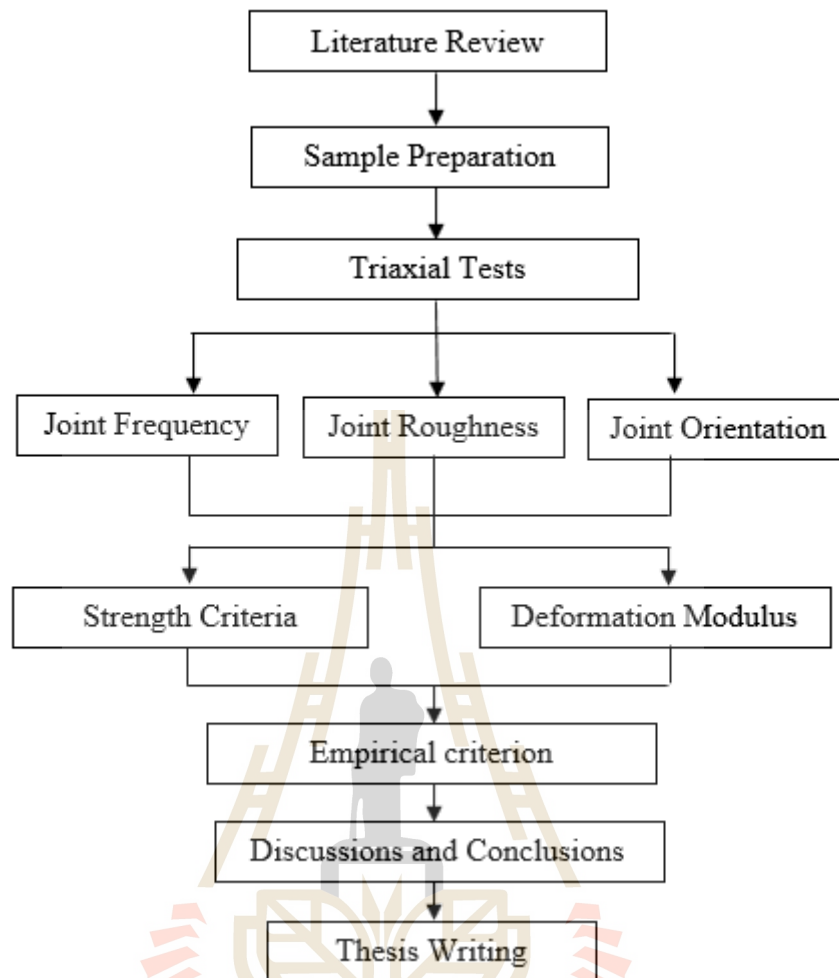


Figure 1.1 Research Methodology.

The simulated joints are tension-induced fractures. Specimens with one joint set, two joint set and three mutually perpendicular joint sets are prepared. There are 1 and 2 joints for each set (36 and 54 joints per meter). For one joint set specimens, the joint are parallel, inclined at 45° and perpendicular to the applied major principal stress.

1.4.3 Triaxial testing

A true triaxial load frame is used to apply constant confining pressures at 0, 1, 3, 5, 7 and 12 MPa. Neoprene sheets are used to minimize the friction at all

interfaces between the loading platens and the rock surface. The tests are performed by increasing the axial stress until failure occurs. The confining pressure is controlled constant by four lateral hydraulic pumps. The digital displacement gages are installed to measure the axial and lateral deformations until failure occurs. The maximum load at failure and failure modes are recorded. They are used to calculate the strength and deformation modulus of the specimen.

1.4.4 Strength criteria

Four criteria that are commonly used to determine rock mass strength are fit to the triaxial strength data. They include the Hoek and Brown (1980), Sheorey et al. (1989), Yudhbir et al. (1983) and Ramamurthy and Arora (1994) criteria. They are all formulated in the terms of σ_1 and σ_3 . The predictive capability of these strength criteria is determined and compared using the coefficient of correlation (R^2) as an indicator. The higher R^2 value indicates the better predictability of the criterion.

1.4.5 Deformation modulus

Four empirical criteria are used to estimate rock mass deformation modulus (E_m). They include the Goodman (1970), Yoshinaka and Yamabe (1986), Ramamurthy (2001) and Thaweeboon et al. (2017). The deformation modulus calculated from the triaxial compression test results are compared with the rock mass deformability criteria. RMR classification is also studied.

1.4.6 Empirical criterion

The test results determine the effects of joint frequency, orientation and set numbers on the deformation modulus of rock mass model. An empirical criterion are derived to describe the deformation moduli of the rock models as affected by joint orientation and frequency.

1.4.7 Discussions and conclusions

Discussions are made on the reliability and adequacies of the approaches used here. Future research needs are identified. All research activities, methods, and results are documented and compiled in the thesis. The research or findings will be published in the conference proceedings or journals.

1.5 Thesis content

This research thesis is divided into eight chapters. The first chapter includes background and rationale, research objectives, scope and limitations and research methodology. **Chapter II** presents results of the literature review to improve an understanding of the strength and deformation of rock mass, the existing strength criteria and the previous relevant testing. **Chapter III** describes sample preparation. **Chapter IV** describes the test method. **Chapter V** presents the experimental results. **Chapter VI** assesses the predictive capability of some rock mass strength criteria, determine the effects of joint frequency, orientation and set numbers on the deformation modulus of rock mass model and to assess the predictive capability of the deformability criteria. **Chapter VII** presents discussions, conclusions and recommendation for future studies.

CHAPTER II

LITERATURE REVIEW

2.1 Introduction

Relevant topics and previous research results are reviewed to improve an understanding of the strength and deformation of rock mass, the existing strength criteria and the previous relevant testing. These include the effects of joint set on rock mass, effects of joint orientation, rock mass strength criterion, strength comparison and elastic modulus of rock mass. Initial review results are summarized below.

2.2 Effects of joint set on rock mass

Yang et al. (1998) perform uniaxial tests on prismatic jointed models with two joint sets (type A) and three joint sets (type B) with different surface roughness and configurations. The failure mode, failure strength and deformation behavior were investigated for each test in order to analyze the fracture mechanism of jointed rock. The model material is a mixture of plaster, sand and water in the proportions of 1:0.25:0.92 by weight. The fundamental properties of the model material are: $\sigma_c = 7.63$ MPa, $\sigma_t = 1.05$ MPa, $E = 4554$ MPa, $\nu = 0.19$, $\gamma = 1.05$ g/cm³, $\phi_b = 31^\circ$. From the axial stress-stress curves of type A mass, it is observed a highly nonlinear and joint orientation dependent behavior representing jointed rocks. To design two identical strengths of joint sets in a mass, the first and third joint sets in model B was arranged symmetrically with respect to the axial loading. In this circumstance, the shear strength of joints in

each set is the same. The steeper set demonstrates a lower shear strength as shown in Figure 2.1. The strengths in some cases of type B are smaller than that in type A.

2.3 Effects of joint orientation

Ramamurthy and Arora (1994) study the jointed rock mass strength to predict strength from joint factor (J_f). The joint factors consist of joint frequency, joint orientation (n) and shear strength along the joint (r). The objective was achieved by simulating joints in intact isotropic rock cores in laboratory. Anisotropy was induced into the intact specimens by developing a number of clean and rough-broken joints at $\beta=0, 30, 40, 50, 60, 70, 80, 90^\circ$ (β is the angle between the joint orientation and vertical axis through the specimen). The strength of a jointed rock mainly depends on the orientation of the joint with respect to the direction of axial loading. The study revealed that rocks exhibit a minimum value of strength when the joints are oriented at $\beta=30-40^\circ$. Similar behavior was also observed in earlier studies. The joint which is closer to

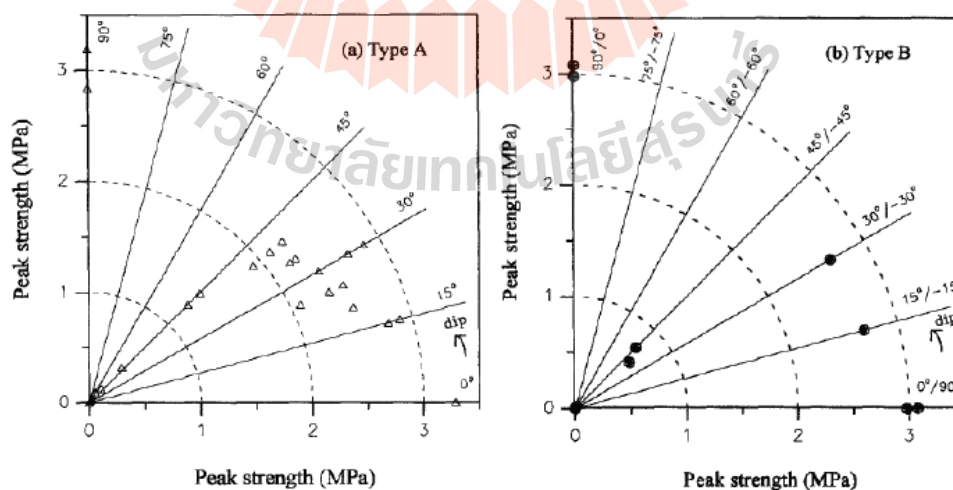


Figure 2.1 Anisotropic strength of rock masses with different dip angle: (a) type A; and (b) type B (Yang et al., 1998).

$(45-\varphi/2)^\circ$ with the major principal stress is the most probable sliding joint and should be considered in estimating the value of J_f .

Colak and Unlu (2004) study the influence of joint orientation (m_i value) for the strength anisotropy. The testing is performed in sandstone (possessing low degree of anisotropy) and siltstone, claystone (medium degree of anisotropy). The rock samples have orientations (β) at 0, 30, 45, 60 and 90° (orientated constant named $m_i(\beta)$). Tests were conducted according to the ISRM suggested standards. It has been noted that values of $m_i(\beta)$ vary with the orientation angle, and this is considered an indication of the strength anisotropy. A suitable function that may be used to define the normalized value of $m_i(\beta)$ has been derived from a similar expression given by Hoek and Brown (1980). Utilizing this equation, the following expression is obtained:

$$\frac{m_{i(\beta)}}{m_{i(90)}} = 1 - A \exp \left[- \left(\frac{\beta - B}{C + D\beta} \right)^4 \right] \quad (2.1)$$

where $m_{i(90)}$ is the reference value of m_i , B is the value of β (in degrees) at which $m_i(\beta)$ is minimum, and A , C and D are statistical parameters given in Table 2.1. Finally, a generalized curve is obtained for all the sedimentary rocks considered (Figure 2.2). In summary, when transversely isotropic intact rock specimens exhibit strength anisotropy, the H-B strength envelope is variable, and it is influenced by the orientation angle. Using the results of basic strength tests on oriented samples, the values of the H-B strength parameter m_i are calculated for different orientation angles by conventional statistical analysis. Then, employing the expression given by Equation (2.1) as a model for non-linear statistical regression, the parameter $m_i(\beta)$ can be obtained as a function of the orientation angle (β). Finally normalized H-B strength envelopes are obtained

according to Equation (2.2), and they also depend on the orientation angles.

$$\sigma_1(\beta)/\sigma_{ci}(\beta) = \sigma_3/\sigma_{ci}(\beta) + (m_i(\beta) \sigma_3/\sigma_{ci}(\beta) + 1)^{0.5} \quad (2.2)$$

In addition, it should be emphasized that this approach is applicable to two dimensional transverse isotropy problems involving intact rocks. Although this approach is applicable only to plane anisotropy problems related to intact rocks, it is anticipated that it will be possible to extend it to include rock masses.

Table 2.1 Results of statistical analyses involving non-linear least squares estimation method (Colak and Unlu, 2004).

Rock type	Statistical parameters				Coefficient of determination(r^2)
	A	B	C	D	
Sandstones	0.38	17.0	14.8	0.47	0.653
Siltstones	0.77	17.4	19.8	0.31	0.840
Claystone	0.61	15.3	17.6	0.40	0.998
All sedimentary rock types considered	0.63	13.4	13.3	0.49	0.606

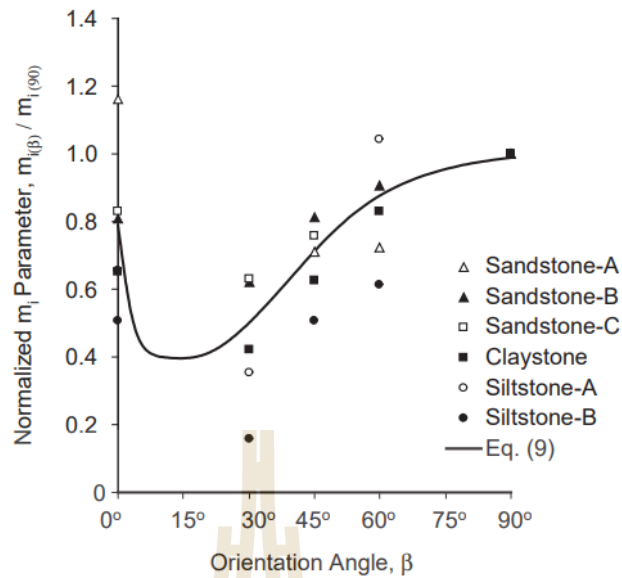


Figure 2.2 Variation of the normalized m_i parameter with the orientation angle for all sedimentary rock type considered (Colak and Unlu, 2004).

2.4 Rock mass strength criterion

Ramamurthy (2001) studies the shear strength response of some geological materials in triaxial compression by proposing a non-linear shear strength failure criterion. This criterion has been verified with the experimental data of 41 different soils from clay to rockfill and with the data of a number of intact rocks, jointed rocks and rock-like materials tested in the axisymmetric triaxial compression exhibiting either brittle or ductile response. Various types of joints introduced into the test specimens by the corresponding test data are included in Figure 2.3 It is found that the compressive strength of a jointed rock can be linked to that of the intact rock through a joint factor, J_r . The strength criterion on jointed rocks is thus

$$\frac{(\sigma'_1 - \sigma'_3)}{\sigma'_3} = B_j \left(\frac{\sigma'_{ci}}{\sigma'_3} \right)^\alpha \quad (2.3)$$

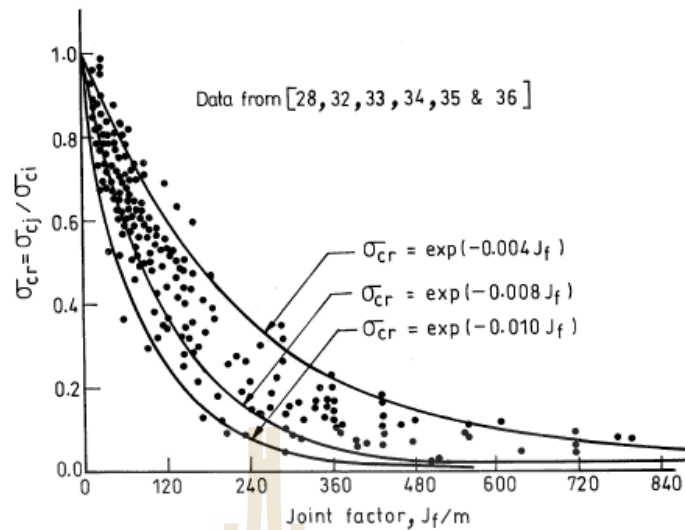


Figure 2.3 Relationship between compressive strength of jointed specimens and joint factor (Ramamurthy, 2001).

where σ_1' and σ_3' are major and minor effective principal stresses, respectively, σ_{cj}' the uniaxial compressive strength of jointed specimen obtained from, B_j and α_j are strength parameters of the jointed rock. The values of α_j and B_j are obtained from the following expressions:

$$\alpha_j / \alpha_i = \left(\frac{\sigma_{cj}}{\sigma_{ci}} \right)^{0.5} \quad (2.4)$$

$$B_i / B_j = 0.13 \exp[2.04 \alpha_j / \alpha_i] \quad (2.5)$$

where α_i and B_i are the values of the strength parameters obtained from triaxial tests on intact specimens of the rock.

Since, the weakness introduced into an intact rock is essentially due to the combined effect of the joints, their inclination/orientation and the strength along these joints, represented by J_r , both compressive strength and modulus are influenced.

Kulatilake et al. (2006) propose a new rock mass failure criterion for biaxial loading conditions (Equation 2.6). To simulate brittle rocks, a mixture of glastone, sand and water was used as a model material. To investigate the failure modes and strength, both the intact material blocks as well as jointed model material blocks of size $35.6 \times 17.8 \times 2.5$ cm having different joint geometry configurations were subjected to uniaxial and biaxial compressive loadings. The results exhibited three different failure modes under different joint geometry configurations: Orientation of joint sets and the level of intermediate principal stress play major roles with respect to the mode of failure. A new intact rock failure criterion is proposed at the 3-D level. Results obtained from both the intact and jointed model material blocks are used to develop a strongly non-linear new rock mass failure criterion for biaxial loading. The criterion incorporates the fracture tensor component and covers the strengths resulting from all the three failure modes observed in the investigation. Equation (2.8) shows the fracture tensor of a jointed mass has the capability of integrating the effects of number of fracture sets (N), fracture density (ρ), and distributions for size (r) and orientation (θ) of the fracture sets. The fracture tensor component in a certain direction quantifies the directional effect of fracture geometry.

$$\frac{\sigma_{u,b}}{\sigma_{u,l}} = \exp(-\omega_0 F_{22}) \quad (2.6)$$

$$\omega = \frac{\omega_0}{a\left(\frac{\sigma_2}{\sigma_{u,l}}\right)^b + 1} \quad (2.7)$$

$$F_{22} = \sum_{m=1}^N (\rho r^2 \sin^2 \theta) \quad (2.8)$$

Saroglou and Tsiambaos (2008) propose the modified Hoek-Brown criterion by incorporating a new parameter (k_β) to account for the effect of strength anisotropy, thus being able to determine the strength of intact anisotropic rock under loading in different orientations of the plane of anisotropy. The uniaxial and triaxial compression tests were performed on gneiss, schist and marble specimens in which the planes of anisotropy were oriented at angles β equal to 0° , 15° , 30° , 45° , 60° , 75° and 90° . The specimen diameter was 54 mm (NX size) with a height/diameter ratio between 2.0 and 2.5. The range of confining pressures used for the triaxial tests was $0 < \sigma_3 < \sigma_{ci}/2$. From the present study were fitted to the proposed failure criterion in Equation (2.9).

$$\sigma_1 = \sigma_3 + \sigma_{c\beta} \left(k_\beta m_i \frac{\sigma_3}{\sigma_{c\beta}} + 1 \right) \quad (2.9)$$

where $\sigma_{c\beta}$ is the uniaxial compressive strength at an angle of loading, β , and k_β is the parameter describing the anisotropy effect. In verification of proposed criterion, plotting the uniaxial compressive strength, determined by tests for different loading directions, $\sigma_{c\beta\text{-lab}}$, against that predicted from the failure criterion for anisotropic intact rock, can also assess the accuracy of the proposed criterion. When loading is performed perpendicular to the planes of “inherent” anisotropy of the intact rock, the parameter k_β is equal to unity ($k_{\beta 0} = 1$) and the strength ($\sigma_{c\beta}$) is equal to the uniaxial compressive

strength σ_{ci} . The minimum value of this parameter, $k_\beta = k_{30}$, occurs when loading is performed at the angle of minimum strength which usually is when the angle β between the major principal stress (σ_1) and the foliation planes is between 30° and 45° . The prediction of uniaxial strength by the proposed criterion is quite good as the majority of the data plot on the diagonal line. Although the proposed modification was studied for metamorphic rocks (gneiss, schist, marble), but could also be applied to other rock types exhibiting ‘‘inherent’’ anisotropy, e.g. sedimentary as well as igneous rocks. The proposed modified criterion is intended for use for prediction of strength of intact rock but can also be extended to rock masses.

Rafiai (2011) proposes a new polyaxial criterion (Equation 2.10) and triaxial criterion (Equation 2.11) for brittle and ductile failure of intact rock and rock masses. A comprehensive database of the results of uniaxial, triaxial, and polyaxial tests on intact rock was utilized for evaluation of the new criterion and comparison of its accuracy with the most accurate and frequently used criteria.

$$\frac{\sigma_1}{\sigma_c} = \frac{\sigma_1^{trx}}{\sigma_c} + \sqrt{C \frac{\sigma_2 + \sigma_3}{\sigma_1^{trx}} \exp\left(-\frac{\sigma_2 + \sigma_3}{\sigma_1^{trx}}\right)} \quad (2.10)$$

where C and D are constants and σ_1^{trx} is the rock strength in triaxial state of stresses ($\sigma_2 = \sigma_3$) that can be calculated as

$$\frac{\sigma_1^{trx}}{\sigma_c} = \frac{\sigma_3}{\sigma_c} + \frac{1+A(\sigma_3/\sigma_c)}{1+B(\sigma_3/\sigma_c)} \quad (2.11)$$

where σ_c is the uniaxial compressive strength of intact rock, A and B are dimensionless constants that depend on the properties of rock ($A \geq B \geq 0$). The parameter r is a strength reduction factor indicating the extent to which, the rock mass has been fractured. For intact rock $r = 0$ and for heavily jointed rock masses $r = 1$.

It shows that the new criterion can maintain its accuracy over a wider range of stresses. In the absence of rock mass strength data, applicability of the new criterion for rock mass was verified by fitting it to typical Hoek–Brown (1988) failure envelopes. Regression analysis of the polyaxial strength data in the form of $(\sigma_3, \sigma_2, \sigma_1)$ for six rock types showed that the new criterion predict the strength more accurately than the Modified Wiebols–Cook (Zhou, 1994) and You criteria (You, 2009) in all cases.

Singh and Singh (2012) state that the Mohr–Coulomb shear strength criterion is the most widely used criterion for jointed rocks. In its present form there are two major limitations of this criterion; firstly it considers the strength response to be linear, and, secondly the effect of the intermediate principal stress on the strength behavior is ignored. A modified non-linear form of Mohr–Coulomb strength criterion has been suggested in this study to overcome these limitations by following equations:

$$(\sigma_1 - \sigma_3) = \left(\sigma_{cj} + \frac{2 \sin \phi_{jo}}{1 - \sin \phi_{jo}} \sigma_3 - \frac{1}{\sigma_{ci}} \frac{\sin \phi_{jo}}{(1 - \sin \phi_{jo})} \sigma_3^2 \right) \quad (2.12)$$

$$\sin \phi_{j0} = \frac{(1 - \text{SRF}) + \left(\frac{\sin \phi_{i0}}{1 - \sin \phi_{i0}} \right)}{(2 - \text{SRF}) + \left(\frac{\sin \phi_{i0}}{1 - \sin \phi_{i0}} \right)}; \text{SRF} = \text{Strength reduction factor} = \frac{\sigma_{cj}}{\sigma_{ci}} \quad (2.13)$$

Equations (2.12) and (2.13) were used to predict σ_1 value for all the triaxial tests with inputting only σ_{ci} , σ_{cj} and ϕ_{io} . Where σ_{ci} is the UCS of the intact rock and ϕ_{io} is the friction angle of the intact rock. On lines similar to intact rock criterion (Singh and Singh, 2012) the strength criterion for jointed rocks in Equation (2.12) is extended to polyaxial stress condition purely on trial basis. The criterion for polyaxial strength is expresses as:

$$(\sigma_1 - \sigma_3) = \sigma_{cj} + \frac{2 \sin \phi_{jo}}{1 - \sin \phi_{jo}} \left(\frac{\sigma_1 - \sigma_3}{2} \right) - \frac{1}{\sigma_{ci}} \frac{\sin \phi_{jo}}{(1 - \sin \phi_{jo})} \left(\frac{\sigma_2^2 + \sigma_3^2}{2} \right); \text{for } 0 \leq \sigma_3 \leq \sigma_2 \leq \sigma_{ci} \quad (2.14)$$

where σ_{cj} is the anisotropic strength of the rock mass under uniaxial loading condition ($\sigma_3 = \sigma_2 = 0$) in the direction of σ_1 , which will depend on the characteristics of the joints (frequency, orientation and surface roughness) and the properties of the intact rock; ϕ_{jo} is the anisotropic friction angle of the rock mass at low confining stress level and may be obtained as a function of SRF and ϕ_{jo} using Equation (2.13). The criterion has been found to work well for those failure patterns where assumption of equivalent continuum is valid and the equivalent properties are function of intact rock properties and joint characteristics. It is suggested that the simple polyaxial strength criterion (Equation 2.14) may be used in the non-linear stress analysis of underground openings in natural rock masses. The applicability of the proposed criterion has been verified by applying it to extensive experimental data on triaxial and polyaxial test results on jointed rocks available from literature.

Hashemnejad et al. (2013) states that a strength criterion should be capable to deal with different conditions of a certain type of rock having different properties. A new empirical criterion (Equation 2.15) is introduced and compared to the Hoek-Brown (1988) criteria, Bieniawski (1974) criteria, Ramamurthy (1989) criteria and as a result.

$$\left(\frac{\sigma_1}{\sigma_3}\right) = \beta \left(\frac{3\sigma_c - 0.5\sigma_3}{\sigma_3}\right)^\alpha \quad (2.15)$$

where β is rock material constant; function of rock type and quality and α is slope of plot between (σ_1 / σ_3) and $((3 \sigma_c - 0.5 \sigma_3) / \sigma_3)$ on log-log plot. The above expression is applicable for all values of $\sigma_3 > 0$. For a discussion and comparison of the forms and the new form presented in this study, triaxial data of 80 samples were collected from different sources. These data are homogeneous and on specimens of almost the same size. In the new criterion defined, failure is as the failure strength and a failure criterion is not associated with the strain. Analysis of individual data sets revealed that none of the existing criteria shows perfect agreement with experimental values of stone strength. The analysis was carried out for different rock types, namely, limestone, granite, granodiorite, shale, sandstone, claystone and liparite. For each particular rock type there found to be a correlation between B in the Bieniawski (1974) criterion and m in the Hoek-Brown (1980) criterion with σ_c . The result show that the triaxial strength can be made by means of the Bieniawski criterion with a variable B dependent upon σ_c and α certain constant σ for each particular material. The only parameter required for this criterion is the unconfined compressive strength which can be determined simply. In Figure 2.4, the results of the regression of this criterion are shown. Finally in Figure 2.5, which compares

the results, obtained from the four criteria actual values obtained from triaxial tests on samples, it is better visible.

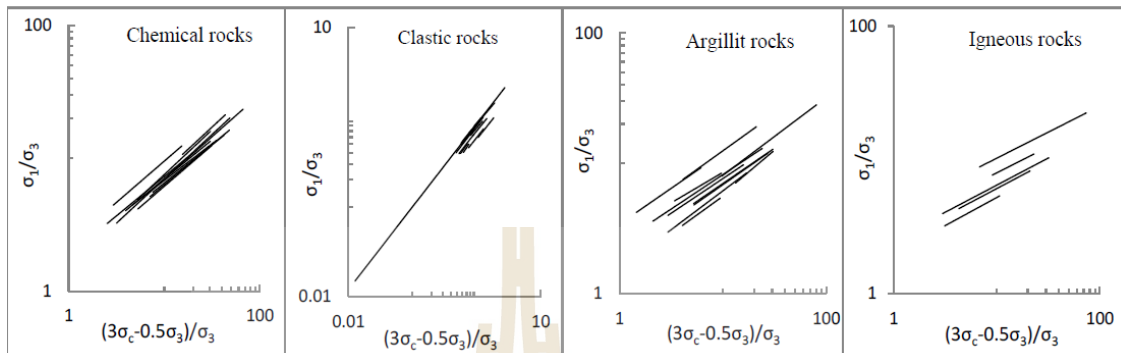


Figure 2.4 Plot of proposed criterion for types of rocks (Hashemnejad et al., 2013).



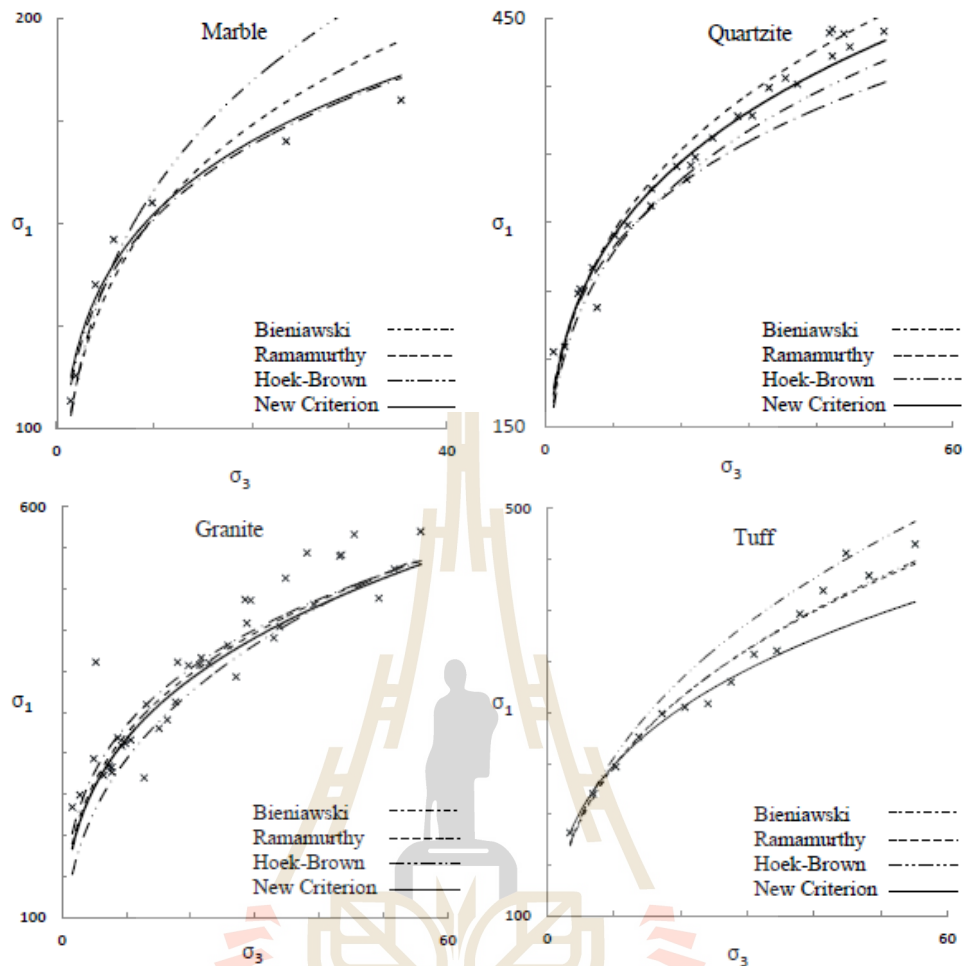


Figure 2.5 Comparison between predicted and measured strength of marble, quartzite, granite and tuff (Hashemnejad et al., 2013).

2.5 Strength comparison

Sridevi and Sitharam (2000) study the strength and moduli of jointed rock to develop a rapid and exact technique based on equivalent continuum approach in which the properties of jointed rock masses are represented as a function of the intact rock properties and the properties of the rock joints, and comparison of empirical strength criteria of joint rock mass. In the analysis shear strength criteria proposed by Hoek and Brown (1980), Yudhbir et al. (1983), Ramamurthy and Arora (1994) and the

conventional Mohr-Coulomb criteria are used to determine the failure stress. The four empirical strength criteria are incorporated in a finite element code to determine the major principal stress at failure. The results have been presented in the form of principal stresses at failure based on the strength criteria used for different joint orientations and material properties. The results are plotted for different strength criteria and compared with the experimental results of Yaji (1984) and Brown and Trollope (1970). The results compare well within the limit of empirical relations of different strength criteria and experimental framework. From a comparison of empirical strength criteria it can be concluded that at higher confining pressures one can use any strength criteria whereas the choice of strength criteria is much more important at lower confining pressures. For jointed rocks the Mohr-Coulomb criterion gives a high estimate of failure stress for single jointed rock but gives a fair estimate of failure stress for block-jointed systems. The Hoek-Brown (1980), Yudhbir et al. (1983) and Ramamurthy (2001) criteria give a fair estimate of the major principal stress at failure for almost all cases although the value given by Ramamurthy's criterion is the best. This analysis, when extended to specimens with filled joints and also to an axisymmetric case, would throw some light on the validity of these criteria in general and also help in arriving at a conclusion at which one is best for a given jointed rock mass.

Edelbro et al. (2007) presents a review of existing methods to estimate the rock mass strength using empirical failure criteria and classification/characterisation systems. To investigate the robustness and quantitatively compare the different selected estimation methods, they were used in three case studies. This paper is concerned with rocks whose failure mechanisms primarily are spalling and/or shear failure. Furthermore, the rock mass must be possible to approximate as a continuum material.

For consideration, the methods had to: (i) present a numerical result that corresponds to the strength, (ii) have been used after the first publication, and (iii) be applicable to underground rock masses. All methods comprise an expression for the uniaxial rock mass compressive strength, see Table 2.2. The results from all methods and all case studies have also been summarized with respect to the span between estimated maximum and minimum values. The results from the Round Robin tests showed that the Hoek–Brown-GSI and Sheorey-RMR76, RMS, and MRMR strength estimation methods gave results that were in poor agreement with the measured strengths. The use of the N, Yudhbir-RMR76, R_{Mi}, Q-, and Hoek–Brown-GSI methods, presented in Table 2.3, yielded reasonable agreement with the measured strengths. These methods are thus considered the best candidates for realistic strength estimation. However, the issue of “user-friendliness” must first be considered. Of these five methods, R_{Mi} seems to be least user-friendly, primarily due to the difficulties of accurately determining block size. The tables used for Hoek–Brown-GSI, are basic, but may be experienced as inaccurate by the user. In conclusion, the selected five estimation methods appear to be applicable for hard rock masses, provided that care is taken when choosing values for each of the included parameters in each method. However, the agreement with measured strengths is still relatively poor, implying that precise estimates cannot be expected with any method. This study has shown that the block volume was difficult to estimate; hence, a better method for block size estimation is warranted. The joint strength is included in most of the methods, where the joint alteration and joint roughness parameters (in Q, R_{Mi} and N) covers more possible geological situations and, according to this study, are better described than the joint condition parameter in RMR (Bieniawski, 1989). The physical scale is not included in

any of the existing methods. The N method considers the tunnel span or diameter (B), but not related to the scale of the rock mass.

Table 2.2 Expressions of the uniaxial compressive strength of the rock mass for the elected estimation methods (Edelbro et al., 2007).

Criterion	Uniaxial compressive strength of rock mass (σ_{cm})					Authors
Hoek-Brown-RMR ₇₆	$\sigma_{cm} = \sigma_c \cdot \sqrt{e^{\frac{RMR_{hoek}-100}{9}}}$					Hoek and Brown (1988)
Yudhbir-RMR ₇₆	$\sigma_{cm} = \sigma_c \cdot e^{[7.65(\frac{RMR_{hoek}-100}{100})]}$					Yudhbir et al. (1983)
Sheorey-RMR ₇₆	$\sigma_{cm} = \sigma_c \cdot e^{\frac{(RMR_{hoek}-100)}{20}}$					Sheorey (1997)
MRMR	$\sigma_{cm} = \sigma_c \cdot \frac{(MRMR\text{-rating for } \sigma_c)}{100}$					Laubscher (1984)
Q	$\sigma_{cm} = 5\rho(Q \cdot \frac{\sigma_c}{100})^{1/3}$					Barton (2002)
N	$\sigma_{cm} = \frac{5.5 \cdot \rho \cdot N^{1/3}}{B^2}$					Singh and Goel (1999)
RMi	RMi = $\sigma_c \cdot JP$					Palmström (1995)
Hoek-Brown-GSI	$\sigma_{cm} = \sigma_c \cdot e^{\frac{(GSI-100)}{9-10}} (\frac{1}{2} + \frac{1}{4}(e^{-GSI/15} - e^{-20/3}))$					Hoek et al. (2002)
RMS	RMS-value ^a	100-81	80-61	60-41	41-20	Stille et al. (1982)
	σ_{cm} (MPa)	30	12	5	2.5	

Table 2.3 Methods with reasonable agreement with the measured strengths (Edelbro et al., 2007).

Methods	Parameters of interest	Remarks
Q	J _r , J _a	The effect on the rock mass strength due to be better defined
RMi	V _b , jL, jR and jA	The block volume and joint length needs to be modified and easier to use
N	B	Could be interesting to study a stress free Q-system, of the newest version to determine the rock mass strength
Yudhbir-RMR ₇₆	-	Study the relation between RMR ₇₆ and the rock mass strength
Hoek-Brown-GSI	m, a, s and GSI	-

Goshashi et al. (2006) evaluate the most suitable criterion for predicting the anisotropic strength of rocks in uniaxial and triaxial compression. Uniaxial and triaxial tests were conducted on specimens having orientation angles (β) of 0, 30, 45, 60, 75 and 90 degrees. The triaxial tests were done at confining pressures of 3, 5 and 10 MPa.

Laboratory tests were carried out in accordance with ISRM standards on cylindrical samples at various orientation angles. Figure 2.6 shows the variation of uniaxial compressive strength versus orientation angles. The results are based on the average experimental data obtained from three to five tests for each orientation. The results clearly show that the slate has a U-shaped anisotropy. Figure 2.7 shows the strength variations with orientation angles at various confining pressures. The plots are drawn by taking the average experimental results of three to five tests. It is clear from the results that the maximum and minimum strengths values are observed at $\beta = 90^\circ$ and 30° respectively. In order to evaluate the most suitable criterion for predicting the anisotropic strength of rocks in uniaxial compression, the Liao and Huang (Liao and Hsieh, 1999) and Ramamurthy criteria (Ramamurthy, 1993) were studied. The predicted values were then plotted and compared with experimental test results. The study clearly shows that both criteria have good agreements with the test results; however, the Liao and Huang criterion predicts the strength more precisely. In order to investigate the most suitable criterion for predicting the anisotropic strength of rocks in triaxial compression, various criteria was used. The most commonly criteria utilized in this study were Donath and Mclamore (Mclamore and Gray, 1967; Fahimifar and Soroush, 2003; Goodman, 1989), Hoek and Brown criterion for anisotropic rocks (Hoek and Brown, 1980), Liao and Huang (Liao and Hsieh, 1999), Tien and Kuo (Tien, and Kuo, 2001) and Ramamurthy (Ramamurthy, 1993; Nasser et al., 2003). Figures 2.8–2.10 exhibit the between the predicted strength values and the data at different confining pressures. These criteria, it is essential to conduct three triaxial tests

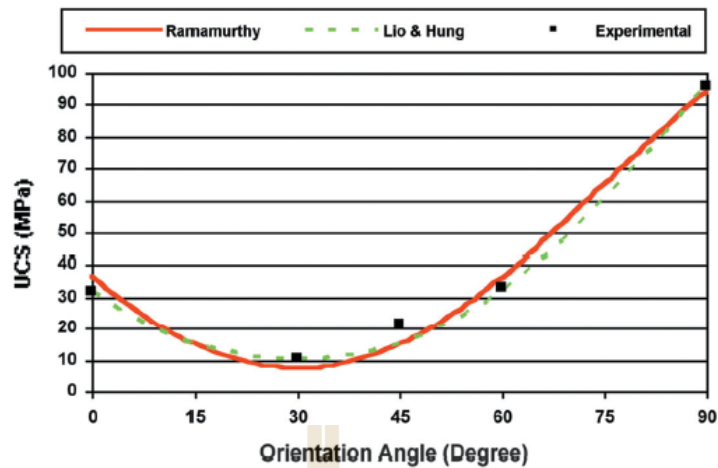


Figure 2.6 Experimental and predicted curves of uniaxial compressive strength of slates (Goshashi et al., 2006).

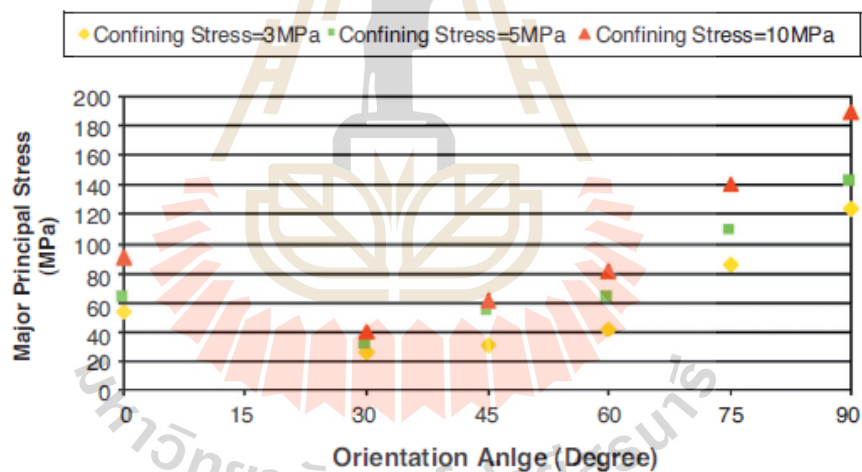


Figure 2.7 Variation of strengths versus orientation angles (Goshashi et al., 2006).

at orientation angles of 0° , 30° , 75° and 90° . In contrast, for the Ramamurthy criterion one only needs to do three uniaxial tests at orientation angles of 0° , 30° and 90° and one triaxial test in 90° at two confining pressures. Hence, it can be concluded that if very precise values are needed, then one should use the Hoek and Brown and McLamore criteria by conducting a large number of tests. If the number of tests is

limited, then the Ramamurthy criterion can be utilized to predict the strength values reasonably.

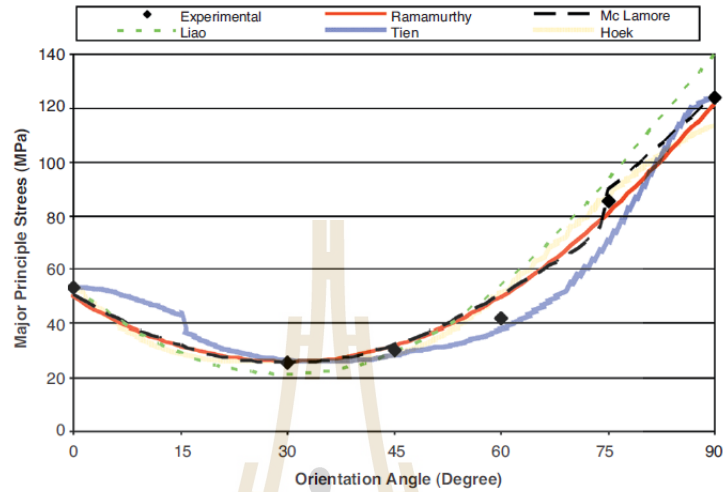


Figure 2.8 Comparison between predicted and experimental strength at $\sigma_3 = 3$ MPa (Goshashi et al., 2006).

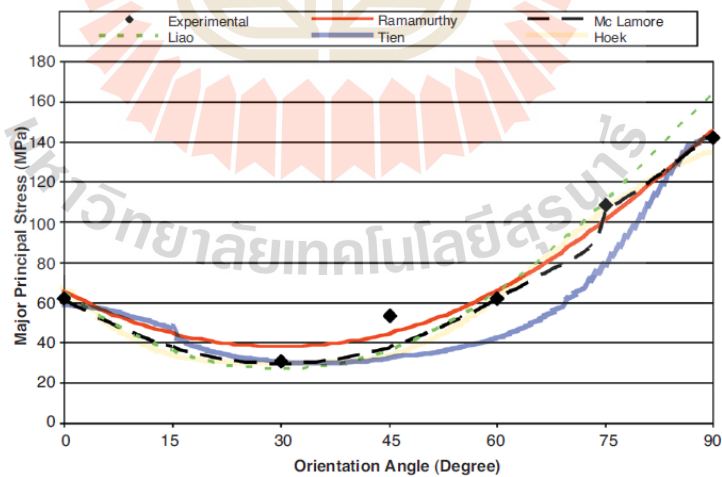


Figure 2.9 Comparison between predicted and experimental strength at $\sigma_3 = 5$ MPa (Goshashi et al., 2006).

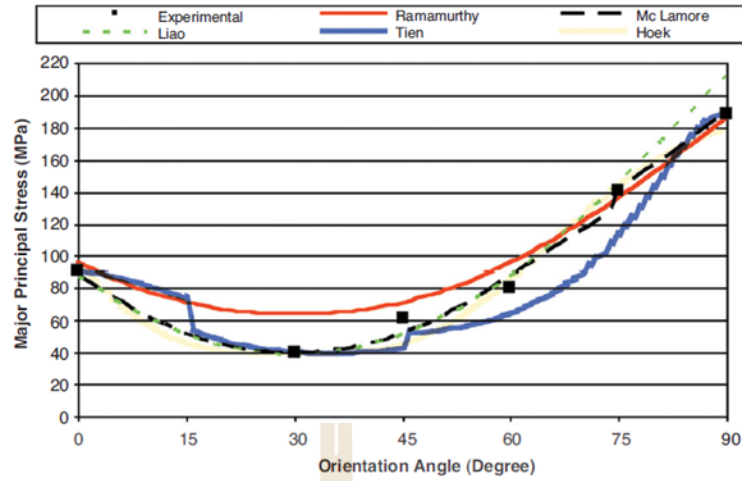


Figure 2.10 Comparison between predicted and experimental strength at $\sigma_3 = 10$ MPa (Goshashi et al., 2006).

2.6 Deformation modulus of rock mass

Yoshinaka and Yamabe (1986) present a constitutive relation for evaluating deformation behavior of regularly jointed rock. Based on the concept of joint stiffness, an equation (2.16) to evaluate the deformation of jointed rock is derived as:

$$\frac{1}{E_t} = \left[\frac{1}{E_c} + \frac{\cos^2 \theta_1}{L_1} \left(\frac{\sin^2 \theta_1}{k_{s1}} + \frac{\cos^2 \theta_1}{k_{n1}} \right) + \frac{\cos^2 \theta_2}{L_2} \left(\frac{\sin^2 \theta_2}{k_{s2}} + \frac{\cos^2 \theta_2}{k_{n2}} \right) \right]^{-1} \quad (2.16)$$

where E_c is elastic modulus of intact rock, θ_1 , θ_2 are the angles of inclination from the applied plane of major principal stress, L_1 and L_2 are joint spacings and k_s and k_n are joint stiffnesses. In order to confirm the constitutive relations derived here, loading tests using jointed rock mass models were carried out and the applicability of the proposed relations was confirmed from the comparison of experimental and numerical results. To obtain the characteristics of joint deformation, joint shear and compression tests were performed in the laboratory using rock specimens with several kinds of roughness

and size. The rock used in the experiments was soft welded-tuff and its physical properties are listed in Table 2.4. Now, as an example, we consider a model of the jointed rock mass shown in Figure 2.11. This model can be expressed by the mechanical model shown in Figure 2.12 with the following conditions. The state of stress is plane stress, $\sigma_3 = 0$. The rock mass has two sets of joints with the same dip direction parallel to the axis of minimum principal stress. Each joint has the joint stiffnesses shown in Figure 2. 12, the angles of inclination at θ_1 and θ_2 from the applied plane of maximum principal stress, and joint spacings L_1 and L_2 , respectively. The intact rock is elastic with properties E_c and ν_c . Loading tests have been performed in two series of rock mass models assembled as 32 element blocks with the smooth or rough surface joints. The loading system arrangement is and the capacities for loading in the two perpendicular horizontal directions are 1 MN and 0.5 MN respectively. The results of the loading tests are clearly shown that the stress-strain curves of jointed rock masses change remarkably according to the confining pressure and joint angle, and the curves have strong non-linearity owing to the characteristics of joint deformation.

Table 2.4 Physical properties of welded-tuff (Ohya-stone) (Yoshinaka and Yamabe, 1986).

Specific Gravity (SG)	Dry density, γ_{Dry} (kN/m ³)	Porosity n (%)	Uniaxial compressive strength, σ_c (MPa)	Tensile strength σ_1 (MPa)
2.40	14.3	41.2	11.2	1.46

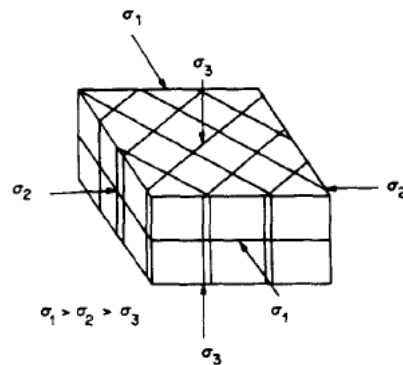


Figure 2.11 Model of a jointed rock mass subjected to three principal stresses (Yoshinaka and Yamabe, 1986).

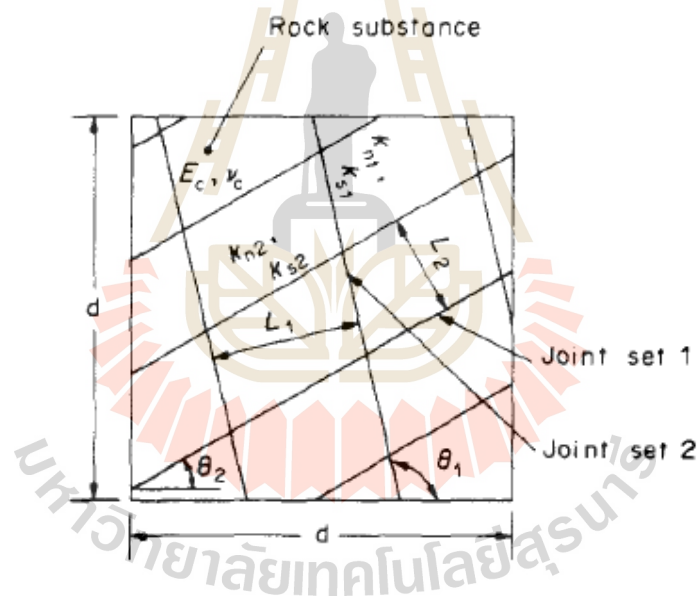


Figure 2.12 Mechanical model for jointed rock mass with two sets of joints (Yoshinaka and Yamabe, 1986).

Yang et al. (1998) describe a series of physical model tests for jointed rock masses with several superimposed joint sets. The objective is to study the effect of joint sets on the deformation of rock mass models. The uniaxial tests are performed on prismatic jointed models with two joint sets and three joint sets with different surface

roughness and configurations. It is observed that the axial deformation behavior of the jointed model is highly nonlinear and joint orientation dependent. The deformation moduli are less than that of the nonjointed rock. The highest value of deformation modulus in the split model only reaches 40% of the nonjointed rocks. The lowest values also occur in the range of the sliding mode. The deformation modulus reduces as the number of joint set increasing.

Ramamurthy (2001) show the modulus ratio is also linked to the failure axial strain of jointed rocks when tested in uniaxial compression. Examination of the available experimental data of the jointed rock specimens tested in uniaxial compression and dense soil specimens also tested in uniaxial compression or under very low confining pressure suggest that when the modulus ratio (E_{ij}/σ_{cj} for jointed rocks and E_t/σ_c for soils, where E_t is the tangent modulus) is less than 50, the material may be considered to behave as a soil; most dense/stiff soils will have this ratio in the range of 50. All the available data on the ratios of moduli, E_{ij}/E_{ti} , obtained from tests in uniaxial compression with J_f for the jointed specimens are presented in Figure 2.13. An average relation may be represented by Equation (2.17):

$$\frac{E_{ij}}{E_{ti}} = \exp(-1.15 \times 10^{-2} J_f) \quad (2.17)$$

Where E_{ij} is the jointed rock deformation modulus, E_{ti} is the intact deformation modulus, and J_f is the joint factor. Figure 13 infer that when a rock mass assumes a value of J_f greater than 200/m, it may be treated to respond as a soil.

Tiwari and Rao (2006) study an experimental on rock mass model with three joint sets under triaxial and true-triaxial stress states to assess the influence of joint geometry and stress ratios on deformational behavior of rock mass. The true-triaxial system (TTS) developed by Tiwari and Rao (2002) was used in the present study. The results from experimental study are used to develop expressions for predicting modulus values of rock mass. As expected, the modulus values are increasing at all dipping with increasing confining stress, σ_3 (see Figure 2.14). The modulus values predicted using the Janbu (1963) and J_f (Ramamurthy, 1993) approaches are presented along with the experimental data for comparison as shown in Table 2.5. The modulus values are

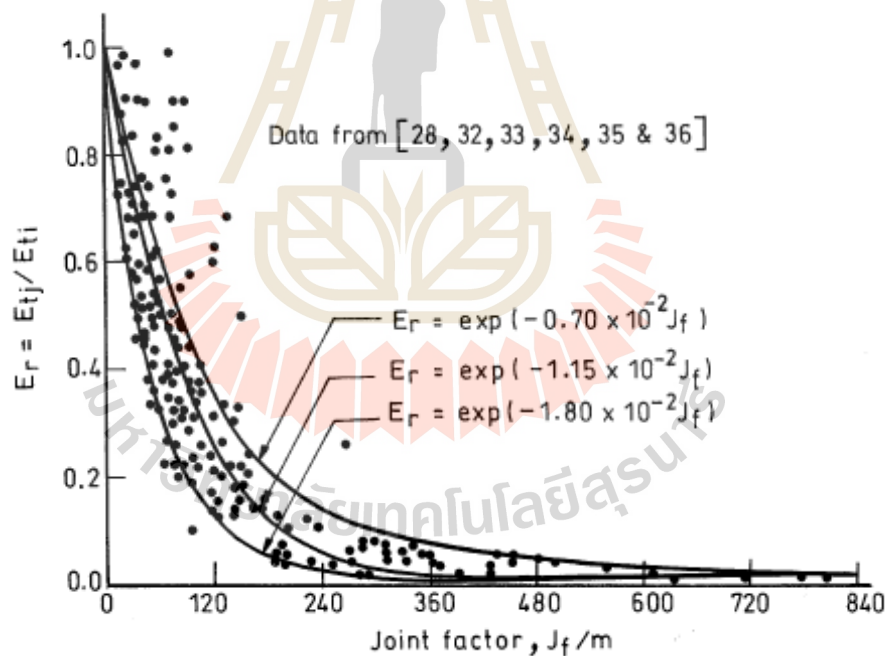


Figure 2.13 Relationship between E_{tj}/E_{ti} and joint factor for jointed specimens (Ramamurthy, 2001).

minimum at $\theta = 60^\circ$ and maximum at $\theta = 90^\circ$ obtained by both approaches and show anisotropy at all confining stresses. It can be seen that joint factor approach may not be

applicable in describing the deformation behavior of rock mass under confining stress state because J_f assumes U shaped anisotropy behavior of jointed rock mass, which is possible in UCS conditions only. In the field a method should be selected based on input parameters available. It can be seen that both approaches require entirely separate type of input parameters for their applicability. Hence, the use of any approach of that method. Further Janbu coefficient approach is recommended over joint factor approach. The modulus value $E_j (=E_{ij} = E_{m50})$ value in triaxial stress state is once known using Janbu's coefficients and joint factor approaches as discussed above.

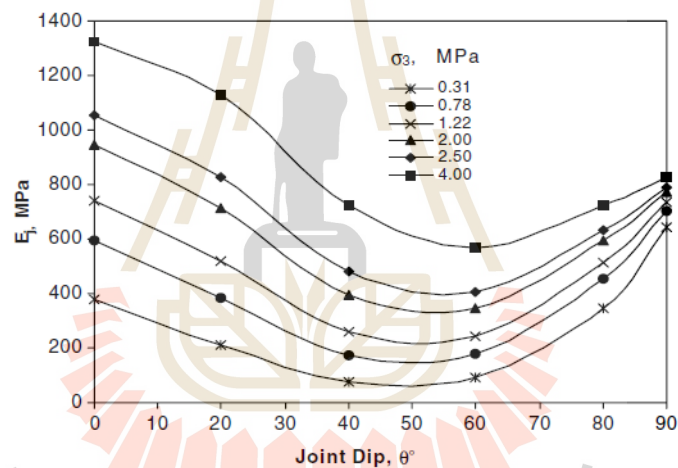


Figure 2.14 Prediction of modulus at different confining pressures using Janbu's coefficients approach (Tiwari and Rao, 2006).

Table 2.5 Comparison of E_j values obtained from different approaches (Tiwari and Rao, 2006).

θ (°)	E_j (MPa)								
	$\sigma_3 = 0.31$ MPa			$\sigma_3 = 0.78$ MPa			$\sigma_3 = 1.22$ MPa		
	Experimental	Janbu approach	J_f approach	Experimental	Janbu approach	J_f approach	Experimental	Janbu approach	J_f approach
0	380.5	378.9	2276.1	711.5	595.5	3325.1	718.0	741.4	4342.2
20	200	209.2	317.8	456.4	384.6	578.2	464.1	516.6	746.1
40	84.5	78.3	49.1	142.2	174.7	61.6	298.8	257.8	65.6
60	32.9	92.5	1.3×10^{-13}	124.3	178.1	1.3×10^{-13}	189.6	244.7	1.3×10^{-13}
80	357.9	345.6	117.4	503.2	451.6	182.5	517.7	514.1	211.7
90	631.5	640.9	1916.9	671.4	702.9	2900.6	723.8	735.0	3822.3

Then, based on the extensive data of true-triaxial test results, the expression of E_j in true-triaxial stress states ($\sigma_2 > \sigma_3$) is suggested as in Equation (2.18):

$$\frac{E_j(\sigma_2 > \sigma_3)}{E_j(\sigma_2 = \sigma_3)} = 1 + T \left(\frac{\sigma_2}{\sigma_3 - 1} \right)^r \quad (2.18)$$

where T , r joint inclination parameters and vary with inclination of joint set-I. Once the E_j value in triaxial stress state is known by any of the approach discussed above, the Equation (2.18) can be conveniently used for prediction of modulus at any joint dip θ of rock mass under true-triaxial stress conditions at any σ_2/σ_3 level.

Maji and Sitharam (2008) use two artificial neural network models for the efficient prediction of the elastic moduli of jointed rocks from the elastic modulus of intact rocks and different joint parameters for various different confining pressure conditions. The important joint parameters which are taken into consideration independently are joint frequency (J_n), joint inclination parameter (n) and joint roughness parameter (r). The results of this analysis are compared with the experimental results of Arora (1987), Roy (1993) and Yaji (1984). First all the 896 experimental data

sets are systematically analyzed to check the correlation among elastic modulus ratio (EMR, ratio of elastic modulus of jointed rock to the intact rock) and joint factor (J_f) which takes care for the joint frequency, joint inclination and joint roughness. Finally, artificial neural network models provide significant advantage for handling problems involving practical discontinuous system. The present work supports the use of neural networks for the successful prediction of elastic properties jointed rocks and opens up the possibility of embedding neural networks into numerical modeling codes for modeling the structures in jointed rocks.

Thaweeboon et al. (2017) study strength and deformability of small-scale rock mass models under large confinements. Triaxial compression tests were performed to determine the strength and deformability of small-scale rock mass models with multiple joint sets and frequencies under confining stresses up to 12 MPa. This rock is classified as fine-grained quartz sandstones with highly uniform texture and density (Boonsener and Sonpiron, 1997). The cubical sandstone specimens ($80 \times 80 \times 80 \text{ mm}^3$) with joint sets simulated by saw-cut surfaces were compressed to failure using a true triaxial load frame. The joint frequencies ranged from 26 to 76 joints per meter. Case studies (Sheorey et al., 1989) and numerical analyses (Halakatevakis and Sofianos, 2010) to determine the effects of joint frequency, joint orientation and joint set number on rock mass strengths. The results indicate that the Hoek–Brown (1980) criterion with two material parameters (m and s) can describe rock mass strengths as well as the three parameter criteria of Sheorey et al. (1989), Yudhbir et al. (1983) and Ramamurthy-Arora (1994). Exhaustive reviews of these criteria have been given elsewhere (Edelbro, 2004; Sheorey, 1997), and hence will not be repeated here. The parameter s notably decreases with increasing joint frequency, while parameter m is less sensitive to joint

frequency. The confining stresses tend to enhance the effects of joint frequencies on rock mass compressive strengths. The deformation moduli in the direction normal to the joints tend to be lower than those parallel to the joints. The joint normal stiffness used here is 381.2 GPa/m which is obtained from Kamonphet et al. (2012). They decrease with increasing joint frequency. Goodman (1970) equation was modified here to allow calculation of the deformation moduli of the rock mass along the three principal directions. The deformation moduli along the major, intermediate and minor principal directions can then be calculated by (Jaeger et al., 2007). The modified equation can sufficiently describe the deformation moduli normal and parallel to the joints for one-joint set and three-joint set specimens under all confining stresses.

Galera et al. (2007) presents the result of comparisons between the modulus of deformation obtained from dilatometer tests and the geomechanical quality of the rock mass using the RMR classification and the basic intact rock properties such as the uniaxial compressive strength and Young's modulus. The first step was to compare the dilatometer with RQD and RMR. Subsequently, it has been decided to use the RMR without considering the lithology, as the differences were found insignificant. Excluding any data with anomalous ratios, the final database consists of 436 cases in which known values of E_m , RMR, S_c and E_i are considered reliable. With this database several correlations were investigated to estimate rock mass deformability improving on the existing criteria of Bieniawski (1978), Serafin-Pereira (1983), Nicholson-Bieniawski (1990) and Hoek et al. (2000). A new relation between RMR and E_m/E_i is recommended.

CHAPTER III

SAMPLE PREPARATION

3.1 Introduction

This chapter describes the preparation of rock samples and their joint characteristics. The tested rocks are from Phu Phan sandstone. Sample preparation is carried out in the laboratory at the Suranaree University of Technology.

3.2 Sample preparation

The rock samples are obtained from Phra Wihan sandstone. This rock is classified as fine-grained quartz sandstone with highly uniform texture and density (Boonsener and Sonpiron, 1997). It is prepared to obtain cubic specimens with nominal dimensions of $55 \times 55 \times 55 \text{ mm}^3$. Appendix A (Tables A.1 through A.8) gives dimensions and density of the rock samples. Artificial joints are induced into the intact specimens by line loading (Figure 3.1) to develop a number of rough joints with different orientations. The specimens are prepared with three different characteristics for triaxial compression tests. Each case is shown in Table 3.1 and is described below.

Case I: One-joint set specimens are prepared to study the effects of joint frequency and major principal stress direction on the strength of rock specimens. The specimens are prepared with joints parallel to the major principal stress direction ($\beta=0^\circ$) (β is the angle between the normal to the jointed plane and vertical axis through the specimen). Joints are prepared by a line load applied to obtain a tension-induced

fracture. There are two joint frequencies (equivalent to 36 and 54 joints per meter). The joint roughness coefficient is averaged as 6.

Case II: One-joint set specimens are prepared to study the effects of joint frequency when the joints are normal to the major principal axis. The numbers of joints are two joints frequencies (equivalent to 36 and 54 joints per meter). The specimens are simulated with joints normal to the major principal stress direction ($\beta=90^\circ$).

Case III: The specimens have two joint set. Joints are parallel to the major principal stress direction. The normal to the fracture plane makes angles of 0° with the major axis of the specimen. This case is simulated to study the effects of joint set number and joint frequency.

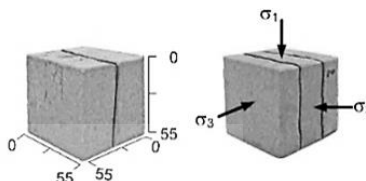
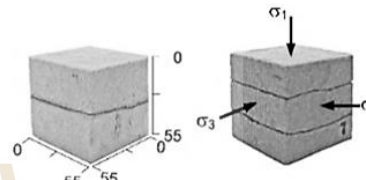
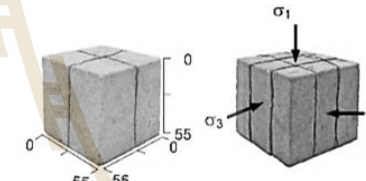
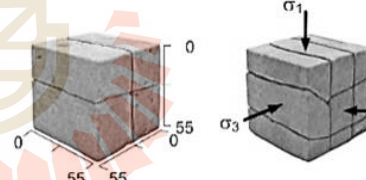
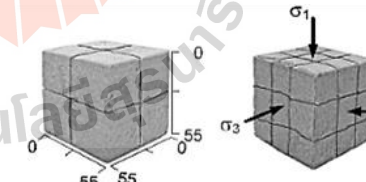
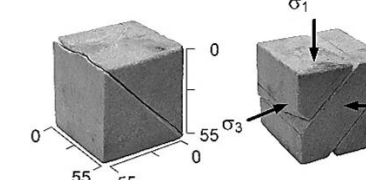
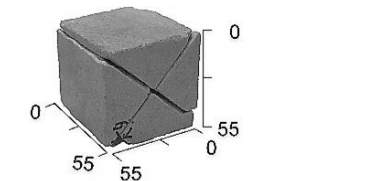
Case IV: Two joint set specimen with two joint frequencies are used in this case. Joints are parallel and normal to the major principal axis.

Case V: Specimens with three-mutually perpendicular joint sets are prepared to study the effects of joint set number and joint frequency. There are 1 and 2 joints frequencies for each set.

Case VI: One joint set specimens are prepared with joint making angles of 45° to the major principal stress. Joint plane simulated by a line load applied to obtain a tension-induced fracture diagonally across the sandstone block to study the effect of joint roughness. There are 1 and 2 joints frequencies for each set.

Case VII: Two joint set specimen with one joint frequency are prepared with joint making angles of 45° to the major principal stress. The numbers of joints are one joints frequency (equivalent to 36 per meter).

Table 3.1 Specimens prepared for triaxial compression test with confining pressures of 0, 1, 3, 5, 7 and 12 MPa.

Cases	Number of joint sets	Orientations of joint with respect to σ_1 axis	Specimens
I	1	Parallel to σ_1	
II	1	Normal to σ_1	
III	2	Two Parallel to σ_1	
IV	2	Parallel and normal to σ_1	
V	3	Two parallel and one normal to σ_1	
VI	1	45° with σ_1	
VII	2	45° and 135° with σ_1	

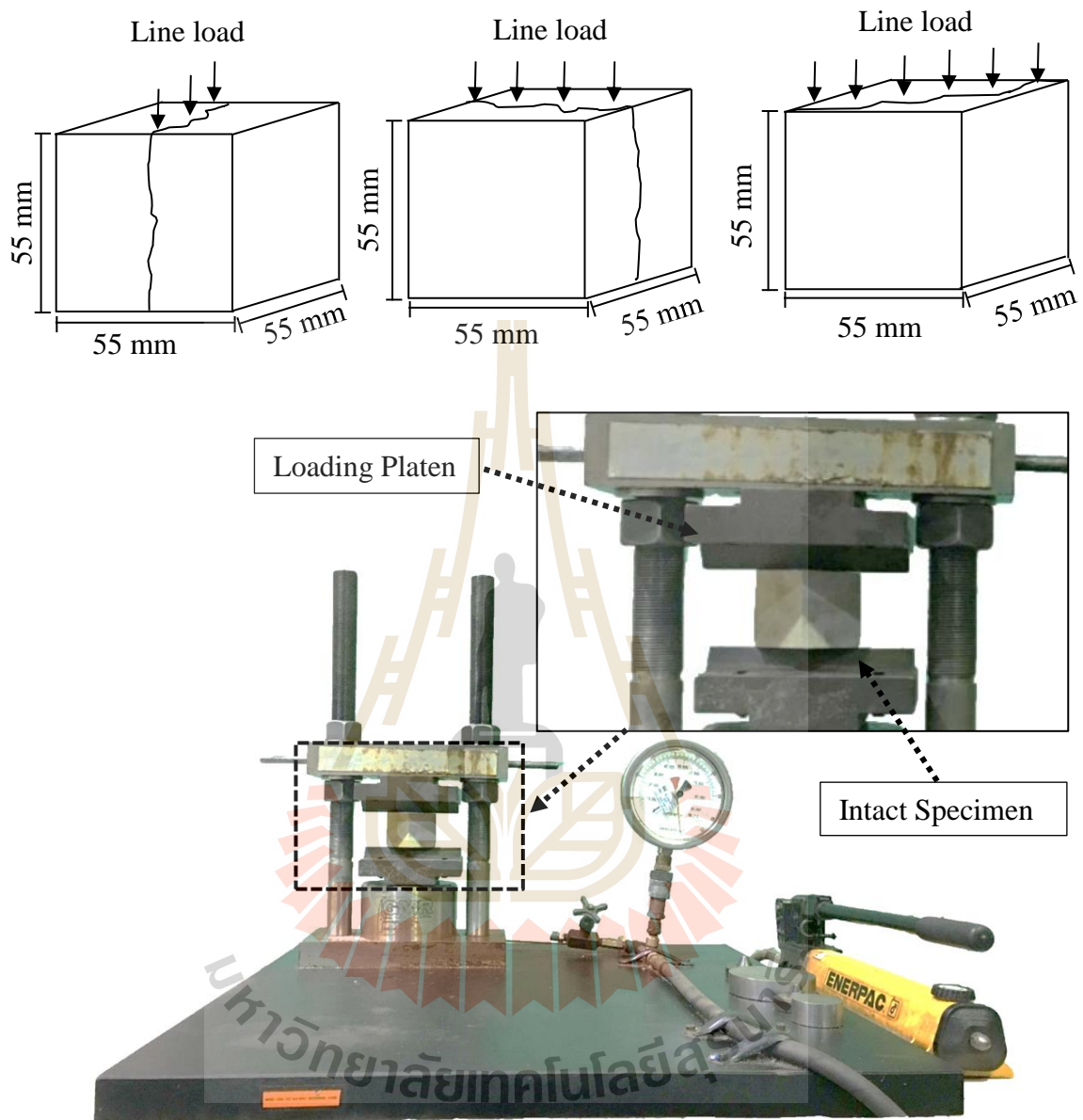


Figure 3.1 Line load applied to obtain tension-induced fracture in specimen all tests are conducted under ambient temperature and dry condition.

CHAPTER IV

TEST METHOD

4.1 Introduction

This chapter describes test apparatus and method of the triaxial compression test on rock samples containing different joint configurations.

4.2 Test apparatus

A polyaxial load frame (Walsri et al., 2009) is used to apply triaxial compression test to the specimens because the cantilever beams with pre-calibrated dead weight can apply a truly constant lateral stress (confining pressure) to the specimen. The lateral stresses are applied by two pairs of 152 cm long cantilever beams set in mutually perpendicular directions. The outer end of each beam is pulled down by a dead weight placed on a lower steel bar linking the two opposite beams underneath. The beam inner end is hinged by a pin mounted between vertical bars on each side of the frame. During testing all beams are arranged nearly horizontally, and hence a lateral compressive load results on the specimen placed at the center of the frame. Using different distances from the pin to the outer weighting point and to the inner loading point, a load magnification of 12 to 1 is obtained. This loading ratio is also used to determine the lateral deformation of the specimen by monitoring the vertical movement of the two steel bars below. Figure 4.1 shows the polyaxial load frame used in thin study. The lateral stresses are parallel and normal to the strike of

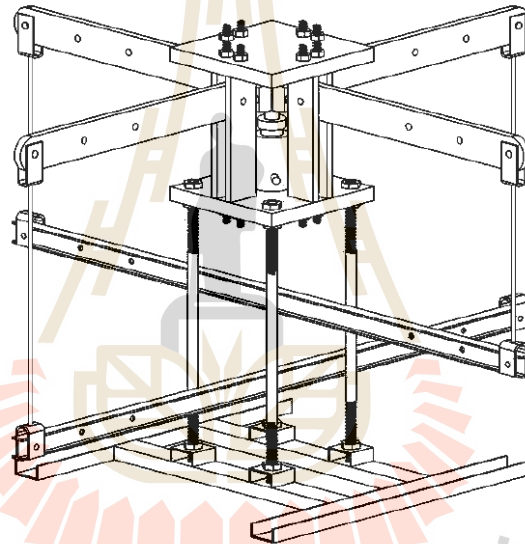
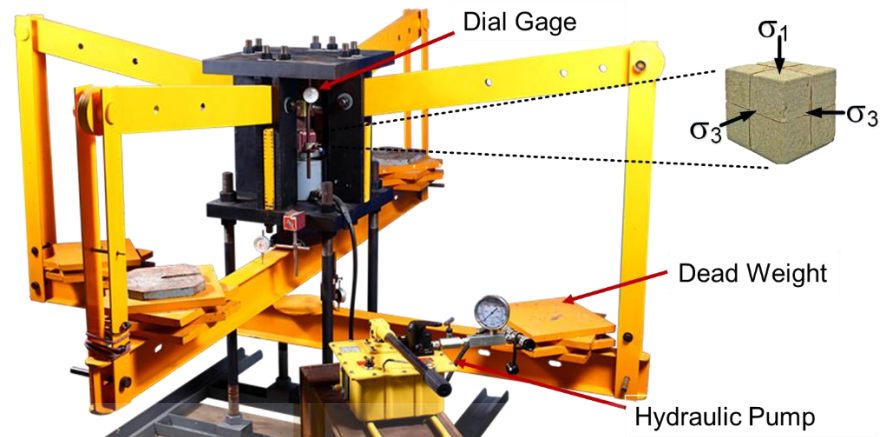


Figure 4.1 Polyaxial load frame developed for compressive and tensile strength testing under true triaxial stress (Walsri et al., 2009).

the fracture plane. Figure. 4.2 shows the directions of the applied stresses with respect to the fracture orientation. Dead weights are placed on the two lower bars to obtain the pre-defined magnitude of the lateral stresses on the specimen. Simultaneously the axial (vertical) stress is increased to the same value with lateral stresses. The specimen is first loaded under hydrostatic condition.

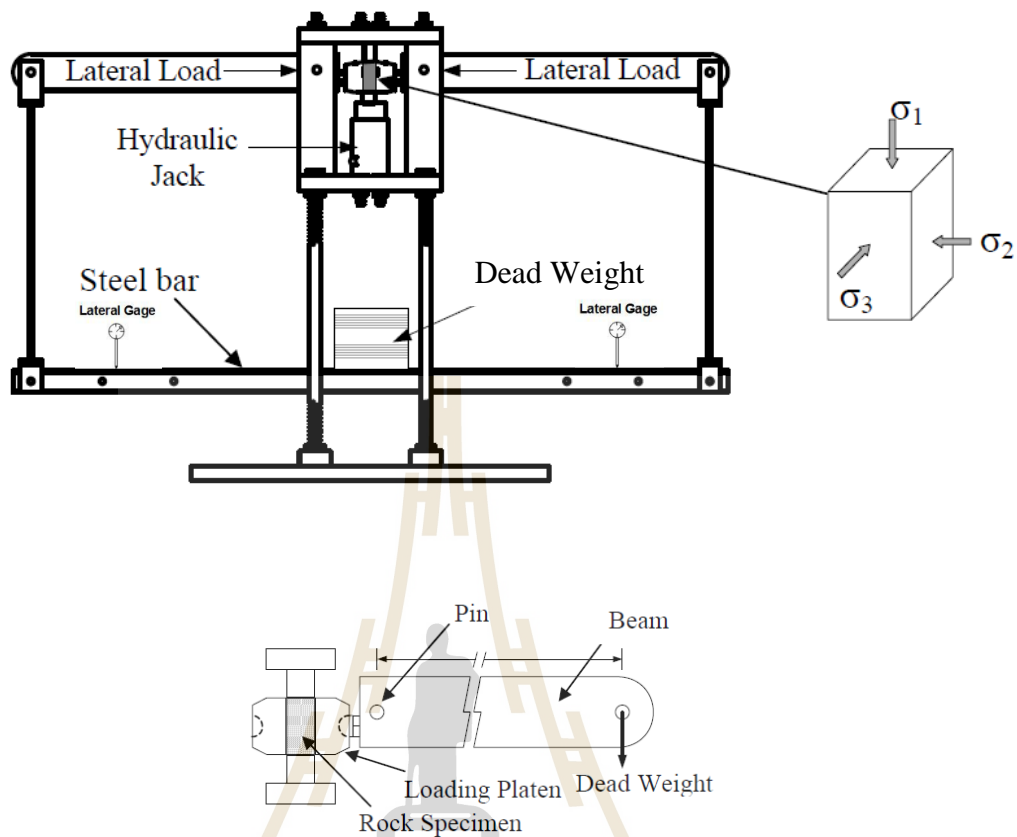


Figure 4.2 Cantilever beam weighed at outer end applies lateral stress to the rock specimen (Walsri et al., 2009).

4.3 Test method

A polyaxial load frame is used to apply axial stress (σ_1) and constant lateral stresses (σ_3) to the intact and jointed rock specimens. Neoprene sheets are placed in all interfaces between the loading platens and specimen surfaces to minimize the friction. Figure. 4.3. The axial stress is applied along the axial direction of the specimen. The constant lateral confining pressures ($\sigma_2=\sigma_3$) on the specimens are from 0, 3, 5, 7 and 12 MPa. After installing the jointed rock specimen into the load frame then four lateral stresses from hydraulic pumps are applied loads to obtain the pre-defined magnitude of

the uniform lateral stress (σ_3) on the specimen. Simultaneously the axial stress is increased to the pre-defined σ_3 value. The test is started by that the axial stress (major principal stress) is increased at a constant rate ($\partial\sigma_1/\partial t$) of 0.1 MPa/s using the hydraulic pump. The specimen deformations are monitored using dial gages in the three loading directions and are used to calculate the principal strains. The readings are recorded every 8.4 kN (equivalent to the 100 psi on the pump pressure gauges) of load increment until the applied axial stress is dropped, which indicates the failure of the specimen. Photograph is taken of the post-test specimens and the modes of failure are identified. All tests are conducted under ambient temperature.

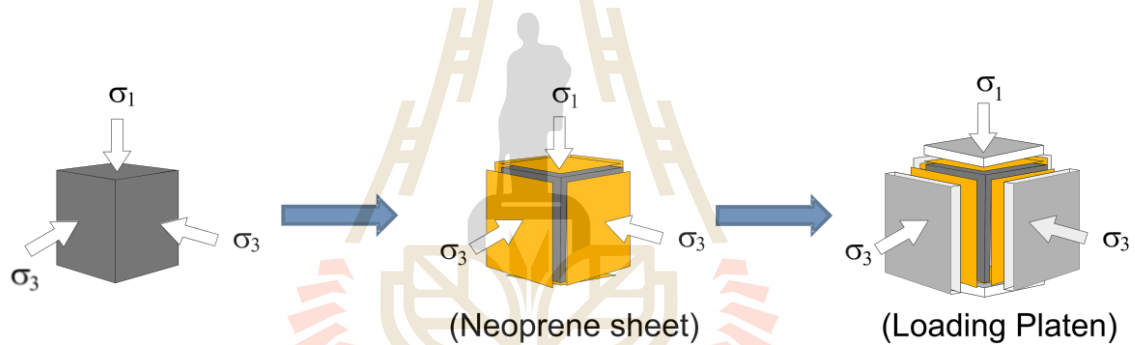


Figure 4.3 Sample preparation before installed into the load frame. (Thaweeboon et al., 2017).

CHAPTER V

TEST RESULTS

5.1 Introduction

This chapter presents the test results of compression test for each fracture configuration. Stress-strain curves, post-test failure modes and specimen strengths are described.

5.2 Stress-strain curves

Figures 5.1 shows stress-strain curves for different numbers of joint per meter and confining pressures for one, two and three joint sets conditions. The stress-strain curves tend to show nonlinear behavior, particularly under high confining pressures and high joint frequencies. Under the same joint frequency, the stress and strain at failure increase with confining pressure. The effect of the joint frequency on the rock models is reflected as the reduction of stresses and increment of strains at failure. Results for the compressive strength, elastic modulus and Poisson's ratio are calculated from these.

5.3 Post-test observations

Table 5.1 to 5.8 summarized the major (σ_1) and minor principal stresses (σ_3) obtains for intact specimens and jointed specimens with different joint sets and frequency. Table 5.9 shows post-test specimens. The specimens fail under different modes, depending upon joint configurations, stress ratios, and stress orientations. The observed failure modes can be divided into 3 groups

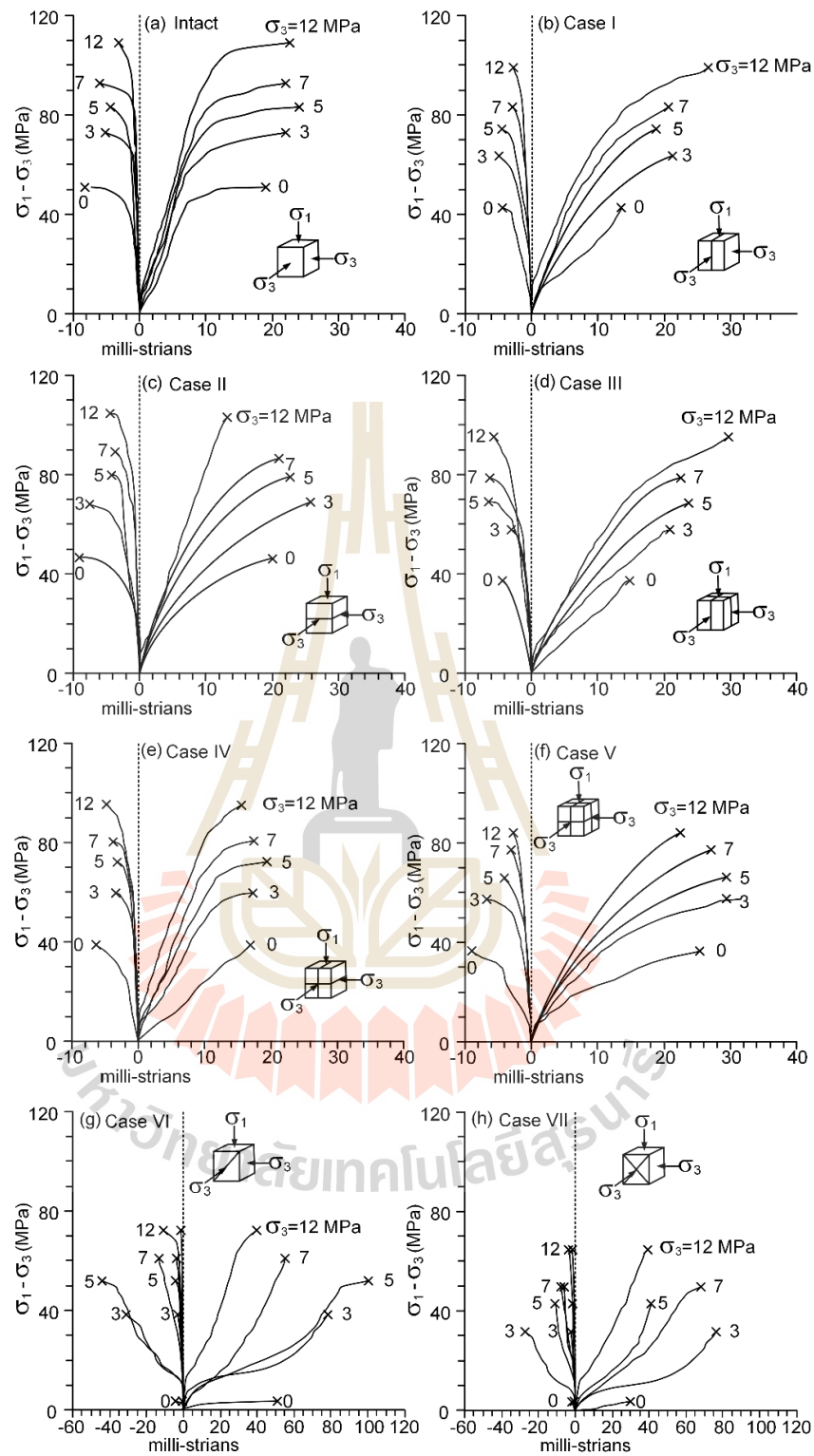


Figure 5.1 Axial and lateral strains measured from various confining pressures for specimens with three mutually perpendicular joint sets, and inclined joint sets.

Table 5.1 Strength results for intact rock specimens.

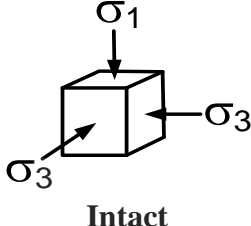
Joint frequency, J_f (joints/m)	σ_3 (MPa)	σ_1 (MPa)
 <p>Intact</p>	0	50.4
	3	72.4
	5	82.6
	7	92.3
	12	108.7

Table 5.2 Strength results for case I

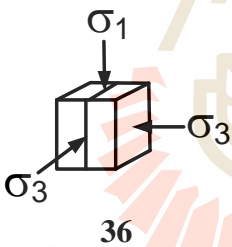
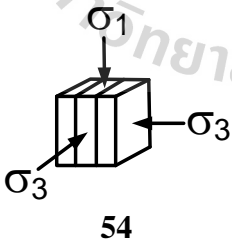
Joint frequency, J_f (joints/m)	σ_3 (MPa)	σ_1 (MPa)
 <p>36</p>	0	39.5
	3	61.4
	5	73.1
	7	82.2
	12	99.1
 <p>54</p>	0	34.2
	3	56.6
	5	68.6
	7	76.9
	12	92.6

Table 5.3 Strength results for case II.

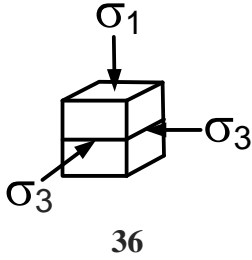
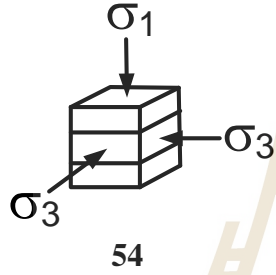
Joint frequency, J_f (joints/m)	σ_3 (MPa)	σ_1 (MPa)
 <p>36</p>	0	41.4
	3	63.9
	5	76.8
	7	86.4
	12	104.7
	 <p>54</p>	0
3		60.3
5		71.7
7		82.6
12		98.7

Table 5.4 Strength results for case III.

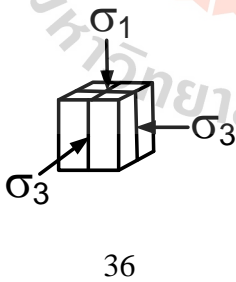
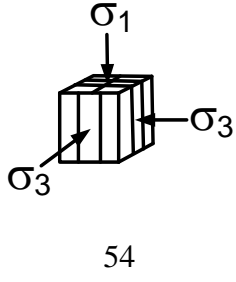
Joint frequency, J_f (joints/m)	σ_3 (MPa)	σ_1 (MPa)
 <p>36</p>	0	36.9
	3	57.1
	5	68.2
	7	78.2
	12	94.8
	 <p>54</p>	0
3		53.2
5		63.4
7		72.7
12		88.3

Table 5.5 Strength results for case IV.

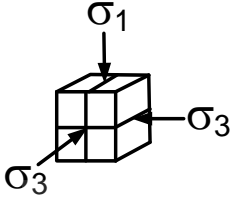
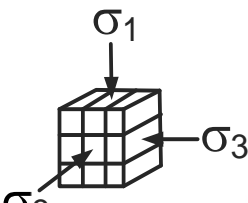
Joint frequency, J_f (joints/m)	σ_3 (MPa)	σ_1 (MPa)
 36	0	38.0
	3	59.6
	5	71.9
	7	80.2
	12	97.0
	 54	0
3		55.7
5		66.9
7		75.5
12		90.8

Table 5.6 Strength results for case V.

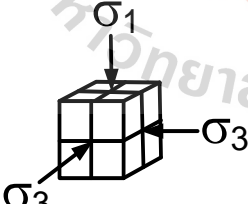
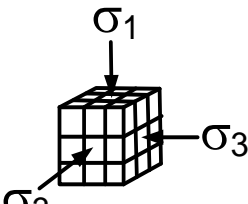
Joint frequency, J_f (joints/m)	σ_3 (MPa)	σ_1 (MPa)
 36	0	36.2
	3	57.2
	5	69.1
	7	76.9
	12	94.0
	 54	0
3		49.0
5		58.2
7		65.4
12		79.2

Table 5.7 Strength results for case VI.

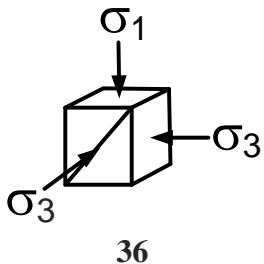
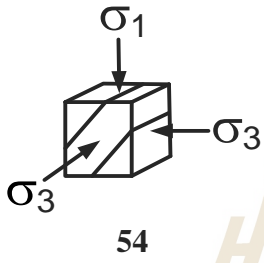
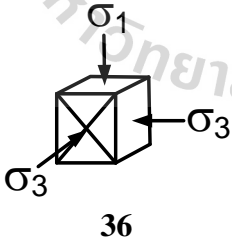
Joint frequency, J_f (joints/m)	σ_3 (MPa)	σ_1 (MPa)
 36	0	4.5
	3	38.5
	5	52.1
	7	61.1
	12	72.5
	 54	0
3		27.5
5		36.0
7		42.0
12		56.9

Table 5.8 Strength results case VII.

Joint frequency, J_f (joints/m)	σ_3 (MPa)	σ_1 (MPa)
 36	0	3.4
	3	31.7
	5	43.0
	7	49.0
	12	64.0

(1) Extensile splitting mode: This mode of failure involves tensile fractures which are parallel and subparallel to the major principal stress direction. The main mechanism of failure is the extensile failure through the intact pieces and pre-existing joints of the specimen.

(2) Sliding mode: This mode of failure is characterized by movement of the intact pieces of the jointed specimens parallel to the joint planes.

(3) Crushing mode: This mode of failure shows combination of large number of minute cracks, tensile fractures, crushed pieces and rock powder. The failure modes in each case are described below.

Intact: The failure of extensile splitting mode with large number of minute cracks. When increasing of confining pressures, the failures tend to show crushing mode.

Cases I and II: Specimens with one joint set and two joints frequencies ranging from 36 and 54 joints per meter are tested under various confining pressures. The specimens show the failure under extensile splitting mode. The specimens under high confining pressures show large number of minute cracks.

Cases III and IV: The two joint sets specimens are tested with two joint frequencies. Under confining pressures and increasing axial stress the specimens show extensile splitting mode.

Case V: The three joint sets specimens show the failure under extensile splitting mode with large number of minute cracks. When increasing the joint frequency, the failures tend to show crushing mode.

Case VI: The specimens with joint making angle of 45° with two joints frequencies ranging of 36 and 54 joints per meter show sliding mode through pre-defined joints under low confining pressures and combinations of extensile splitting

fracture and sliding under high confining pressures. When joint frequency is increased, the failures tend to show crushing mode.

Case VII: The two joint sets specimens with joints making angle of 45° and one joint frequency show sliding mode under low confining pressures and combinations of extensile splitting fracture and sliding under high confining pressures.

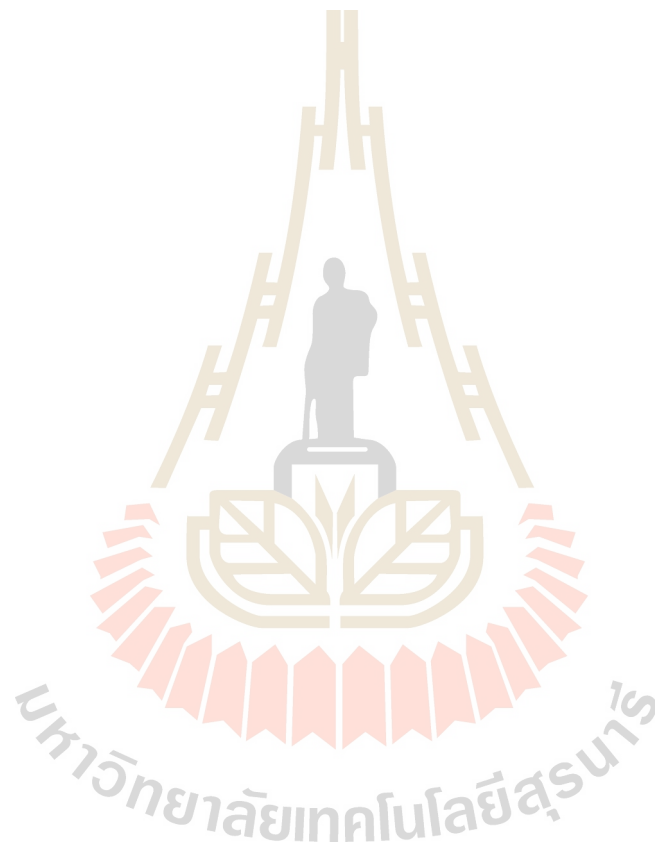


Table 5.9 Some post-test specimens.

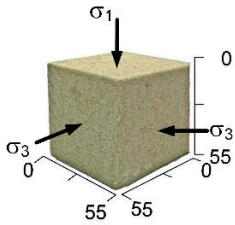
Case	pre-test specimens		post-test specimens	
Intact				
Case I	 36 joints/meter	 54 joints/meter	 36 joints/meter	 54 joints/meter
Case II	 36 joints/meter	 54 joints/meter	 36 joints/meter	 54 joints/meter
Case III	 36 joints/meter	 54 joints/meter	 36 joints/meter	 54 joints/meter
Case IV	 36 joints/meter	 54 joints/meter	 36 joints/meter	 54 joints/meter
Case V	 36 joints/meter	 54 joints/meter	 36 joints/meter	 54 joints/meter

Table 5.9 Some post-test specimens (continuou).

Case	Pre-test specimens		Post-test specimens	
Case VI	 36 joints/meter	 54 joints/meter	 36 joints/meter	 54 joints/meter
Case VII	 36 joints/meter		 36 joints/meter	

5.4 Strength results

The effect of joint frequency on the rock specimens can be observed by the reduction of failure stresses and the increase of failure strains. The effects of the confining stresses on the strength of the specimens can be observed from the σ_1 - σ_3 diagrams for all cases, as shown in Figure 5.2. The relations between σ_1 and σ_3 at failure tend to be non-linear for the intact sandstone and for the specimens with all joint frequencies. The specimens with higher joint frequencies (J_f) show lower strengths than those with lower joint frequencies. The effect of joint frequency on the strength tends to be greater for the specimens with joint parallel to σ_1 direction (Cases I and III), as compared to those with joints normal to σ_1 direction (Cases II and IV). For example, for specimens with the strengths of the specimens with 54 joints/m decreases by about 14% from the intact strength. Under this joint frequency, the strengths for specimens

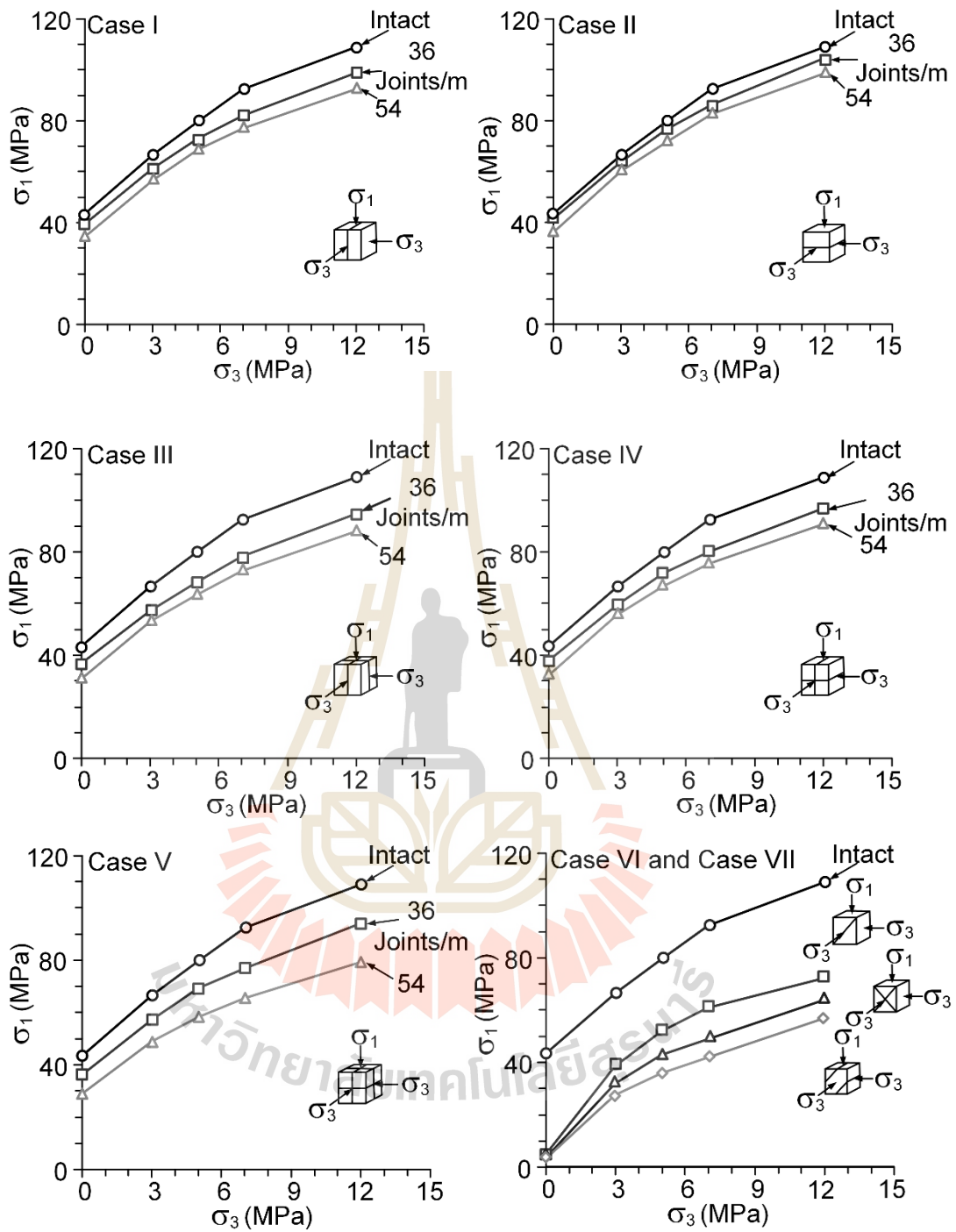


Figure 5.2 Major principal stresses at failure as a function of confining pressure for various joint orientation.

with joint normal to σ_1 (Case II) decrease by about 18%. The effects of joint frequency are greatest for the three-joint set specimens (Case V). The strengths of specimens containing three joint sets with 54 joints per meter drop by nearly 26% from the intact strength. The single joint set specimens with joints normal to σ_1 (Cases II and IV) show higher strength than those with joints parallel to σ_1 (Cases I and III). Joints making angle of 45° to σ_1 (Cases VI and VII) show lowest strength. The strength discrepancies are primarily due to the fact that σ_1 direction is parallel to small plates of the sandstone forming the rock mass models. The height-to-width ratios of these plates are relatively high (varying from 2 to 3, depending on the joint frequencies). Under axial loading, each plate can laterally dilate (toward the thinner sides), and hence the extensile fractures can be induced in vertical or nearly vertical directions. The pre-existing joints also help the induce extensile fractures to propagate through the specimen models. The induced fractures can propagate more easily for the specimens with higher joint frequency, as compared to those with lower joint frequencies. This explains why the strengths of specimens with joint parallel to σ_1 decrease with increasing joint frequency. Under large confinement, the lateral dilation of the sandstone pates toward the pre-existing joints becomes more difficult, and hence some shear fractures are induced across the specimen models. For the specimens with σ_1 normal to joint planes, the specimens cannot dilate easily under loading, and therefore the compressive shear fractures are predominant. As a result the strengths of specimens with joint normal to σ_1 tend to be greater than those with joint parallel to σ_1 . These shear fractures for specimens with joint normal to σ_1 can propagate easier for the specimens with higher

joint frequencies and under lower confining stresses, as compared to those with lower joint frequencies and higher confining stresses. Under the same joint frequency the strengths of Case III specimens are lower than those of Cases I and II because each sandstone block has an additional free face to dilate (i.e., there are two mutually perpendicular joint sets parallel to σ_1 direction).

The compressive strength results can be presented in terms of the octahedral shear stress at failure ($\tau_{\text{oct},f}$) as a function of mean stress (σ_m), as shown in Tables 5.10 through 5.17 and in Figure 5.3, where (Jaeger et al., 2007):

$$\tau_{\text{oct},f} = \left\{ (1/3) [(\sigma_1 - \sigma_2)^2 + (\sigma_2 - \sigma_3)^2 + (\sigma_3 - \sigma_1)^2] \right\} \quad (5.1)$$

$$\sigma_m = (1/3) (\sigma_1 + \sigma_2 + \sigma_3) \quad (5.2)$$

where $\tau_{\text{oct},f}$ and σ_m are octahedral shear stresses and mean stress at failure, and σ_1 , σ_2 and σ_3 are the compressive strength, intermediate principal stress and minor principal stress.

The relations between $\tau_{\text{oct},f}$ and σ_m at failure tend to be non-linear for the intact sandstone and for the specimens with all joint frequencies. The specimens with higher joint frequencies (J_f) show lower octahedral shear stress at failure than those with lower joint frequencies. The effect of joint frequency on the octahedral shear stress tends to be greater for the specimens with joint parallel to σ_1 (Cases I and III), as compared to those with joints normal to σ_1 (Cases II and IV). The single joint set specimens with joints normal to σ_1 (Cases II and IV) show higher octahedral shear stress than those

with joints parallel to σ_1 (Cases I and III) and joints making angle of 45° to σ_1 (Cases VI and VII) show lowest octahedral shear stress at failure.



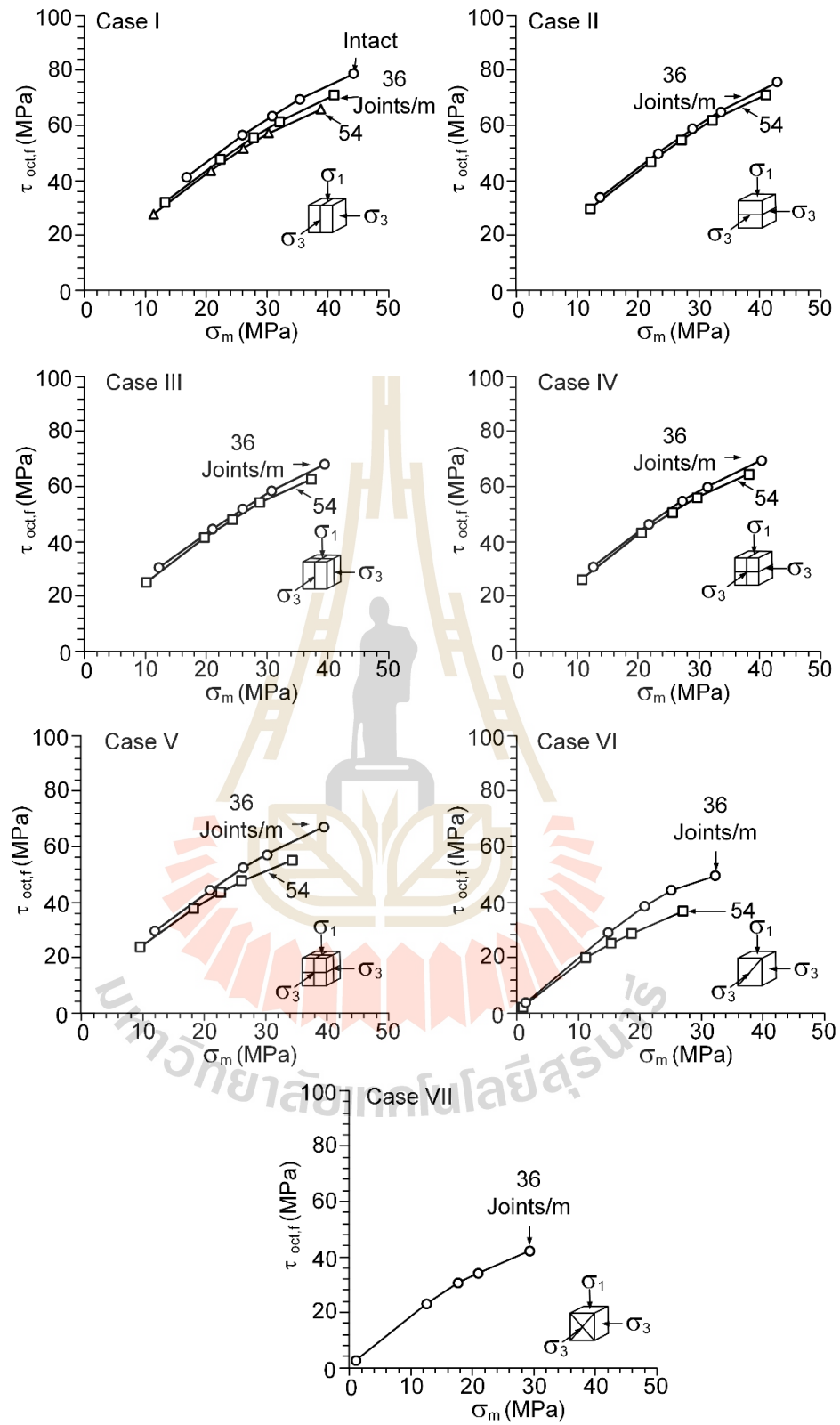


Figure 5.3 Octahedral shear stresses at failure ($\tau_{oct,f}$) as a function of mean stress (σ_m).

Table 5.10 Octahedral shear stresses at failure (case I).

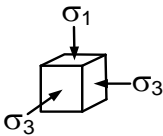
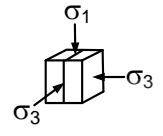
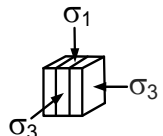
specimens	σ_3 (MPa)	σ_m (MPa)	$\tau_{oct,f}$ (MPa)
 intact	0	16.8	41.2
	3	26.1	56.7
	5	30.9	63.4
	7	35.4	69.6
	12	44.2	79.0
 36 joints/meter	0	13.2	32.3
	3	22.5	47.7
	5	27.7	55.6
	7	32.1	61.4
	12	41.0	71.1
 54 joints/meter	0	11.4	27.9
	3	20.9	43.8
	5	26.2	51.9
	7	30.3	57.1
	12	38.9	65.8

Table 5.11 Octahedral shear stresses at failure (case II).

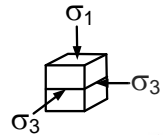
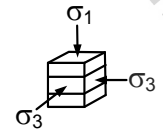
specimens	σ_3 (MPa)	σ_m (MPa)	$\tau_{oct,f}$ (MPa)
 36 joints/meter	0	13.8	33.8
	3	23.3	49.7
	5	28.9	58.6
	7	33.5	64.8
	12	42.9	75.7
 54 joints/meter	0	12.1	29.6
	3	22.1	46.8
	5	27.2	54.5
	7	32.2	61.7
	12	40.9	70.8

Table 5.12 Octahedral shear stresses at failure (case III).

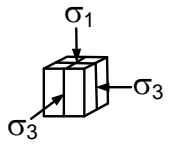
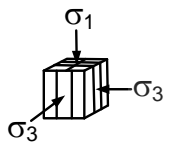
specimens	σ_3 (MPa)	σ_m (MPa)	$\tau_{oct,f}$ (MPa)
 36 joints/meter	0	12.3	30.1
	3	21.0	44.2
	5	26.1	51.6
	7	30.7	58.1
	12	39.6	67.6
 54 joints/meter	0	10.2	25.1
	3	19.7	41.0
	5	24.5	47.7
	7	28.9	53.6
	12	37.4	62.3

Table 5.13 Octahedral shear stresses at failure (case VI).

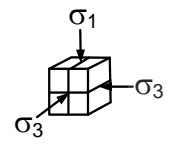
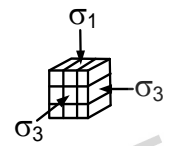
specimens	σ_3 (MPa)	σ_m (MPa)	$\tau_{oct,f}$ (MPa)
 36 joints/meter	0	12.7	31.0
	3	21.9	46.2
	5	27.3	54.6
	7	31.4	59.8
	12	40.3	69.4
 54 joints/meter	0	10.7	26.3
	3	20.6	43.0
	5	25.6	50.5
	7	29.8	55.9
	12	38.3	64.3

Table 5.14 Octahedral shear stresses at failure (case V).

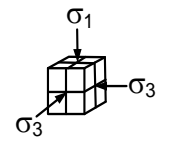
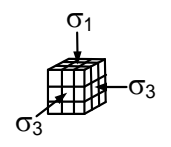
specimens	σ_3 (MPa)	σ_m (MPa)	$\tau_{oct,f}$ (MPa)
 36 joints/meter	0	12.1	29.6
	3	21.1	44.3
	5	26.4	52.3
	7	30.3	57.1
	12	39.3	67.0
 54 joints/meter	0	9.6	23.6
	3	18.3	37.6
	5	22.7	43.4
	7	26.5	47.7
	12	34.4	54.9

Table 5.15 Octahedral shear stresses at failure (case VI).

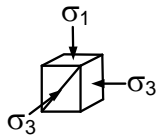
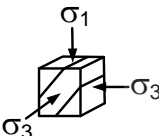
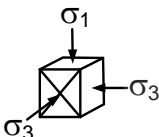
specimens	σ_3 (MPa)	σ_m (MPa)	$\tau_{oct,f}$ (MPa)
 36 joints/meter	0	1.5	3.7
	3	14.8	29.0
	5	20.7	38.5
	7	25.0	44.2
	12	32.2	49.4
 54 joints/meter	0	1.0	2.4
	3	11.2	20.0
	5	15.3	25.3
	7	18.7	28.6
	12	27.0	36.7

Table 5.16 Octahedral shear stresses at failure (case VII).

specimens	σ_3 (MPa)	σ_m (MPa)	$\tau_{oct,f}$ (MPa)
 36 joints/meter	0	1.1	2.8
	3	12.6	23.4
	5	17.7	31.0
	7	21.0	34.3
	12	29.3	42.5

5.5 Deformation moduli

The deformation parameters are determined from the tangent of the stress-strain curves at about 50% of the failure stress. An attempt is made to calculate the deformation moduli along the three loading directions. It is initially assumed that the Poisson's ratio (ν) of the specimens is the same for all principal planes. The deformation moduli along the major, intermediate and minor principal directions can then be calculated by (Jaeger et al., 2007):

Case: I

$$\varepsilon_{1,p} = \sigma_1/E_{1,p} - \nu(\sigma_3/E_{3,p} + \sigma_3/E_{3,n}) \quad (1)$$

$$\varepsilon_{3,p} = \sigma_3/E_{3,p} - \nu(\sigma_1/E_{1,p} + \sigma_3/E_{3,n}) \quad (2)$$

$$\varepsilon_{3,n} = \sigma_3/E_{3,n} - \nu(\sigma_1/E_{1,p} + \sigma_3/E_{3,p}) \quad (3)$$

Case: II

$$\varepsilon_{1,n} = \sigma_1/E_{1,n} - \nu(\sigma_3/E_{3,p} + \sigma_3/E_{3,p}) \quad (4)$$

$$\varepsilon_{3,p} = \sigma_3/E_{3,p} - \nu(\sigma_1/E_{1,p} + \sigma_3/E_{3,n}) \quad (5)$$

$$\varepsilon_{3,p} = \sigma_3/E_{3,p} - \nu(\sigma_1/E_{1,n} + \sigma_3/E_{3,p}) \quad (6)$$

Case: III, IV

$$\varepsilon_{1,p} = \sigma_1/E_{1,p} - \nu(\sigma_3/E_{3,p} + \sigma_3/E_{3,p}) \quad (4)$$

$$\varepsilon_{3,p} = \sigma_3/E_{3,p} - \nu(\sigma_1/E_{1,p} + \sigma_3/E_{3,n}) \quad (5)$$

$$\varepsilon_{3,p} = \sigma_3/E_{3,p} - \nu(\sigma_1/E_{1,n} + \sigma_3/E_{3,p}) \quad (6)$$

where $\varepsilon_{1,p}$ and $\varepsilon_{1,n}$ are the major principal strains parallel and normal to the joints, $\varepsilon_{3,p}$ and $\varepsilon_{3,n}$ are the minor principal strains parallel and normal to the joints, and $E_{1,p}$, $E_{1,n}$, $E_{1,n}$ and $E_{3,n}$, are the deformation moduli parallel and normal to the joints in the directions of major and minor principal stresses.

Case: V, VI, VII

$$\varepsilon_1 = \sigma_1/E_1 - \nu(\sigma_3/E_3 + \sigma_3/E_3) \quad (7)$$

$$\varepsilon_3 = \sigma_3/E_3 - \nu(\sigma_1/E_1 + \sigma_3/E_3) \quad (8)$$

$$\varepsilon_3 = \sigma_3/E_3 - \nu(\sigma_1/E_1 + \sigma_3/E_3) \quad (9)$$

where ε_1 , ε_2 and ε_3 are the major and minor principal strains, and E_1 , E_2 and E_3 are the deformation moduli along the major, and minor principal directions. Tables 5.17 through 5.23 show the calculation results. The calculated Poisson's ratios tend to be independent of the joint frequency and loading direction. The results show that for one joint set specimens the deformation moduli that are parallel to the joint planes show highest values compared to those that are normal to the joints. This is true for all joint frequencies as shown in Figure 5.4. For three joint set specimens, the deformation moduli are similar for all principal directions. The deformation modulus decreases with increasing joint frequency, and tends to increase with confining pressure (Figure 5.5). The Poisson's ratio of the specimens with different joint frequencies ranges from 0.15 to 0.29. The effect of the confining pressure on the Poisson's ratio cannot be clearly observed from the test results. This may be due to the intrinsic variability among the test models.

Table 5.17 Deformation moduli for intact rock specimens.

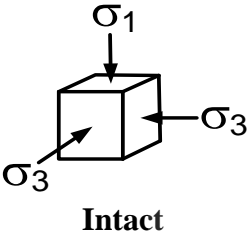
Joint frequency, J_f (joints/m)	σ_3 (MPa)	ν	E_1 (GPa)	E_2 (GPa)	E_3 (GPa)
 Intact	0	0.21	10	10	10
	3	0.29	10.3	10.1	10.2
	5	0.18	11.1	11	11.1
	7	0.20	10.2	9.8	10.7
	12	0.18	11.0	11.9	10.3

Table 5.18 Deformation moduli for case I.

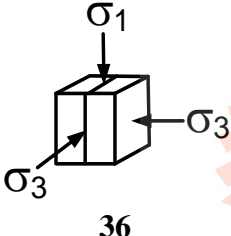
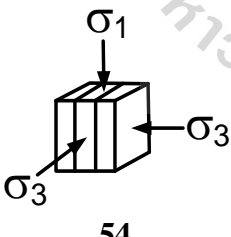
Joint frequency, J_f (joints/m)	σ_3 (MPa)	ν	$E_{1,p}$ (GPa)	$E_{3,p}$ (GPa)	$E_{3,n}$ (GPa)
 36	0	0.27	6.5	6.3	5.8
	3	0.22	5.6	6.1	5.6
	5	0.16	6.2	6.2	5.8
	7	0.27	6.4	6.4	5.6
	12	0.21	6.0	6.5	6.0
 54	0	0.28	4.8	4.8	4.8
	3	0.16	5.0	4.6	4.4
	5	0.22	5.7	4.8	4.6
	7	0.21	4.4	4.9	4.5
	12	0.29	6.3	4.9	4.6

Table 5.19 Deformation moduli for case II.

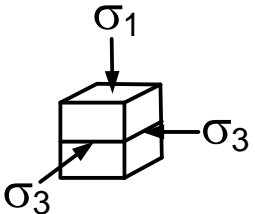
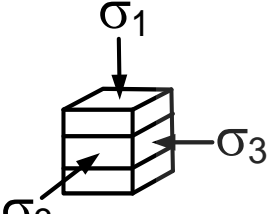
Joint frequency, J_f (joints/m)	σ_3 (MPa)	ν	$E_{1,n}$ (GPa)	$E_{3,p}$ (GPa)	$E_{3,p}$ (GPa)
 36	0	0.18	5.3	5.3	5.3
	3	0.19	5.6	6	5.6
	5	0.28	5.7	5.7	5.8
	7	0.20	5.1	5	5.9
	12	0.22	4.8	4.8	5.2
 54	0	0.24	3.1	2.8	3.8
	3	0.22	3.1	3.7	3.7
	5	0.28	3.9	4.4	3.9
	7	0.22	3.2	3.1	3.8
	12	0.28	3.4	3.3	3.5

Table 5.20 Deformation moduli for case III.

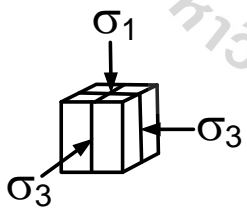
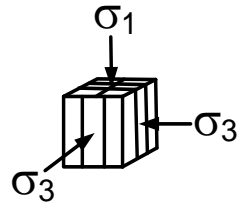
Joint frequency, J_f (joints/m)	σ_3 (MPa)	ν	$E_{1,p}$ (GPa)	$E_{3,p}$ (GPa)	$E_{3,p}$ (GPa)
 36	0	0.17	5	5.2	5
	3	0.20	4.5	5	5.2
	5	0.23	4.3	5.2	5.0
	7	0.29	5.3	5.5	5.1
	12	0.29	6.5	5.5	5.3
 54	0	0.26	3.4	4.2	3.8
	3	0.24	4.1	4	4
	5	0.25	3.6	4.1	3.8
	7	0.25	3.5	3.6	3.5
	12	0.27	3.0	4.0	3.4

Table 5.21 Deformation moduli for case IV.

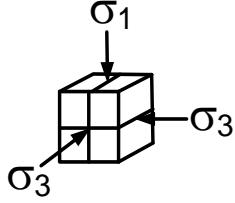
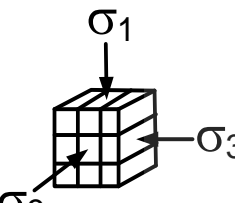
Joint frequency, J_f (joints/m)	σ_3 (MPa)	ν	$E_{1,p}$ (GPa)	$E_{3,p}$ (GPa)	$E_{3,p}$ (GPa)
 36	0	0.28	4.9	4	4.7
	3	0.26	3.8	4.6	4.2
	5	0.24	4.3	4.3	4.3
	7	0.24	4.3	4.7	4.1
	12	0.27	4.3	4	4.4
 54	0	0.24	4.1	4.6	2.4
	3	0.26	3.2	3.6	2.9
	5	0.25	2.6	2.5	2.6
	7	0.29	3.6	3.2	3
	12	0.26	2.8	2.6	2.9

Table 5.22 Deformation moduli for case V.

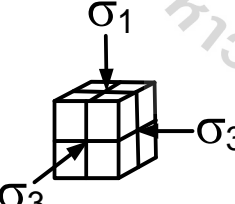
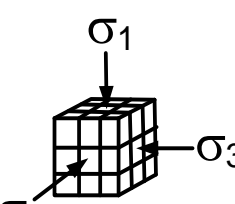
Joint frequency, J_f (joints/m)	σ_3 (MPa)	ν	E_1 (GPa)	E_2 (GPa)	E_3 (GPa)
 36	0	0.17	4.3	4.2	4.2
	3	0.17	4.4	4.4	4.3
	5	0.22	3.8	3.4	4.3
	7	0.28	4.2	4.2	4.5
	12	0.23	4.0	4.0	4.3
 54	0	0.20	3.1	3.5	3.2
	3	0.24	2.8	2.8	2.9
	5	0.29	2.7	2.7	2.7
	7	0.26	2.9	3.3	2.4
	12	0.24	2.9	3.0	2.6

Table 5.23 Deformation moduli for case VI.

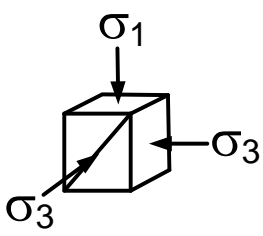
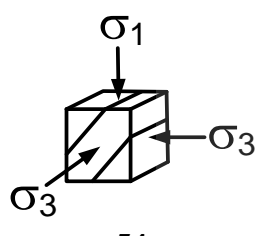
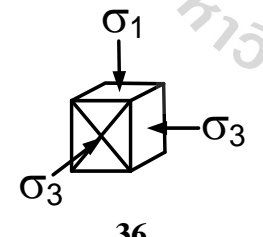
Joint frequency, J_f (joints/m)	σ_3 (MPa)	ν	E_1 (GPa)	E_2 (GPa)	E_3 (GPa)
 36	0	0.24	5.9	2.8	2.8
	3	0.24	5.7	1.7	1.2
	5	0.28	5.4	1.6	1.3
	7	0.23	5.2	1.1	2.3
	12	0.24	5.0	1.7	1.0
 54	0	0.27	5.4	2.0	0.9
	3	0.16	5.2	1.2	0.4
	5	0.15	4.9	1.6	1.0
	7	0.24	4.6	1.3	1.1
	12	0.23	4.4	1.2	2.1

Table 5.24 Deformation moduli for case VII.

Joint frequency, J_f (joints/m)	σ_3 (MPa)	ν	E_1 (GPa)	E_2 (GPa)	E_3 (GPa)
 36	0	0.27	0.6	1.4	5.4
	3	0.25	0.9	0.5	5.4
	5	0.24	1.5	0.5	4.4
	7	0.27	0.7	1.4	3.5
	12	0.24	0.8	0.9	3.5

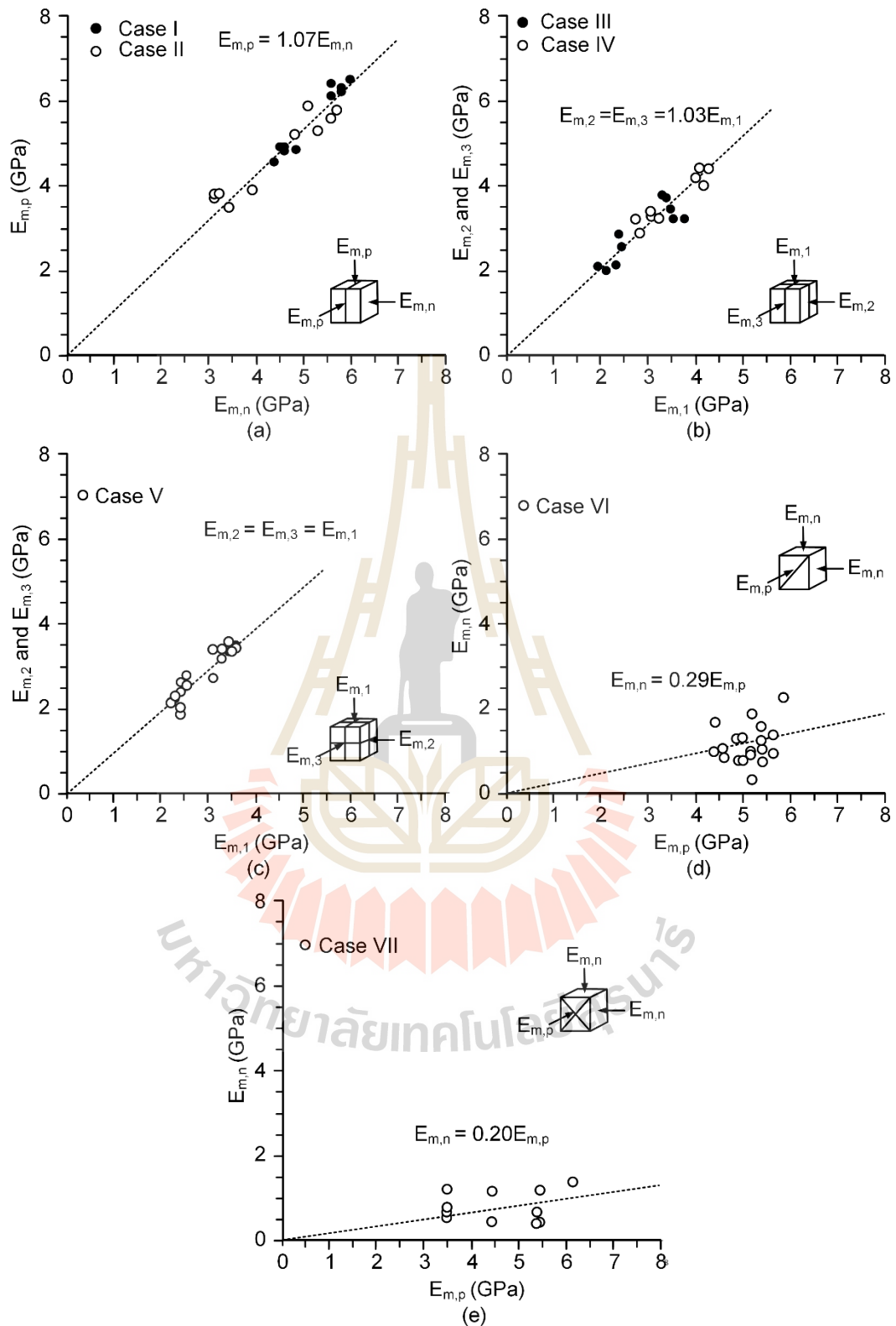


Figure 5.4 Deformation moduli calculated along the intermediate and minor principal axes as a function of the major principal axis.

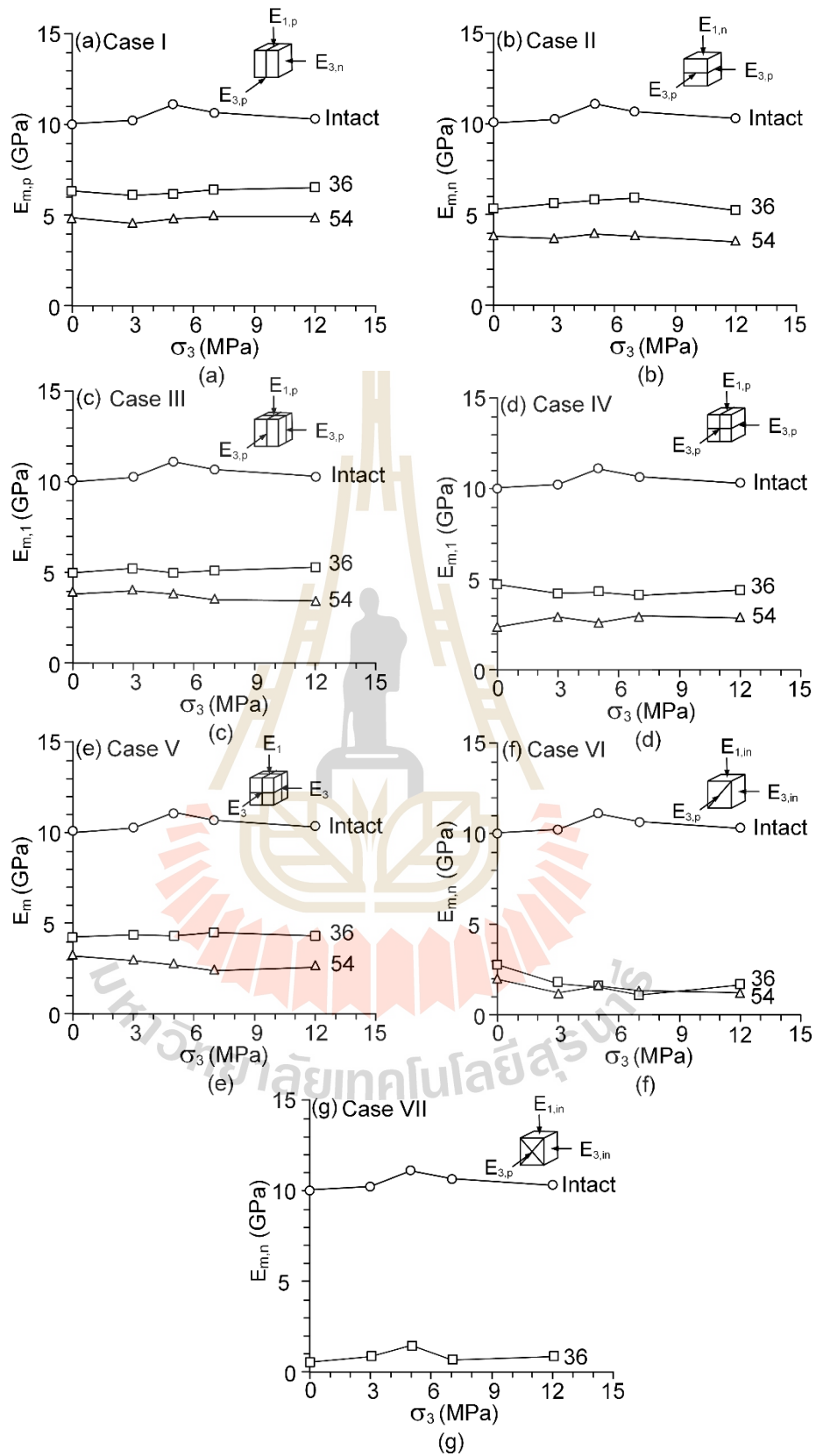


Figure 5.5 Deformation modulus as a function of confining pressure.

CHAPTER VI

TEST RESULTS ANALYSIS

6.1 Introduction

This chapter determines the predictive capability of rock mass strength criteria developed by Hoek and Brown (1980), Sheorey (1989), Yudhbir (1983) and Ramamurthy and Arora (1994) by comparing with the test results. The effects of joint frequency, orientation and set numbers on the deformation modulus of rock mass model are determined. The predictive capability of the empirical criteria developed by Goodman (1970), Yoshinaka and Yamabe (1986), Ramamurthy (2001) and Thaweeboon (2017) is also evaluated by comparing with the test results.

6.2 Strength criteria

Four strength criteria that are commonly used to determine rock mass strength are compared against the triaxial strength data obtained from different joint configurations. These include the Hoek and Brown (1980), Sheorey (1989), Yudhbir (1983) and Ramamurthy and Arora (1994) criteria. They are all formulated in the terms of σ_1 and σ_3 . The predictive capability of these strength criteria is determined and compared using the coefficient of correlation (R^2) as an indicator. The higher R^2 value indicates the better predictability of the criterion. Governing equations of these strength criteria used in the regression are described briefly below.

The Hoek and Brown criterion defines the relationship between the major and minor stresses at failure by

$$\sigma_1 = \sigma_3 + (m\sigma_c\sigma_3 + s\sigma_c^2)^{1/2} \quad (6.1)$$

where m and s are constants which depend on the properties of the rock.

The sheorey criterion defines the relationship between the major and minor principal stresses at failure by:

$$\sigma_1 = \sigma_{cm} + [1 + (\sigma_3 / \sigma_{tm})]^{bm} \quad (6.2)$$

where b_m is a constant, σ_{cm} is the uniaxial compressive strength of rock mass, and σ_{tm} is the uniaxial tensile strength of rock mass.

Yudhbir et al. (1983) modify the original Bieniawski criterion (1974). The new criterion can be written in a more general form as:

$$\sigma_1 / \sigma_c = A + B(\sigma_3 / \sigma_c)^\alpha \quad (6.3)$$

where A is a dimensionless parameter whose value depends on rock mass quality, and B is material constant depending on rock type.

Ramamurthy and Arora (1994) present a nonlinear shear strength response of intact rocks in the form of a modified Mohr-Coulomb theory. For a jointed rock mass the criterion can be written as:

$$(\sigma_1 - \sigma_3) / \sigma_3 = \beta(\sigma_{cm} / \sigma_3)^\alpha \quad (6.4)$$

where α and B are the material constants for the rock mass, and σ_{cm} is the uniaxial compressive strength of rock mass. The results show that σ_{cm} is the most effective parameter to dictate the strength of rock mass. However, this criterion cannot be used to predict rock mass strength under unconfined condition. Ramamurthy suggests an alternative formula in terms of joint factor J_f which can be written by:

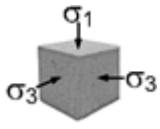
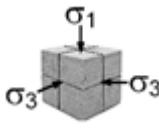
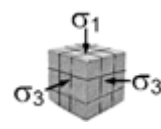
$$\sigma_{cm} = \sigma_c \exp(-0.008J_f) \quad (6.5)$$

$$B_i/B_j = 0.13 \exp[2.04\alpha_j/\alpha_i] \quad (6.6)$$

$$\alpha_j/\alpha_i = (\sigma_{cj}/\sigma_{ci})^{0.5} \quad (6.7)$$

The constants calculated from SPSS program for strength criteria are shown in Table 6.1. Major principal stresses at failure are compared between tension-induced fractures with those of smooth fractures (Figure 6.1). The model with tension-induced fractures give greater major principal stresses than those with smooth fractures. All criteria can provide good correlation with the test data, with R^2 greater than 0.9. Figure 6.2 compares the test data with curve fits of the strength criteria in terms of σ_1 as a function of σ_3 at failure. Figure 6.3 shows the decrease of parameters m and s of Hoek-Brown criterion as the joint frequency increases. The parameters m and s of one joint set specimen are greater than those of the three joint set specimens.

Table 6.1 Strength criteria and their constants calibrated from the test data.

Strength criteria	Parameters	Joint frequencies (joints/m)		
		Intact	36	54
				
Hoek-Brown (1980) $\sigma_1 = \sigma_3 + (m \sigma_c \sigma_3 + s \sigma_c^2)^{1/2}$	m	14.10	10.10	8.20
	s	1.00	0.68	0.51
	R ²	0.977	0.978	0.979
Sheorey et al. (1989) $\sigma_1 = \sigma_{cm}(1 + \sigma_3/\sigma_{tm})^{b_m}$	σ_{cm}	43.00	34.40	30.00
	σ_{tm}	2.60	2.30	2.10
	b_m	0.55	0.55	0.55
	R ²	0.996	0.997	0.996
Yudhbir et al. (1993) $\sigma_1/\sigma_c = A + B(\sigma_3/\sigma_c)^\alpha$	A	0.97	0.79	0.70
	B	4.15	3.43	3.07
	α	0.73	0.73	0.73
	R ²	0.988	0.982	0.978
Ramamurthy and Arora (1994) $(\sigma_1 - \sigma_3)/\sigma_3 = \beta(\sigma_{cm}/\sigma_3)^\alpha$	σ_{cm}	43.40	35.80	31.50
	β	1.10	1.05	1.00
	α	0.70	0.70	0.70
	R ²	0.988	0.979	0.976

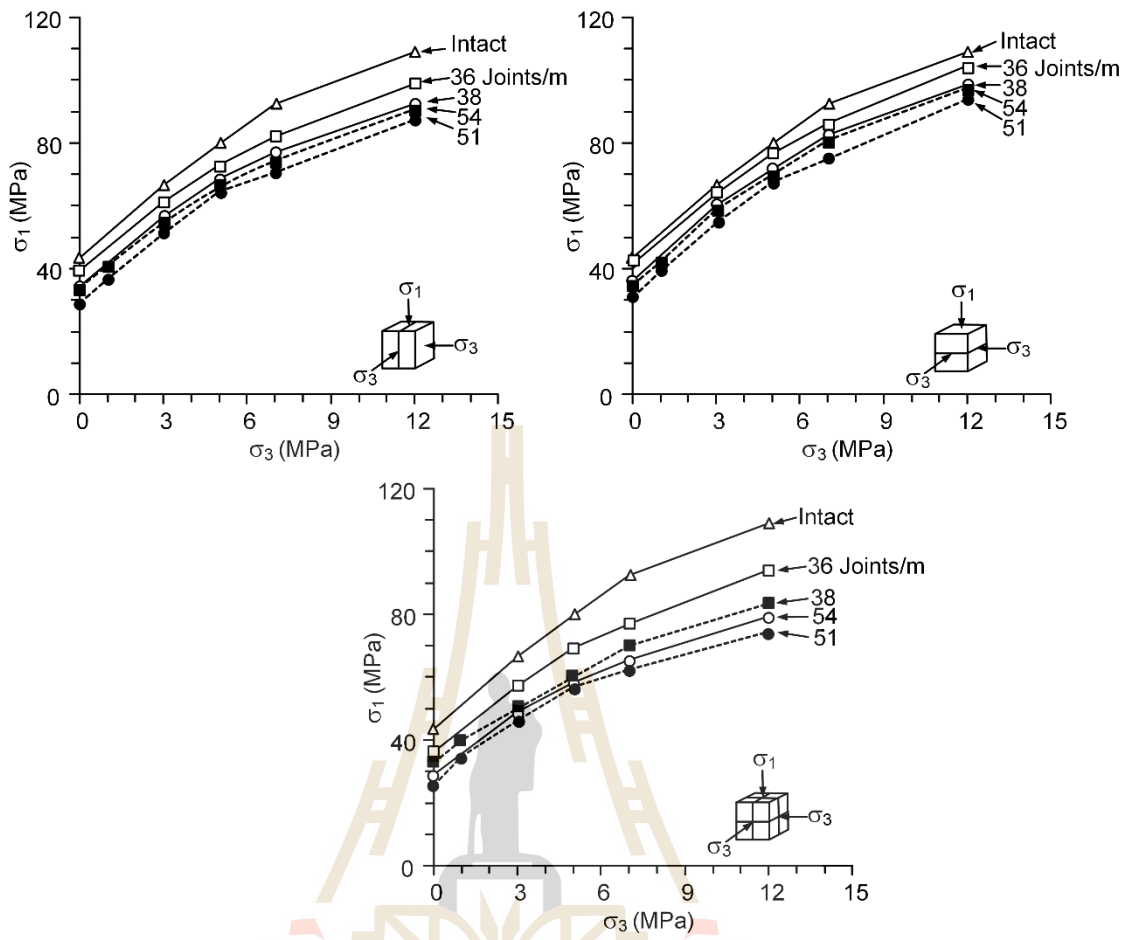


Figure 6.1 Major principal stresses at failure are comparing the model with tension-induced fractures (solid lines) with those of smooth fractures (dash line) of Thaweeboon et al. (2017).

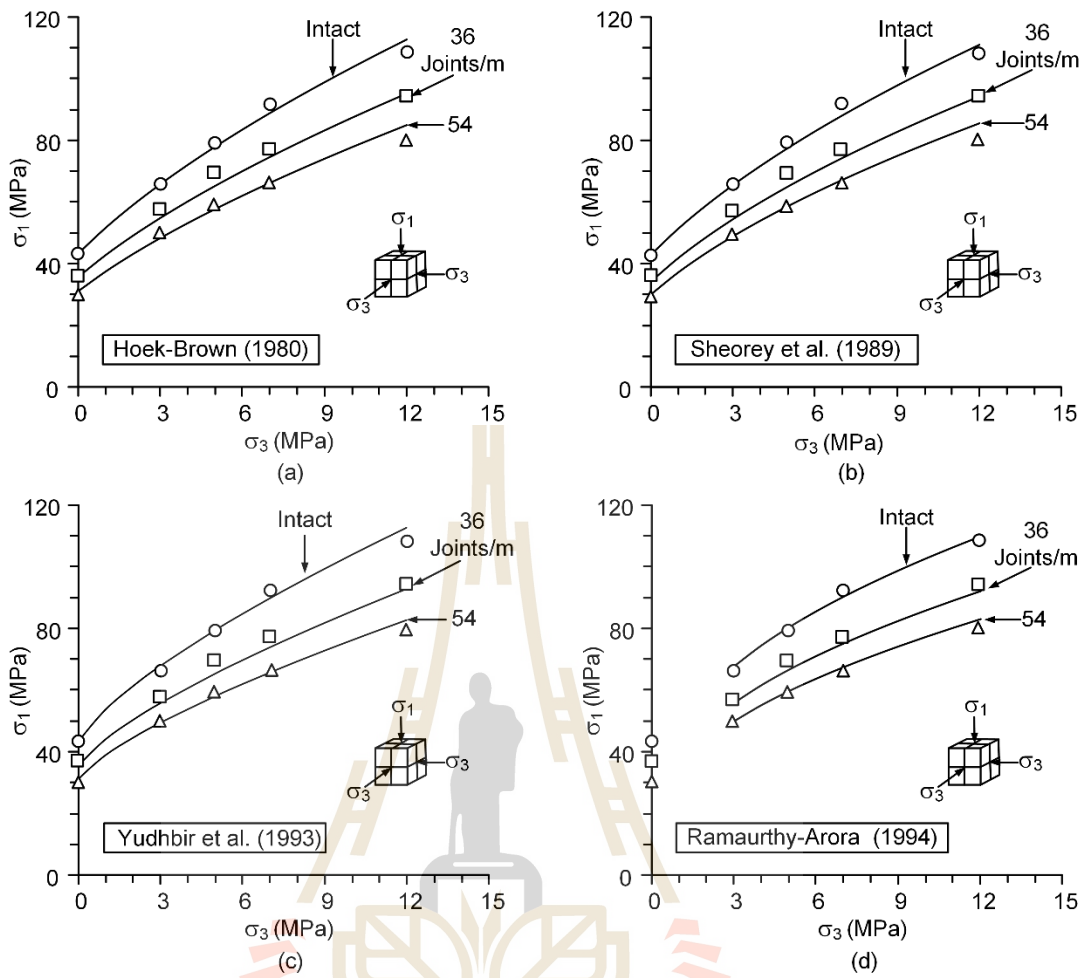


Figure 6.2 Test data (points) and curve fits of four strength criteria.

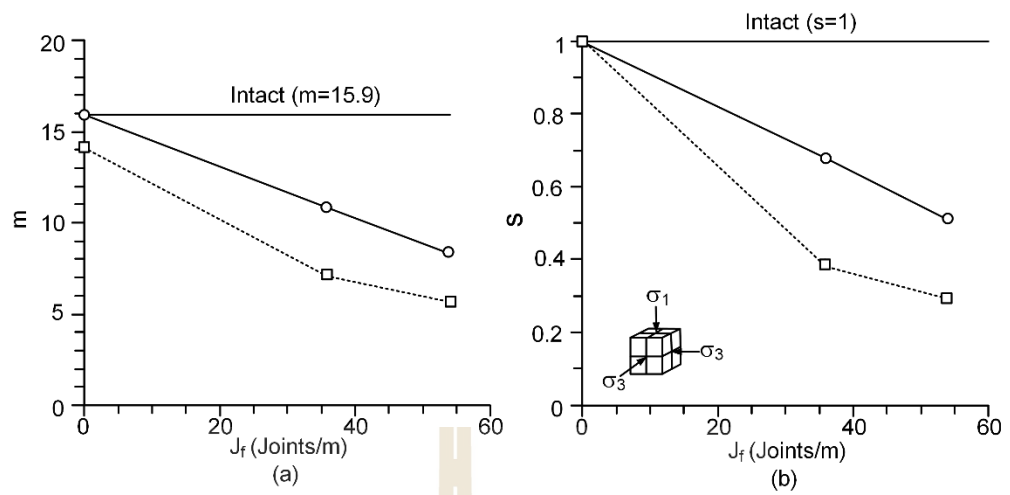


Figure 6.3 Hoek–Brown parameters m (a) and s (b) comparing the model with tension-induced fractures (solid lines) with those of smooth fractures (dash lines) of Thaweboon et al. (2017).

6.3 Deformability criteria

Four empirical criteria are used to estimate rock mass deformation modulus (E_m). They include the Goodman (1970), Yoshinaka and Yamabe (1986), Ramamurthy criteria (2001) and Thaweboon et al. (2017). The deformation modulus calculated from the triaxial compression test results for each case are compared with the rock mass deformability criteria. A brief description of each criterion is described below.

Goodman (1970) has presented a method to evaluate the elastic constants for an equivalent continuous material representative of a rock mass regularly crossed by a single set of joints using the concept of joint stiffness. The criterion can be written as:

$$\frac{1}{E_r} = \frac{1}{E_i} + \frac{1}{sk_n} \quad (6.8)$$

where E_r is the rock mass deformation modulus, k_n is the joint normal stiffness, s is the average joint spacing and E_i is the equivalent deformation modulus.

Yoshinaka and Yamabe (1986) study the stress-strain behavior of a discontinuous rock mass. Based on the concept of joint stiffness, an equation to evaluate the deformation of jointed rock is derived as:

$$\frac{1}{E_t} = \frac{1}{E_c} + \frac{\cos^2\theta_1}{L_1} \left(\frac{\sin^2\theta_1}{k_{s1}} + \frac{\cos^2\theta_1}{k_{n1}} \right) + \frac{\cos^2\theta_2}{L_2} \left(\frac{\sin^2\theta_2}{k_{s2}} + \frac{\cos^2\theta_2}{k_{n2}} \right) \quad (6.9)$$

where E_c is elastic modulus of intact rock, θ_1, θ_2 are the angles of inclination from the applied plane of major principal stress, L_1 and L_2 are joint spacings and k_s and k_n are joint stiffnesses.

Ramamurthy (2001) defines the relationship between the ratios of moduli, E_{ij}/E_{ti} and J_F , which can be represented by:

$$E_{ij}/E_{ti} = \exp(-1.15 \times 10^{-2} J_F) \quad (6.10)$$

where E_{ij} is the jointed rock deformation modulus, E_{ti} is the intact deformation modulus, and J_F is the joint factor which has been defined by the following relation:

$$J_F = \frac{J_f}{n \times r} \quad (6.11)$$

where J_f is joint frequency, i.e. number of joints per meter, n is inclination parameter depending upon the orientation of the joint β , r is joint strength parameter dependent upon the joint condition.

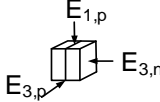
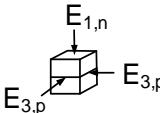
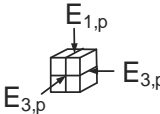
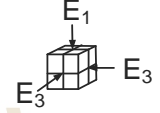
Thaweboon et al. (2017) modify Goodman (1970) equation to determine the deformation modulus along three principal directions. It is proposed as:

$$\frac{1}{E_m} = \frac{1}{E_i} + \frac{N}{sk_n} \quad (6.12)$$

The N values are defined by the direction of deformation moduli with respect to the joint plane as shown in Table 6.2.

The elastic moduli parallel and normal to the joints are plotted as a function of joint frequency for single joint set specimens (see Figure 5.5). Their average value (data point) and standard deviation (shown as error bars) obtained from all confining

Table 6.2 Parameter N defined for modified Goodman's equation.

Number of joint sets	Orientation of joint with respect to σ_1 axis	Model	N
1	Parallel to σ_1		0.5 ^a
1	Normal to σ_1		1.0 (original Goodman's equation)
2	Parallel and normal to σ_1		1.5
3	Two parallel and one normal to σ_1		2.0 ^a

^a Verified by test results

pressures are shown in the figure. The joint normal stiffness used here is 381.2 GPa/m, which is obtained from Kamonphet et al. (2015).

The joint factors of Ramamurthy (2001) used in this study are summarized in Table 6.3. The Ramamurthy (2001) equation gives a good estimation for the deformation moduli parallel to the joint planes and normal to the joint planes. The Goodman (1970) and Yoshinaka and Yamabe (1986) equations can also describe the deformation moduli normal to joint planes. Yoshinaka and Yamabe's (1986) equation adequately describes the deformation moduli of the rock specimens with three-joint sets. Note that Yoshinaka and Yamabe (1986) cannot describe the deformation modulus of the rock mass along the axis that is parallel to the joint plane. The comparisons between the test data and predictions are shown in Figure 6.4. Results indicate that the Goodman (1970) and Yoshinaka and Yamabe (1986) equations give good prediction

Table 6.3 Joint factors calculated for this study.

Joint orientation	Joint frequency (J_f)	n	r	Joint factor (J_F)
One-joint set parallel to the major principal axis	Intact	1	0.8	-
	36	0.85	0.8	47.3
	54	0.85	0.8	70.9
One-joint set joint making angles of 45° to the major principal axis	Intact	1	0.8	-
	36	0.28	0.8	160.7
	54	0.28	0.8	241.1
One-joint set normal to the major principal axis	Intact	1	0.8	-
	36	0.98	0.8	45.9
	54	0.98	0.8	68.9

for the deformation modulus normal to joint planes, $E_{1,n}$ ($R^2=0.911$). Yoshinaka and Yamabe (1986) equation also predicts the deformation modulus of rock mass model with three joint sets given $R^2=0.975$. Ramamurthy (2001) equation gives a fair estimation for the deformation modulus normal to the joint planes, $E_{1,n}$ ($R^2=0.986$). It gives a slightly better prediction ($R^2=0.924$) for the deformation modulus that is parallel to the joint planes ($E_{1,p}$).

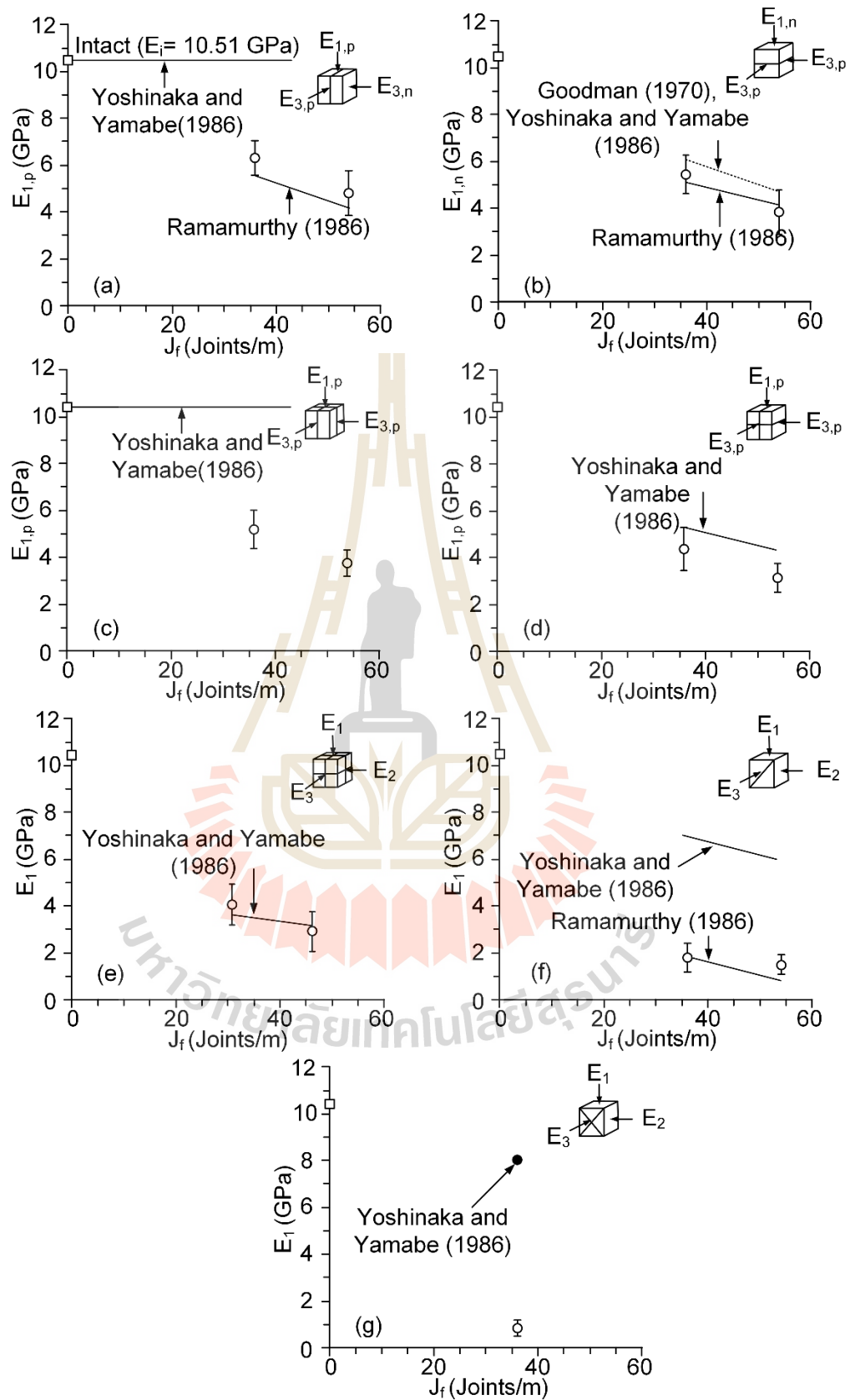


Figure 6.4 Comparisons between the test data (points) and predictions (lines).

6.4 Modified Goodman equation by Thaweeboon et al. (2017)

The Goodman (1970) equation is modified by Thaweeboon et al. (2017) to determine deformation modulus in different directions. It is proposed as:

$$\frac{1}{E_m} = \frac{1}{E_i} + \frac{N}{sk_n} \quad (6.13)$$

where E_m is the jointed rock deformation modulus, E_i is the intact deformation modulus, s is the joint spacing, k_n is the joint normal stiffness and N is a parameter which value depends on joint set direction (Table 6.4). The equation shows well prediction for all cases as shown in Table 6.5 and Figure 6.5. The proposed equation however can only predict the deformation modulus in the directions normal and parallel to the joint planes. Equation is modified to determine deformation modulus in different directions (Eq. 6.13), which gives good correlation with the test data of with R^2 greater than 0.9 (Figure 6.6).

Table 6.4 Parameter N defined for modified Goodman equation by Thaweboon et al. (2017).

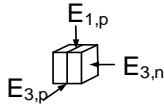
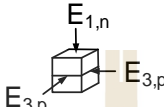
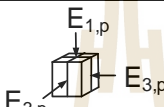
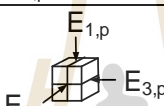
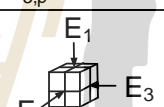
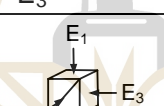
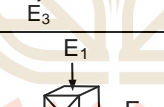
Cases	Model	N
I		0.5
II		1.0 (original Goodman's equation)
III		1.0
IV		1.5
V		2.0
VI		4.0
VII		8.0

Table 6.5 Coefficients of correlation of each criterion.

Criteria	R ²						
	Case I	Case II	Case III	Case VI	Case V	Case VI	Case VII
Goodman (1970)	-	0.911	-	-	-	-	-
Yoshinaka and Yamabe (1986)	-	0.911	-	0.875	0.975	0.123	0.178
Ramamurthy (2001)	0.924	0.986	-	-	-	0.882	-
Modified Goodman	0.936	0.976	0.992	0.988	0.956	0.987	0.943

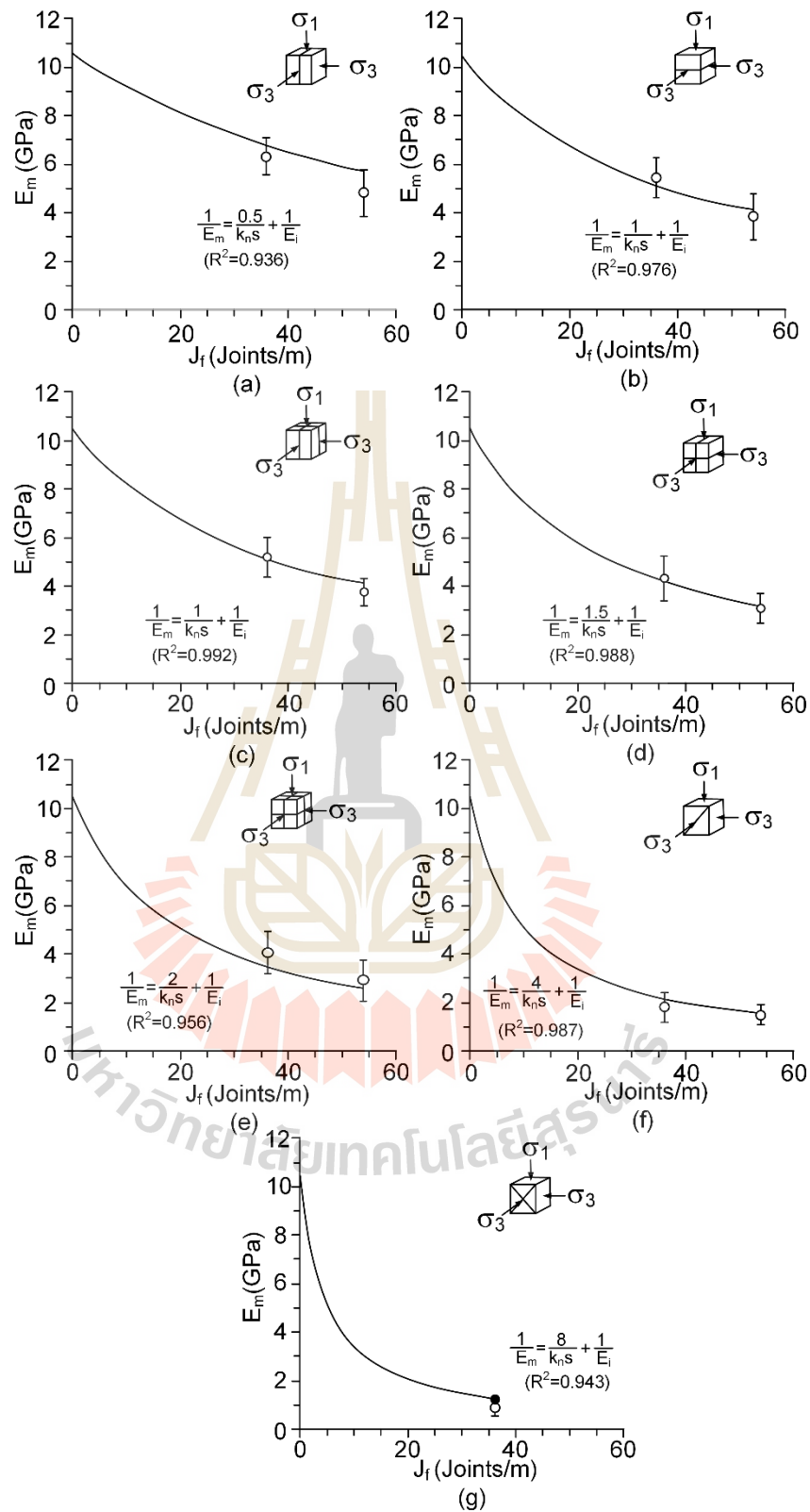


Figure 6.5 Comparisons between the test data (points) and modified Goodman equation by Thaweeboon et al. (2017) (lines).

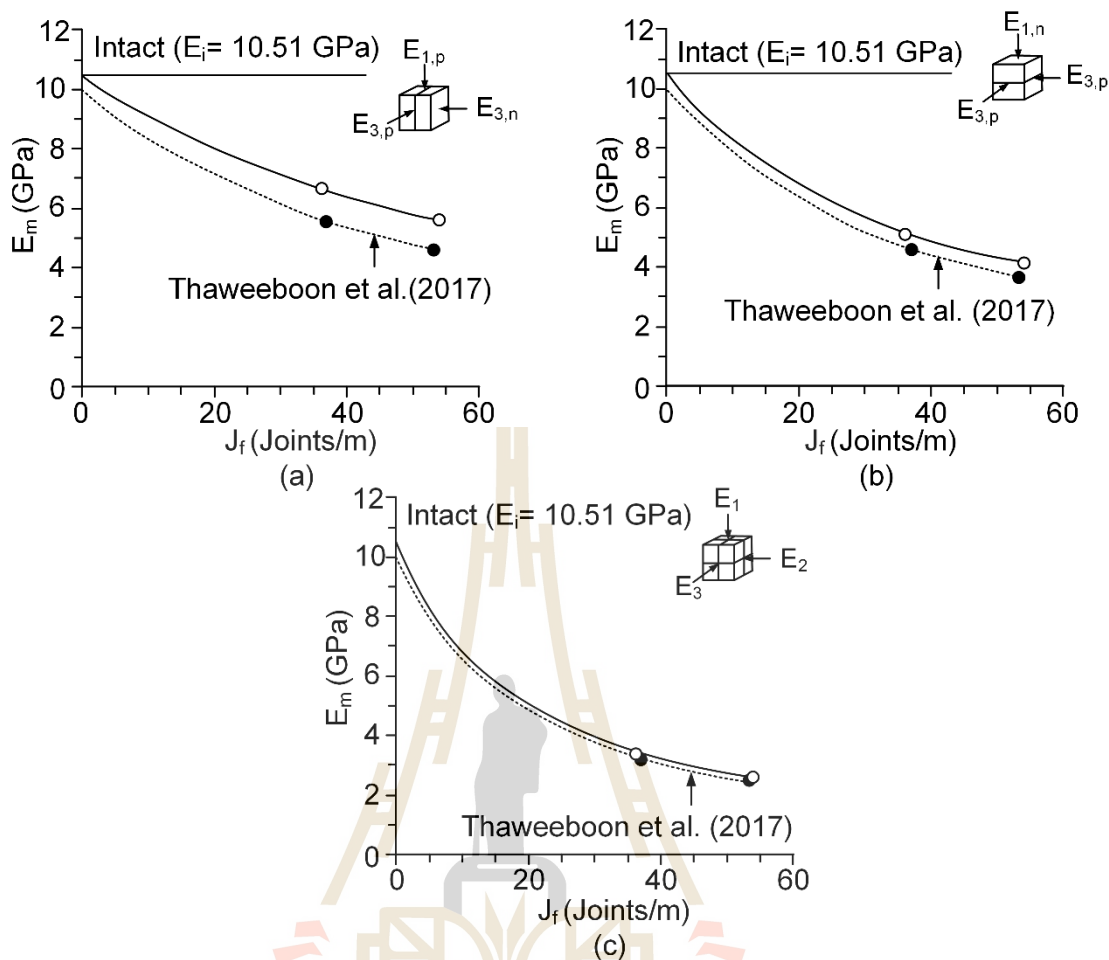


Figure 6.6 Deformation moduli for tension-induced fractures (solid lines) and smooth fractures (dash lines) of Thaweeboon et al. (2017).

6.5 Relationship between deformation modulus and RMR system

Galera et al. (2007) developed relationship between modulus ratio (E_m/E_i) and RMR from Nicholson and Bieniawski (1990). RMR rating and modulus ratio are used in this study, as shown in Tables 6.6 through 6.14. The results obtained in this study have been compared with Galera et al. (2007). Figure 6.7 shows that the results from this study agree reasonably well with those predicted Galera et al. (2007).

Table 6.7 Rock Mass Rating system for I (after Bieniawski 1989).

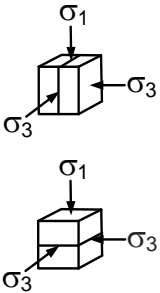
Models	Classification parameters		RMR Rating
	Compressive strength of rock material (Intact rock)	50.4 MPa	7
	Rock Quality Designation (RQD)	0	5
	Spacing of discontinuities	< 60 mm	5
	Condition of discontinuities	Rough surfaces Separation < 0.1 mm	28
	Groundwater conditions	None	15
	Total Rating		60

Table 6.8 Rock Mass Rating system for II (after Bieniawski 1989).

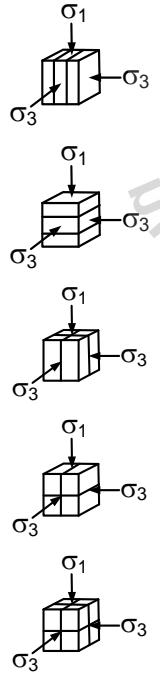
Models	Classification parameters		RMR Rating
	Compressive strength of rock material (Intact rock)	50.4 MPa	7
	Rock Quality Designation (RQD)	0	5
	Spacing of discontinuities	< 60 mm	5
	Condition of discontinuities	Slightly rough surfaces Separation < 1 mm	25
	Groundwater conditions	None	15
	Total Rating		57

Table 6.9 Rock Mass Rating system for III (after Bieniawski 1989).

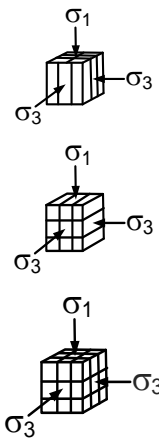
Models	Classification parameters		RMR Rating
	Compressive strength of rock material (Intact rock)	50.4 MPa	7
	Rock Quality Designation (RQD)	0	5
	Spacing of discontinuities	< 60 mm	5
	Condition of discontinuities	Slightly rough surfaces Separation < 5 mm	22
	Groundwater conditions	None	15
	Total Rating		

Table 6.10 Deformation modulus ratio and rock mass rating for case I.

Case I	E_m (GPa)	E_i (GPa)	E_m / E_i	RMR
36	6.5	10.5	0.62	60
	5.6	10.5	0.53	60
	6.2	10.5	0.59	60
	6.4	10.5	0.61	60
	6.0	10.5	0.57	60
54	4.8	10.5	0.46	57
	4.6	10.5	0.43	57
	4.8	10.5	0.45	57
	4.9	10.5	0.47	57
	4.9	10.5	0.46	57

Table 6.11 Deformation modulus ratio and rock mass rating for case II.

Case II	E_m (GPa)	E_i (GPa)	E_m / E_i	RMR
36	5.3	10.5	0.50	60
	5.6	10.5	0.53	60
	5.7	10.5	0.54	60
	5.1	10.5	0.48	60
	4.8	10.5	0.45	60
54	3.1	10.5	0.30	57
	3.1	10.5	0.29	57
	3.9	10.5	0.37	57
	3.2	10.5	0.30	57
	3.4	10.5	0.32	57

Table 6.12 Deformation modulus ratio and rock mass rating for case III.

Case III	E_m (GPa)	E_i (GPa)	E_m / E_i	RMR
36	5.2	10.5	0.49	57
	5.0	10.5	0.48	57
	5.2	10.5	0.49	57
	5.5	10.5	0.52	57
	5.5	10.5	0.52	57
54	3.4	10.5	0.32	54
	4.1	10.5	0.39	54
	3.6	10.5	0.34	54
	3.5	10.5	0.33	54
	3.0	10.5	0.29	54

Table 6.13 Deformation modulus ratio and rock mass rating for case IV.

Case IV	E_m (GPa)	E_i (GPa)	E_m / E_i	RMR
36	4.9	10.5	0.47	57
	3.8	10.5	0.36	57
	4.3	10.5	0.41	57
	4.3	10.5	0.41	57
	4.3	10.5	0.41	57
54	4.1	10.5	0.39	54
	3.2	10.5	0.31	54
	2.6	10.5	0.25	54
	3.6	10.5	0.34	54
	2.8	10.5	0.26	54

Table 6.14 Deformation modulus ratio and rock mass rating for case V.

Case V	E_m (GPa)	E_i (GPa)	E_m / E_i	RMR
36	4.3	10.5	0.41	57
	4.4	10.5	0.42	57
	3.8	10.5	0.36	57
	4.2	10.5	0.40	57
	4.0	10.5	0.38	57
54	3.1	10.5	0.29	54
	2.8	10.5	0.27	54
	2.7	10.5	0.26	54
	2.9	10.5	0.28	54
	2.9	10.5	0.28	54

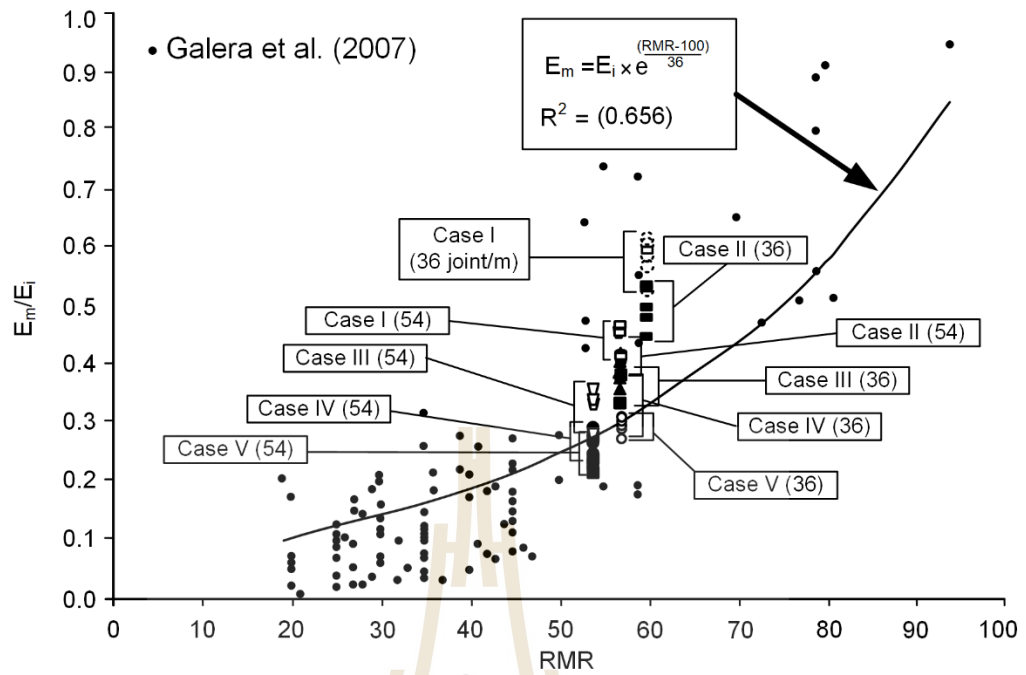


Figure 6.7 Deformation modulus ratio as a function of rock mass rating (RMR).

CHAPTER VII

DISCUSSIONS AND CONCLUSIONS

7.1 Discussions and conclusions

Triaxial compression tests have been performed to determine compressive strength and deformation modulus of small-scale rock mass models with single joint and multiple joint sets and frequencies under large confinements. The joints are artificially made by tension-inducing method. It is found that the compressive strengths decrease with increasing joint frequency. This agrees with the experimental observations by Ramamurthy and Arora (1994) on jointed specimens of plaster of Paris and with Thaweeboon et al. (2017) on artificial joints in sandstone specimens. For one-joint set specimens the strengths of rock specimens with joints normal to σ_1 axis are always greater than those with joints parallel to σ_1 axis. The lowest strengths are obtained when the joint planes make angles 45° with the major principal stress. This agrees with experimental observations by Colak and Unlu (2004), Saroglou and Tsiambaos (2008) and Goshtasbi, et al. (2006) and with Thaweeboon et al. (2017). The decrease of rock mass strengths as the joint frequency increases tends to act equally throughout the range of confining stresses used here (0-12 MPa). All strength criteria used here can well predict the strengths of the rock mass specimens under the confining stresses up to 12 MPa. The Hoek-Brown criterion with only two constants (m and s) can describe the rock mass strengths as well as the three parameters criteria. The parameters m and s of the one and two-joint set specimens are higher than those of the

three-joint set specimens. This suggests that decreasing joint set numbers will increase the rock mass strength. Comparison of the m and s parameters obtained here with those of Thaweboon et al. (2017), who performed similar test on the some sandstone with smooth saw-cut surfaces, shows that under the same joint frequencies the rough joints (tested here) show higher m and s values than those of the smooth joints of Thaweboon et al. (2017).

The parameter s decreases rapidly with increasing joint frequency while parameters m tend to be insensitive with the joint frequency, ranging between 8.2 and 14.1. The parameters m and s of the one joint set specimens are higher than those of the three joint set specimens. This agrees with the conclusion drawn by Thaweboon et al. (2017).

The deformation parameters are determined from the tangent of the stress-strain curves at about 50% of the failure stress. An attempt is made to calculate the deformation moduli along the three loading principal directions. The results show that for one joint set specimens the deformation moduli that are parallel to the joint planes (Case I) show highest values compared to those that are normal to the joints (Case II). Joints making angle of 45° to σ_1 (Cases VI and VII) show lowest deformation moduli. This is true for all joint frequencies. For three mutually perpendicular joint set specimens, the deformation moduli are similar for all principal directions. The deformation modulus decreases with increasing joint frequency, and tends to increase with the confining pressure. This agrees with the experimental observations by Tiwari and Rao (2006). The Poisson's ratio of the specimens with different joint frequencies ranges from 0.15 to 0.29. The effect of the confining pressure on the Poisson's ratio

cannot be clearly observed from the test results. This may be due to the intrinsic variability among the test models.

Four empirical criteria are used to estimate rock mass deformation modulus (E_m). They include the Goodman (1970), Yoshinaka and Yamabe (1986), Ramamurthy criteria (2001) and Thaweeboon et al. (2017). The deformation modulus calculated from the triaxial compression test results for each case are compared with the rock mass deformability criteria. The Ramamurthy (2001) equation gives a good estimation for the deformation moduli parallel to the joint planes and normal to the joint planes. The Goodman (1970) and Yoshinaka and Yamabe (1986) equations can also describe the deformation moduli normal to joint planes. Yoshinaka and Yamabe (1986) equation adequately describes the deformation moduli of the rock specimens with three-joint sets. Yoshinaka and Yamabe (1986) cannot describe the deformation modulus of the rock mass models along the axis that is parallel to the joint plane. The Goodman (1970) equation is modified by Thaweeboon et al. (2017) to determine deformation modulus in different directions. The parameter N was introduced, whose values depend on joint set directions. Results from this study show that the Thaweeboon's modified equation can adequately describe the deformation moduli parallel and normal to the joints planes for one-joint set and three-joint set specimens. The deformation moduli between tension-induced fractures obtained here and smooth-fractures obtained by (Thaweeboon et al., 2017) gives good correlation with the test data of with R^2 greater than 0.9. The tension-induced fractures show higher deformation modulus than those of the smooth-fractures of Thaweeboon et al. (2017).

7.2 Recommendations for future studies

The uncertainties of the investigation and results discussed above lead to the recommendations for further studies.

1. More testing is required to assess the effect of the intermediate principal stress on the rock mass strength and deformability. The results can be used to predict the strength and deformability of rock mass in true triaxial stress condition.

2. More investigation is also desirable to confirm or verify the effect of joint frequency based on the rock mass classification system which can be used to predict the rock mass behavior in real practice.

3. More testing is required to assess the effects of pore pressure on the rock compressive strengths and elasticity is also desirable. The results can be used to design the rock mass excavation where the groundwater have influencing on the designed structure.

4. The rock mass models used here are relatively small. Larger tested models are needed to confirm the conclusion drawn in the study. The results can be predicted for real rock mass properties in in-situ condition.

5. The test results under higher confining pressure should be obtained to obtaining the strength and deformability of rock mass at the great depth.

REFERENCES

- Arora, V.K. (1987). Strength and Deformational Behaviour of Jointed Rocks. **Ph.D. Thesis**, Indian Institute of Technology, Delhi, India.
- Bieniawski, Z.T. (1974). Estimating the strength of rock materials. **Journal of The South African Institute of Mining and Metallurgy**. 74: 312-320.
- Bieniawski, Z. T. (1978). Determining rock mass deformability: experience from case histories. In **International journal of rock mechanics and mining sciences & geomechanics abstracts**. 15(5): 237-247.
- Bieniawski, Z.T. (1989). **Engineering Rock Mass Classifications: A Complete Manual for Engineers and Geologists in Mining, Civil, and Petroleum Engineering**. John Wiley & Sons.
- Boonsener, M. and Sonpiron, K. (1997). Correlation of tertiary rocks in northeast, Thailand. In **Proceeding of International Conference on Stratigraphy and Tectonic Evolution of Southeast Asia and the South Pacific** (pp. 656-661). Bangkok.
- Brown, E.T. and Trollope, D.H. (1970). Strength of model of jointed rock. **Journal of Soil Mechanics and Foundation Division**. 96(SM2): 685–704.
- Colak, K. and Unlu, T. (2004). Effect of transverse anisotropy on the Hoek–Brown strength parameter ' m_i ' for intact rocks. **International Journal of Rock Mechanics and Mining Sciences**. 41(6): 1045-1052.
- Edelbro, C. (2004). Evaluation of rock mass strength criteria. **Ph.D. Thesis**, Lulea University of Technology, Sweden.

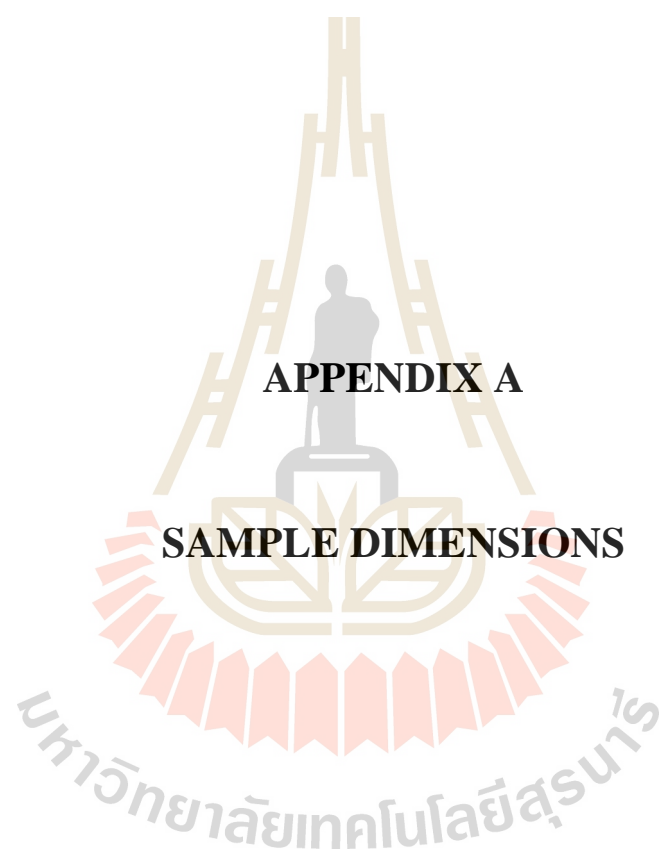
- Edelbro, C., Sjoberg, J., and Nordlund, E. (2007). A quantitative comparison of strength criteria for hard rock masses. **Tunnelling and Underground Space Technology**. 22(1): 57-68.
- Fahimifar, A. and Soroush, H. (2003). Geotechnical parameters characteristics for a kind of schist in Iran. In **Proceedings of 10th ISRM Congress**. South Africa.
- Galera, J. M., Álvarez, M., and Bieniawski, Z. T. (2007). Evaluation of the deformation modulus of rock masses using RMR: comparison with dilatometer tests. In **Proceeding of Underground Works under Special Conditions**. Madrid, Spain.
- Goodman, R.E. (1970). **The Deformability of Joints: In Determination of the In-Situ Modulus of Deformation of Rock**. ASTM Special Tech. Publ. Philadelphia: American Society for Testing and Materials. 477:(174-196).
- Goodman, R.E. (1989). **Introduction to Rock Mechanics**, John Wiley & Sons, New York.
- Goshtashi, K., Ahmadi, M., and Seyedi, J. (2006). Anisotropic strength behavior of slates in the Sirjan-Sanandaj zone. **Journal of the South African Institute of Mining and Metallurgy**. 106: 71-76.
- Halakatevakis, N. and Sofianos, A.I. (2010). Strength of a blocky rock mass based on an extended plane of weakness theory. **International Journal of Rock Mechanics and Mining Sciences**. 47: 568-582.
- Hashemnejad, A., Aghamolaei, I., Ghafoori, M., and Lashkaripour, G. (2013). Providing a new empirical failure criterion for intact rock and comparing it with three criteria Bieniawski, Ramamurthy and Hook-Brown. **International Journal of Emerging Technology and Advanced Engineering**. 3(5): 43-49.

- Hoek, E. and Brown, E.T. (1980). Empirical strength criterion for rock masses. **Journal of Geotechnical Engineering ASCE**. 160(GT9): 1013-1035.
- Hoek, E. and Brown, T. (1988). The Hoek-Brown failure criteria- a 1988 update. In **Proceeding of the Canadian Rock Mechanics. Symposium** (pp. 3-31).
- Hoek, E., Kaiser, P. K., and Bawden, W. F. (2000). **Support of underground excavations in hard rock**. CRC Press.
- Jaeger, J.C., Cook, N.G.W., and Zimmerman, R.W. (2007). **Fundamentals of rock mechanics**, Blackweel: Oxford.
- Janbu, N. (1963). Soil compressibility as determined by odometer and triaxial tests. In **Proceedings of International Conferences on Security Metasploit Framework Expert** (pp.19-25). Essen, Germany.
- Kamonphet, T., Khamrat, S., and Fuenkajorn, K. (2015). Effects of cyclic shear loads on strength, stiffness and dilation of rock fractures. **Songklanakarinn Journal of Science and Technology**. 37(6): 683-690.
- Kulatilake, P.H.S., Park, J., and Malama, B. (2006). A new rock mass failure criterion for biaxial loading conditions. **Geotechnical and Geological Engineering**. 24: 871-888.
- Liao, J.J. and Hsieh, H.Y. (1999). **Triaxial Residual Strength of an Anisotropic Rock**. Rock mechanics for industry, Amadei et al, Balkema, Rotterdam.
- Maji, V.B. and Sitharam, T.G. (2008). Prediction of elastic modulus of jointed rock mass using artificial neural networks. **Geotechnical and Geological Engineering**. 26: 443-452.

- Mclamore, R. and Gray, K.E. (1967). The mechanical behaviour of anisotropic sedimentary rocks. **Transactions of the American Society of Mechanical Engineers**. 89 (1): 62–79.
- Nasser, M.H.B., Rao, K.S., and Ramamurthy, T. (2003) Anisotropic strength and deformational behavior of Himalayan schists. **International Journal of Rock Mechanics and Mining Sciences**. 40(1): 3-23.
- Nicholson, G. A. and Bieniawski, Z. T. (1990). A nonlinear deformation modulus based on rock mass classification. **International Journal of Mining and Geological Engineering**. 8(3): 181-202.
- Rafiai, H. (2011). New empirical polyaxial criterion for rock strength. **International Journal of Rock Mechanics and Mining Sciences**. 48(6): 922-931.
- Ramamurthy, T. (1989). Stability of rock mass. **Indian Geotechnical Journal**. 16(1):1-74.
- Ramamurthy, T. (1993). **Strength, Modulus Responses of Anisotropic Rocks**. In: Hudson JA, editor. *Comprehensive rock engineering* (pp. 313–329). Oxford: Pergamon Press.
- Ramamurthy, T. (2001). Shear strength response of some geo-logical materials in triaxial compression. **International Journal of Rock Mechanics and Mining Sciences**. 38(5): 683-697.
- Ramamurthy, T. and Arora, V.K. (1994). Strength predictions for jointed rocks in confined and unconfined states. **International Journal of Rock Mechanics and Mining Sciences**. 31(1): 9-22.
- Roy, N. (1993). Engineering behaviour of rock masses through study of jointed models. **Ph.D. Thesis**, Indian Institute of Technology, Delhi.

- Saroglou, H. and Tsiambaos, G. (2008). A modified Hoek–Brown failure criterion for anisotropic intact rock. **International Journal of Rock Mechanics and Mining Sciences**. 45(2): 223-234.
- Sheorey, P.R. (1997). **Empirical Rock Failure Criterion**, Balkema, Rotterdam.
- Sheorey, P.R., Biswas, A.K., and Choubey, V.D. (1989). An empirical failure criterion. **Journal of the Soil Mechanics and Foundations Division**. 99(3): 229–248.
- Singh, M. and Singh, B. (2012). Modified Mohr-Coulomb criterion for non-linear triaxial and polyaxial strength of jointed rocks. **International Journal of Rock Mechanics and Mining Sciences**. 51: 43-52.
- Sridevi, J. and Sitharam, T. G. (2000). Analysis of strength and moduli of jointed rocks. **Geotechnical and Geological Engineering**. 18: 3-21.
- Thaweeboon, S., Dasri, R., Sartkaew, S., and Fuenkajorn, K. (2017). Strength and deformability of small-scale rock mass models under large confinements. **Bulletin of Engineering Geology and the Environment**. 76(3), 1129-1141.
- Tien, Y.M. and Kuo, M.C. (2001). A failure criterion for transversely isotropic rocks. **International Journal of Rock Mechanics and Mining Sciences**. 38: 399-412.
- Tiwari, R. and Rao, K.S. (2006). Deformability characteristics of a rock mass under true-triaxial stress compression. **Geotechnical and Geological Engineering**. 24: 1039-1063.
- Walsri, C., Poonprakon, P., Thosuwan R., and Fuenkajorn, K. (2009). Compressive and tensile strengths of sandstones under true triaxial stresses. In **Proceeding 2nd Thailand Symposium on Rock Mechanics** (pp. 199-218). Chonburi, Thailand.

- Yaji, R.K. (1984). Shear strength and deformation response of jointed rock. **Ph.D. Thesis**, Indian Institute of Technology, Delhi.
- Yang, Z.Y., Chen, J. M., and Huang, T.H. (1998). Effect of joint sets on the strength and deformation of rock mass models. **International Journal of Rock Mechanics and Mining Sciences**. 35(1): 75-84.
- Yoshinaka, R. and Yamabe, T. (1986). Joint stiffness and the deformation behaviour of discontinuous rock. **International Journal of Rock Mechanics and Mining Sciences**. 23(1): 19-28.
- You, M.Q. (2009). True-triaxial strength criteria for rock. **International Journal of Rock Mechanics and Mining Sciences**. 46: 115-127.
- Yudhbir, Y., Lemanza, W., and Prinzl, F. (1983). An empirical failure criterion for rock masses, In Proceedings of the 5th International Congress Society of Rock Mechanics Melbourne (pp.1-8).
- Zhou, S. (1994). A program to model the initial shape and extent of borehole breakout. **Computers and Geosciences**. 20(7-8):1143–1160.



APPENDIX A

SAMPLE DIMENSIONS

Table A.1 Intact rock specimens.

Specimen No.	Dimension (mm³)	Density (g/cc)
PWSS-01	55.12×54.55×55.23	2.22
PWSS-02	54.72×54.55×55.53	2.33
PWSS-03	55.20×55.55×55.03	2.31
PWSS-04	55.12×55.45×54.20	2.24
PWSS-05	55.10×54.95×55.13	2.28

Table A.2 Rock specimens for case I.

Specimen No.	Dimension (mm³)	Density (g/cc)
PWSS-01-I	54.20×54.52×54.73	2.25
PWSS-02-I	54.65×54.56×54.03	2.30
PWSS-03-I	55.27×55.45×55.43	2.29
PWSS-04-I	55.32×54.40×54.80	2.21
PWSS-05-I	55.00×54.75×54.93	2.26

Table A.3 Rock specimens for case II.

Specimen No.	Dimension (mm³)	Density (g/cc)
PWSS-01-II	54.22×54.32×54.53	2.28
PWSS-02-II	55.05×55.16×55.23	2.28
PWSS-03-II	54.25×54.40×55.53	2.25
PWSS-04-II	55.22×54.70×54.97	2.24
PWSS-05-II	55.00×55.55×55.40	2.27

Table A.4 Rock specimens for case III.

Specimen No.	Dimension (mm³)	Density (g/cc)
PWSS-01-III	56.52×56.42×55.53	2.23
PWSS-02-III	56.00×55.87×56.10	2.23
PWSS-03-III	55.25×55.00×55.00	2.25
PWSS-04-III	55.40×55.00×54.50	2.27
PWSS-05-III	55.10×55.50×55.50	2.28

Table A.5 Rock specimens for case IV.

Specimen No.	Dimension (mm³)	Density (g/cc)
PWSS-01-IV	56.22×56.80×55.50	2.33
PWSS-02-IV	55.60×56.70×56.19	2.25
PWSS-03-IV	54.25×54.24×55.09	2.24
PWSS-04-IV	54.50×55.50×54.55	2.23
PWSS-05-IV	55.00×55.90×55.59	2.26

Table A.6 Rock specimens for case V.

Specimen No.	Dimension (mm³)	Density (g/cc)
PWSS-01-V	56.34×54.00×55.00	2.30
PWSS-02-V	55.87×56.35×56.95	2.20
PWSS-03-V	54.54×55.46×56.00	2.22
PWSS-04-V	55.50×55.50×55.85	2.26
PWSS-05-V	55.60×55.82×55.34	2.27

Table A.7 Rock specimens for case VI.

Specimen No.	Dimension (mm³)	Density (g/cc)
PWSS-01-VI	55.40×55.00×55.00	2.28
PWSS-02-VI	55.05×55.50×55.80	2.24
PWSS-03-VI	54.86×55.65×55.94	2.20
PWSS-04-VI	55.50×55.50×55.50	2.21
PWSS-05-VI	55.00×55.32×55.59	2.23

Table A.8 Rock specimens for case VII.

Specimen No.	Dimension (mm³)	Density (g/cc)
PWSS-01-VII	56.00×56.21×54.60	2.24
PWSS-02-VII	56.25×55.00×55.00	2.27
PWSS-03-VII	55.60×56.50×55.50	2.29
PWSS-04-VII	55.89×55.20×55.55	2.24
PWSS-05-VII	55.09×55.23×55.77	2.25



BIOGRAPHY

Mr. Kiattisak Seephan was born on October 2, 1994 in Ubon Ratchathani Province, Thailand. He received her Bachelor's Degree in Engineering (Geotechnology) from Suranaree University of Technology in 2017. For his post-graduate, he continued to study with a Master's degree in the Geological Engineering Program, Institute of Engineering, Suranaree university of Technology. During graduation, 2017-2019, she was a part time worker in position of research assistant at the Geomechanics Research Unit, Institute of Engineering, Suranaree University of Technology.

